

A xanthine monophosphate-specific phosphatase is involved in ureide biosynthesis in nodules of tropical legumes and initiates purine nucleotide catabolism in *Arabidopsis thaliana* in dark-induced carbon starvation and in plant defense

Von der Naturwissenschaftlichen Fakultät der
Gottfried Wilhelm Leibniz Universität Hannover

zur Erlangung Grades
Doktorin der Naturwissenschaften (Dr. rer. nat.)

genehmigte Dissertation
von
Katharina Johanna Heinemann, geb. Winkel, M. Sc.

2021

Referent: Prof. Dr. rer. nat. Claus-Peter Witte

Korreferent: Dr. rer. nat. Sascha Offermann

Tag der Promotion: 24.11.2021

1 Abstract

Purine metabolism is a fundamental pathway of plant primary metabolism and is also known to be used in tropical legumes like soybean and common bean to produce ureides for long-distance nitrogen transport. Some enzymes and transporters involved in ureide biosynthesis are yet unknown. This work describes the identification of a novel xanthosine monophosphate-specific phosphatase, XMPP. By LC-MS-based metabolite analysis of *XMPP*-deficient nodules generated using CRISPR-Cas9 mutagenesis, it was demonstrated that this phosphatase is involved in ureide biosynthesis. *XMPP* is conserved in vascular plants so that another aim of this thesis was its characterization in *Arabidopsis thaliana*. Metabolite analysis of *XMPP* mutants in context of other mutants of the purine catabolism showed that XMP dephosphorylation represents an entry point into purine catabolism and that it is operative in seeds, seedlings, vegetative and reproductive rosettes and that it is of special importance in extended darkness and likely also under biotic stress. It was found that the expression of XMPP protein is under tight control and that it is strongly induced in the extended night and under plant defense-related conditions like methyl jasmonate treatment and infiltration with *Pseudomonas syringae*. In the context of the extended night a new model is proposed which suggests that nucleotides, in particular adenylylates, may serve as transient alternative energy source at the beginning of the extended night when the starch reservoir is depleted and amino acids are not yet available as alternative respiratory substrates. In the context of plant defense, it is suggested that XMPP and purine catabolism could be part of the innate immune response to contain oxidative bursts to the infection sites and thereby protect the surrounding plant tissue.

Keywords: Purine nucleotide metabolism, XMP phosphatase, darkness, carbon starvation, plant defense, ureide biosynthesis, hairy roots, soybean, Arabidopsis

Table of Contents

1	Abstract	I
2	List of Abbreviations	IV
3	Introduction	1
3.1	How excessive nitrogen fertilization changed the world	1
3.2	Nitrogen remobilization from RNA contributes to nitrogen use efficiency	2
3.3	Nucleotides in plants	3
3.4	Purine metabolism	4
3.5	In tropical legumes purine metabolism is used to produce ureides for long-distance nitrogen transport	7
3.6	Current knowledge gaps	8
3.7	Aim of this study	9
4	Results	10
4.1	Candidate list for the identification of enzymes and transporters involved in ureide biosynthesis	10
4.2	Establishment of a workflow to examine candidates in soybean root nodules	13
4.2.1	Choice of nutrient solution	14
4.2.2	Choice of plant substrate and nutrient concentration	16
4.2.3	Further improvements were made for the production of transgenic nodules	18
4.3	Characterization of the XMPP candidate, GSDA and XDH in nodules	20
4.3.1	Characterization of the XMPP candidate and XDH in nodules of common bean	25
4.4	Characterization of XMP Phosphatase in Arabidopsis	28
4.4.1	<i>XMPP</i> phylogeny, gene expression analysis and <i>in vitro</i> enzyme characterization	28
4.4.2	<i>XMPP</i> in Arabidopsis seed development	32
4.4.3	<i>XMPP</i> in Arabidopsis seedlings	40
4.4.4	<i>XMPP</i> in Arabidopsis rosette leaves	47
5	Discussion	52
5.1	Identification of enzymes and transporters involved in nodule ureide biosynthesis of tropical legumes	52
5.2	Characterization of <i>XMPP</i> , GSDA, and XDH in nodule ureide biosynthesis	52
5.2.1	Production of mutant nodules	52
5.2.2	XMP dephosphorylation is possibly the main route to ureide production	53
5.3	Characterization of the XMP Phosphatase of Arabidopsis	55
5.3.1	XMP dephosphorylation is an entry point for purine nucleotide catabolism	55
5.3.2	<i>XMPP</i> in seed development	56

5.3.3	XMPP in seedlings and its role in the extended night _____	58
5.3.4	XMPP in rosettes and in context of extended night and nutrient remobilization _____	58
5.3.5	XMPP represents a switch for the induction of purine catabolism _____	60
5.3.6	The role of XMPP and purine catabolism in plant energy metabolism _____	62
5.3.7	XMPP and purine catabolism in pathogen response _____	71
6	Summary _____	73
7	Material and Methods _____	74
7.1	Plant material and cultivation _____	74
7.2	Cloning _____	76
7.3	Transformation of bacteria _____	78
7.4	Fragment length analysis _____	78
7.5	Protein affinity purification and phosphatase activity assay _____	79
7.6	Immunoblots _____	80
7.7	Production of custom-made polyclonal anti-XMPP antibody _____	80
7.8	Metabolite analysis _____	81
7.9	Statistical Analyses _____	83
7.10	Software _____	83
8	References _____	84
9	List of Figures _____	94
10	List of Tables _____	95
11	Appendix _____	96
	Additional Figures _____	96
	Additional Tables _____	104
	Curriculum Vitae _____	106
	Publications _____	106

2 List of Abbreviations

AEC	Adenylate energy charge
bp	Base pairs
CRISPR	Clustered regularly interspaced short palindromic repeats
DW	Dry weight
FLA	Fragment Length Analysis
FW	Fresh weight
G	Sum of guanylates, guanosine and guanine
HA	hemagglutinin
HPLC	High performance liquid chromatography
KO	Knockout
LC-MS	Liquid chromatography coupled to mass spectrometry
n_b	number of biological replicates
n_t	number of technical replicates
nt	nucleotide(s)
NUE	Nitrogen Use Efficiency
NUtE	Nitrogen Utilization Efficiency
Page	Polyacrylamide gel electrophoresis
PCR	Polymerase chain reaction
PPP	Pentose Phosphate Pathway
RNAseq	RNA sequencing
RPKM	Reads per kilobase of transcript per million mapped reads
RT	Room temperature
SDS	Sodium dodecyl sulfate

3 Introduction

3.1 How excessive nitrogen fertilization changed the world

In 1913, a landmark for agriculture was set by BASF in Ludwigshafen when they put the first plant for the fixation of atmospheric nitrogen into operation. The so-called Haber-Bosch process enabled the production of liquid ammonia which could be used as nitrogen fertilizer (BASF, 1908). Insufficient nitrogen fertilization was until then a common limiting factor of crop growth. Although guano, saltpeter, sal ammoniac extracted from coal and manure were used for nitrogen fertilization before, the production of synthetic nitrogen fertilizer produced by the Haber-Bosch process was largely expanding the nitrogen fertilizer availability. Increased nitrogen supply improved crop yields and initiated a drastic growth of worldwide food supply, livestock farming and eventually world population (Fig. 1, Erisman *et al.*, 2008). In this time sustainability and nitrogen use efficiency in particular were not considered in crop breeding and agriculture. It is only now, that sustainable agriculture has reached public awareness, also recently promoted by the “Fridays for Future” movement.

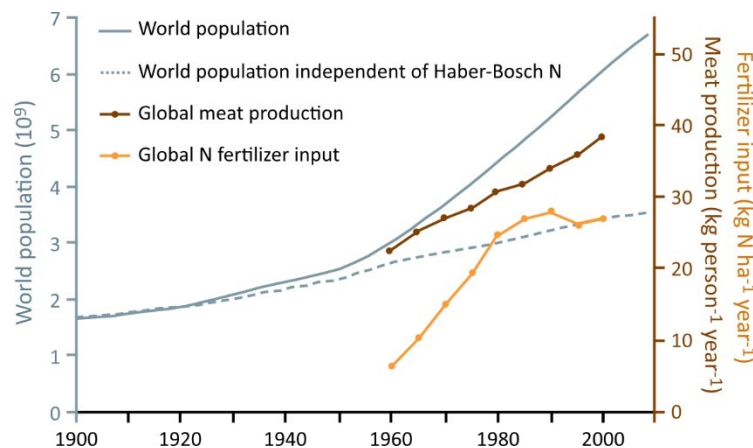


Figure 1 Development of global nitrogen fertilizer use, global meat production and world population after the invention of the Haber-Bosch process at the beginning of the 20th century. The dashed line shows an estimation of the world population that was fed independently of nitrogen fertilizer produced by the Haber-Bosch process. Adapted from Erisman *et al.* (2008).

The Haber-Bosch process is energy-demanding and significantly drives the greenhouse effect by emitting about 4 kg carbon dioxide for 1 kg fixed atmospheric nitrogen (Umweltbundesamt, 2020). With a global production volume of 144 million tons of ammonia in 2018 accordingly 576 million tons of carbon dioxide were generated, which corresponds to 76% of the total carbon dioxide emitted by Germany in the same year (Apodaca, 2020; Strogies and Gniffke, 2020). Additionally, the application of nitrogen fertilizers in the field releases great amounts of the climate gas nitrous oxide (N₂O). Nitrification and denitrification reactions catalyzed by soil bacteria generate nitrous oxide from fertilizer nitrogen (Tian *et al.*, 2020). Nitrous oxide has a comparatively low atmospheric lifetime of about 116 years, but its global warming potential in a 100 year frame is 300 times higher than of carbon dioxide (Prather *et al.*, 2015; IPCC, 2013). Anthropogenic nitrous oxide emissions almost equal natural emissions with contributions of 57% and 43%, respectively (Tian *et al.*, 2020). Of the anthropogenic contribution 70% are caused by fertilizer use. Moreover, 10 - 19% of the applied nitrogen fertilizer is lost by volatilization of ammonia (Bouwman *et al.*, 2002). This promotes the global warming and ozone depletion, and increases concentrations of ammonia and nitrous oxide gases in the atmosphere

Introduction

Nitrogen compounds dissolved in raindrops and the deposition of nitrogen-containing aerosols and airborne particles cause the eutrophication of natural ecosystems (Umweltbundesamt, 2011). Nitrogen fertilizer in form of nitrate can also be washed out easily from the fields by rain and reaches the ground and surface waters like rivers and lakes. According to the EU Water Framework Directive from 2015, 73.6% of 732 monitored German lakes were rated as too eutrophic (Völker *et al.*, 2016). In natural ecosystems, the low nitrogen availability is limiting plant growth, which is directly promoted by nitrogen pollution. Some plant species profit more from the additional nitrogen input and can overgrow plant species adjusted to limited nitrogen availability. In lakes this can be frequently observed as algal blooms. Lawns of algae deprive underneath-growing plants of sun light. Plants die and sink to the ground, where bacteria break down the plant material under oxygen consumption. In heavily affected lakes the oxygen content is strongly reduced eventually resulting in the death of numerous species ranging from mollusks and snails to crabs and fish. Often lakes stabilize in new equilibria with a reduced set of species. The extinction of individual species from ecosystems can have far-reaching consequences also for the survival of other species. Also in terrestrial ecosystems like forests nitrogen-responsive species can overgrow long-term established species due to anthropogenic nitrogen input. Especially for terrestrial plants the nitrogen-dependent fast growth can lead to fragile shoots and roots, which are more sensitive to wind, frost and pests.

In summary, the production and use of synthetic nitrogen fertilizer drives the greenhouse effect and causes progressive eutrophication of terrestrial and aquatic ecosystems which greatly endangers biodiversity. This is why the integration of biological nitrogen fixation and the increase of nitrogen use efficiency have been in focus of plant research in the past decades to reduce the environmentally harmful production of synthetic nitrogen fertilizer and the overall nitrogen fertilizer input.

3.2 Nitrogen remobilization from RNA contributes to nitrogen use efficiency

A target for the reduction of nitrogen fertilizer use is the improvement of nitrogen use efficiency (NUE). Various definitions of NUE exist, which all indicate a ratio of nitrogen found in harvested plant parts and initially applied nitrogen amounts intended for plant use. NUE is determined by the nitrogen uptake and utilization efficiency of the plant. The uptake is depending on the nitrogen availability in the rhizosphere which is influenced by soil composition, aeration, pH, temperature, form of nitrogen but also by plant characteristics like the size and architecture of roots, strength of transpiration flow, and most importantly nitrogen demand and transporter activities. Nitrogen utilization efficiency (NUE) describes a ratio of nitrogen used in harvested plant parts and the total plant nitrogen content (Moll *et al.*, 1982). NUE is depending on nitrogen metabolization, allocation and remobilization in the plant. Nitrogen fertilization is commonly important in the vegetative phase of the plant life cycle, while nitrogen remobilization from vegetative tissues becomes essential in the reproductive phase (Perchlik and Tegeder, 2017). Grain nitrogen of cereals for example is derived by 60 to 92% from remobilization (Barbottin *et al.*, 2005). The main source of remobilized nitrogen are proteins, in particular those related to photosynthesis (Masclaux *et al.*, 2000). But nitrogen is also recovered from chlorophyll and nucleic acids, ribosomal RNA (rRNA) in particular. Pyrimidine nucleotides contain two to three nitrogen atoms and purine nucleotides even four to five (Fig. 2). Total RNA consists to about 80% of rRNA. By autophagy, rRNA is imported into the vacuole where it is hydrolyzed to nucleotides with the contribution of Ribonuclease 2 (RNS2; MacIntosh and Bassham, 2011). Nucleotides are dephosphorylated by unknown phosphatases to nucleosides which are the export product of the vacuolar RNA degradation. Nucleosides are transported by the Equilibrative Nucleoside Transporter 1 (ENT1) from the vacuole to the cytosol where they can either be salvaged to nucleotides or further

degraded by the purine and pyrimidine catabolic pathways.

Initiation of nucleotide degradation can also take place in the cytosol where RNA-derived nucleotides are dephosphorylated. Supposedly, mainly mRNA is degraded via the cytosolic pathway. Although the contribution of nitrogen remobilized from RNA is 25 times smaller than from proteins, nitrogen remobilization from RNA was suggested to play an important role in leaf senescence (Masclaux *et al.*, 2000; Soltabayeva *et al.*, 2018). Soltabayeva *et al.* showed that *Arabidopsis* plants mutated in genes involved in purine catabolism exhibited early nitrogen starvation responses especially in the old rosette leaves when grown under reduced nitrogen supply. Consistently, Takagi *et al.* (2018) found that purine catabolism mutants showed decreased nitrogen use efficiency rates, although they could not rescue the mutant phenotypes by external nitrogen supply.

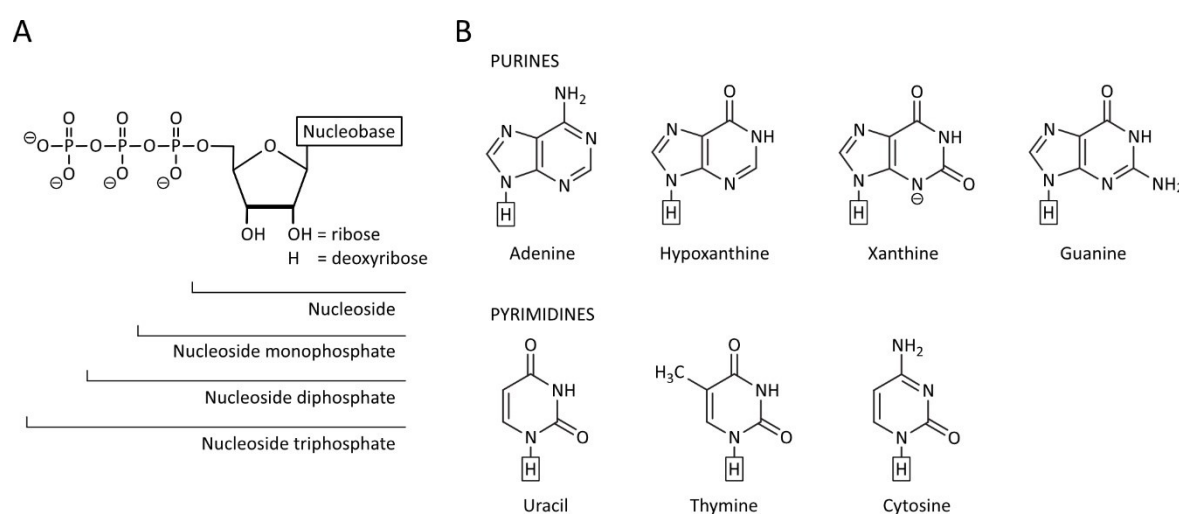


Figure 2 Structure of purine and pyrimidine nucleotides. **A**, General structure of nucleotides. Depending on the number of phosphate groups a nucleoside, nucleoside monophosphate (NMP), nucleoside diphosphate (NDP) or nucleoside triphosphate (NTP) is formed. Nucleosides can contain a ribose or a deoxyribose. **B**, Structure of purine and pyrimidine nucleobases. Nucleobases can be linked to the sugar, as indicated in A, by a glycosidic bond replacing the proton which is surrounded by a box. Adapted from Witte and Herde (2020).

3.3 Nucleotides in plants

Nucleotides are essential for life. As building blocks of DNA and RNA, they store genetic information and allow the processing of this information. Nucleotides comprise a purine or pyrimidine base linked to a phosphorylated sugar (Fig. 2). Depending on the number of phosphates, nucleotides are grouped into nucleoside monophosphates (NMPs), nucleoside diphosphates (NDPs) or nucleoside triphosphates (NTPs). The sugar moiety of RNA nucleotides is ribose whereas DNA nucleotides contain a 2'-deoxyribose and are therefore named deoxynucleotides (dNMPs, dNDPs, dNTPs). The canonical nucleobases that occur in nucleic acids are the purine bases adenine and guanine and the pyrimidine bases cytosine, thymine and uracil. Purine and pyrimidine nucleotides are formed by independent biosynthetic routes which both require phosphoribosylpyrophosphate (PRPP) derived from the pentose phosphate pathway intermediate ribose-5-phosphate (Witte and Herde, 2020). The nucleotide *de novo* biosynthesis is very energy-demanding which is why nucleosides and nucleobases can be recycled by salvage reactions. However, purine and pyrimidine nucleobases can also be fully catabolized through independent routes (Witte and Herde, 2020).

Introduction

Besides being building blocks of RNA and DNA, nucleotides are also important for energy metabolism. The purine nucleotides GTP and especially ATP play central roles as energy carrier in reactions that require energetic coupling. Nucleotides are also building blocks of co-substrates like nicotinamide adenine dinucleotide (NAD), flavin adenine dinucleotide (FAD) and Coenzyme A which contain adenylate moieties. Nucleotides are used for the activation of sugars as in the case of UDP-glucose and are required for other cell-relevant molecules like S-adenosyl methionine, molybdenum cofactor, B-class vitamins like riboflavin, thiamine and folates or the hormone cytokinin (Zrenner *et al.*, 2006).

3.4 Purine metabolism

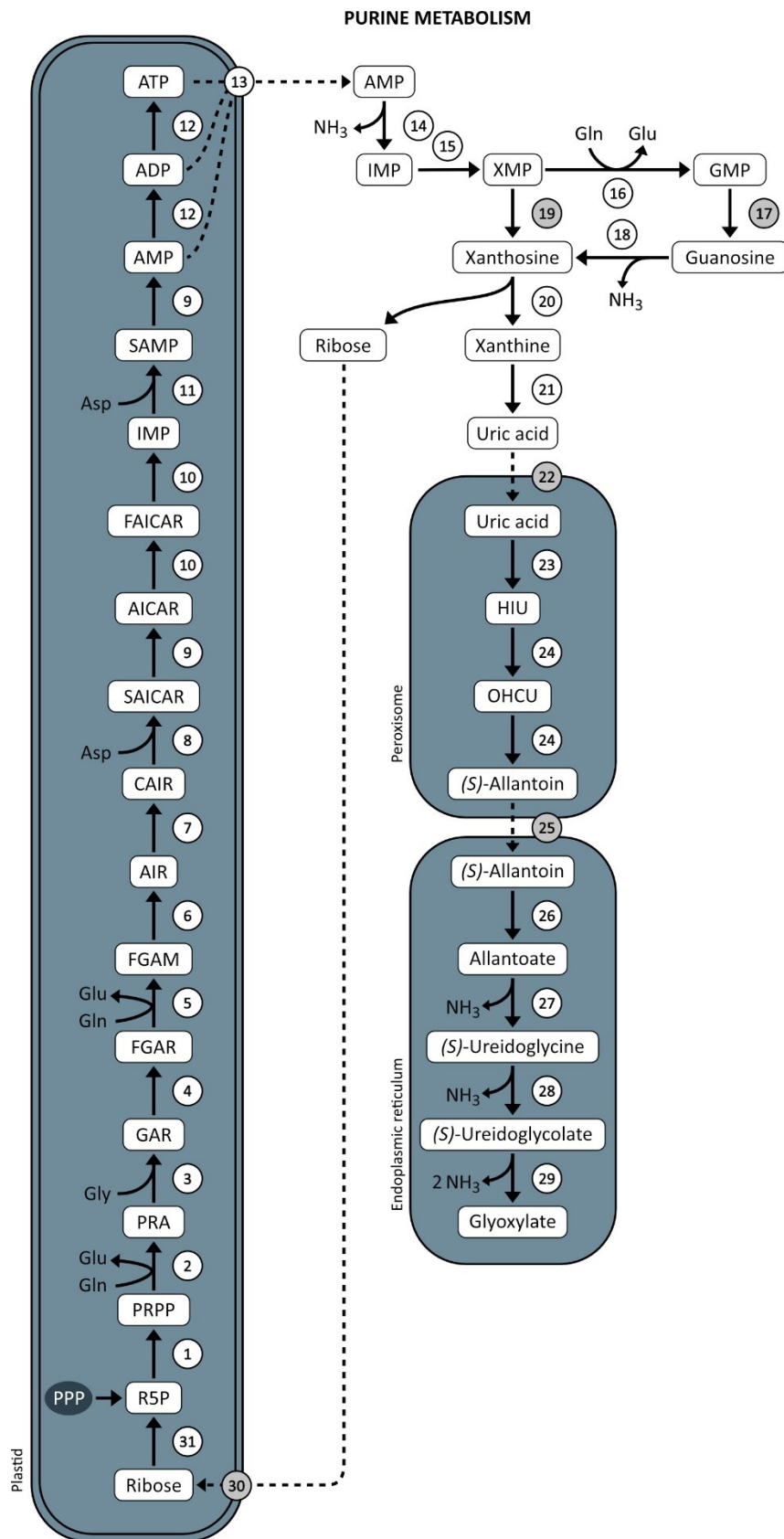
Purine *de novo* biosynthesis requires ribose-5-phosphate (R5P) provided by the pentose phosphate pathway (PPP) in plastids (Zrenner *et al.*, 2006, Witte and Herde, 2020). PRPP is formed from R5P by PRPP synthase and delivers the sugar at which the purine ring system is formed. First the imidazole and subsequently the pyrimidine ring is built up in ten consecutive steps to finally produce inosine 5'-monophosphate (IMP; Fig. 3). IMP is aminated via adenylosuccinate (SAMP) to AMP and can be phosphorylated to ADP and ATP. The adenylate transporter Brittle 1 (BT1) is exporting the adenylate nucleotides into the cytosol. For GMP biosynthesis, AMP is deaminated to IMP which is oxidized to XMP. XMP is aminated to GMP from which GDP and GTP can be produced by phosphorylation.

Degradation of purine nucleoside monophosphates in the cytosol is initiated by yet unknown phosphatases. The nucleosides adenosine, inosine, xanthosine and guanosine are formed by the dephosphorylation of the corresponding nucleoside monophosphates AMP, IMP, XMP and GMP, respectively (Table A - 1). In recent years, it was demonstrated that neither the AMP – adenosine – adenine route nor the IMP – inosine – hypoxanthine route is involved in purine catabolism (Yin *et al.*, 2014; Baccolini and Witte, 2019). By contrast it has been shown that the route GMP – guanosine – xanthosine – xanthine is the main route of purine nucleotide catabolism (Dahncke and Witte, 2013; Baccolini and Witte, 2019). Interestingly, mammals and many bacteria possess a guanine deaminase instead of a guanosine deaminase so that the GMP catabolic route proceeds through GMP – guanine – xanthine. Metabolite analyses of *GSDA NSH1* double mutants showed that the mutation of *Guanosine Deaminase* (*GSDA*, Fig. 3, #18) was not sufficient to completely block the xanthosine accumulation caused by the mutation of *Nucleoside Hydrolase 1* (*NSH1*, #20; Baccolini and Witte, 2019). This indicated that also the shorter route XMP – xanthosine may be operative in the purine catabolism of *Arabidopsis*. The existence of an XMP phosphatase (#19) was already proposed based on feeding experiments using cell-free extracts of soybean and cowpea nodules where the purine metabolism is used for the production of ureides to export previously fixed nitrogen to the shoot (Triplett *et al.*, 1980; Atkins, 1981). So far neither an XMP phosphatase nor a GMP phosphatase (#17) have been identified.

Salvage reactions can recycle nucleosides and nucleobases to nucleotides in an energy-efficient manner. The salvage of purine nucleobases using PRPP is catalyzed by Hypoxanthine Guanine Phosphoribosyltransferase (HGPRT) for hypoxanthine and guanine, and by Adenine Phosphoribosyltransferase (APRT) for adenine (Witte and Herde, 2020). The purine nucleosides adenosine, inosine and guanosine can be salvaged by kinases. It is interesting to note that neither xanthosine nor any of the downstream metabolites can be salvaged (Yin *et al.*, 2014). The production of xanthosine therefore initiates the irreversible degradation of the purine ring system. Xanthosine is hydrolyzed by a heterocomplex of Nucleoside Hydrolases 1 (*NSH1*) and Nucleoside Hydrolase 2 (*NSH2*, #20) releasing ribose and the nucleobase xanthine (Baccolini and Witte, 2019). Ribose is transported to the plastids where it is phosphorylated by Ribokinase to recycle R5P (*RBSK*, #31;

Schröder *et al.*, 2018). The oxidation of xanthine is catalyzed by Xanthine Dehydrogenase (XDH, #21) yielding uric acid, which is imported into the peroxisomes (Werner and Witte, 2011). Uric acid is oxidized by the Urate Oxidase (UOX, #23) to 5-hydroxyisourate (HIU). In contrast to mammals which secrete uric acid in their urine, plants are capable to fully degrade the purine ring system to recover the valuable nitrogen (Werner and Witte, 2011). Allantoin Synthase (ALNS; #24) further breaks down HIU to (*S*)-allantoin, which is transported to the endoplasmic reticulum where the pyrimidine ring is hydrolytically opened by Allantoinase (ALN, #26) forming allantoate. Uric acid, allantoin and allantoate are special intermediates of purine catabolism, as they have been assigned multiple physiological functions. Allantoin was shown to play a role in drought, salt and osmotic stress responses (Watanabe *et al.*, 2014; Irani and Todd, 2016; Lescano *et al.*, 2016). Uric acid and allantoin were proposed to be important for quenching reactive oxygen species (Brychkova *et al.*, 2008; Watanabe *et al.*, 2014; Irani and Todd, 2016; Ma *et al.*, 2016). Allantoin and allantoate are moreover used as nitrogen storage and long-distance transport compounds. In perennial plants like maple and comfrey, high concentrations of ureides are found in dormant roots which supply the shoot with nitrogen in spring (Schubert and Boland, 1990). For Arabidopsis, it has been suggested that the ureides allantoin and allantoate may serve to remobilize nitrogen under limited nitrogen supply (Soltabayeva *et al.*, 2018). Especially important are the ureides in tropical legumes like soybean and common bean, where they transport nitrogen from symbiotic fixation to the shoot (Pate and Atkins, 1983). When required, plants can fully degrade the ureides, releasing carbon dioxide, four molecules of ammonia and glyoxylate (Werner and Witte, 2011).

Figure 3 Purine Metabolism. Purine *de novo* biosynthesis takes place in plastids where R5P is derived from the Pentose Phosphate Pathway (PPP). PRPP is produced from R5P which provides the sugar for the step-wise construction of the purine ring system. Nitrogen for the purine ring system is delivered by the amino acids Gln, Gly and Asp. Adenylates are formed in the plastids whereas guanylates are subsequently formed in the cytosol. Purine nucleotide catabolism can be initiated in the cytosol and proceeds in peroxisomes and the endoplasmic reticulum to fully degrade the purine ring system and recover nitrogen which is released as ammonia. Released ribose is recycled. Salvage reactions for nucleotide biosynthesis are not shown. Adapted from Zrenner *et al.* (2006), Werner and Witte (2011) and Witte and Herde (2020). Intermediates: PRPP, 5-phosphoribosyl-1-pyrophosphate; PRA, 5-phosphoribosylamine; GAR, glycinamide ribonucleotide; FGAR, formylglycinamide ribonucleotide; FGAM, formylglycinamide ribonucleotide; AIR, 5-aminoimidazole ribonucleotide; CAIR, 4-carboxyaminoimidazole ribonucleotide; SAICAR, N-succinyl-5-aminoimidazole-4-carboxamide ribonucleotide; AICAR, 5-aminoimidazole-4-carboxamide ribonucleotide; FAICAR, 5-formaminoimidazole-4-carboxamide ribonucleotide; IMP, inosine monophosphate; SAMP, adenylosuccinate; AMP, adenosine monophosphate; ADP, adenosine diphosphate; ATP, adenosine triphosphate; XMP, xanthosine monophosphate; GMP, guanosine monophosphate; HIU, 5-hydroxyisourate; OHCU, 2-oxo-4-hydroxy-4-carboxy-5-ureido-imidazole; R5P, ribose-5-phosphate. Circled numbers represent genes: 1, PRPP Synthase 1 (PRS1); 2, PRPP Amidotransferase (Atase); 3, GAR Synthase (GARS); 4, GAR Formyltransferase (GART); 5, FGAM Synthase (FGAMS); 6, AIR Synthase (AIRS); 7, AIR Carboxylase (AIRC); 8, SAICAR Synthase (SAICARS); 9, Adenylosuccinate Lyase (ASL); 10, AICAR Transformylase/IMP Cyclohydrolase (ATIC); 11, Adenylosuccinate Synthase (ASS); 12, Adenylate Kinases (AMKs); 13, Brittle 1 (BT1); 14, AMP Deaminase (AMPD); 15, IMP Dehydrogenases (IMPDHs); 16 GMP Synthetase (GMPS); 17, unknown GMP Phosphatase (GMPP); 18, Guanosine Deaminase (GSDA); 19, unknown XMP Phosphatase (XMPP); 20, Nucleoside Hydrolase 1 and 2 heterocomplex (NSH1/2); 21, Xanthine Dehydrogenase (XDH); 22, unknown uric acid transporter; 23, Urate Oxidase (UOX); 24, Allantoin Synthase (ALNS); 25, unknown allantoin transport process; 26, Allantoinase (ALN); 27, Allantoate Amidohydrolase (AAH); 28, Ureidoglycine Aminohydrolase (UGLYAH), 29, Ureidoglycolate Amidohydrolase (UAH); 30, unknown ribose importer; 31, Ribokinase (RBSK). Black numbers marked in grey indicate unidentified genes. Dashed lines symbolize transport processes.



3.5 In tropical legumes purine metabolism is used to produce ureides for long-distance nitrogen transport

Nitrogen is commonly a limiting factor for plant growth although the air consists of 78% dinitrogen gas (N₂). Most plants cannot access the atmospheric nitrogen but legumes are the main exception. In symbiosis with soil bacteria of the genus rhizobia, nitrogen is fixed in symbiosis-induced spherical root organs called nodules (Hellriegel and Wilfarth, 1889). After the invasion of the root, the bacteria differentiate in infected nodule cells to plant-cell organelles, which are referred to as bacteroids (Bergersen, 1958). In these organelles the highly energy-demanding fixation of atmospheric nitrogen is catalyzed by the nitrogenase enzyme which consumes sixteen ATP for each fixed dinitrogen. In this symbiosis plants exchange nitrogen in form of ammonia in exchange for carbon skeletons serving as carbon and energy source for the bacteroids (Udvardi and Poole, 2013; Weir, 2016). Important crop legumes for food and forage production are soybean, lupin, alfalfa, peas and beans.

Legumes can be divided into two groups, the temperate and tropical legumes depending on their natural occurrence. These two groups differ in the metabolites which are used to transport nitrogen to the shoot (Pate and Atkins, 1983). Temperate legumes like *Medicago truncatula* and *Lotus japonicus* mainly export the amides glutamine and asparagine for shoot nitrogen supply. In contrast, tropical legumes like soybean (*Glycine max*) and common bean (*Phaseolus vulgaris*) export nitrogen in form of the ureides allantoin and allantoate. Allantoin and allantoate account for 60 to 90% of the total nitrogen transported in the xylem of different tested tropical legumes (Schubert, 1986).

For ureide biosynthesis, the purine metabolism is used. Bacteroids fix nitrogen producing ammonia, which is provided to the plant cell where it is assimilated into amino acids (Lodwig and Poole, 2003). The amino acids glutamine, aspartate and glycine are used for purine nucleotide biosynthesis (Fig. 3). From purine nucleotides, xanthine is generated by a yet unresolved route. Xanthine is further oxidized to form the ureides which are exported from the nodules to the shoot. In the sink tissues ureides can be used for nitrogen storage or can be fully degraded to reassimilate the released ammonia into amino acids. Feeding experiments of cell free extracts of cowpea nodules with purine nucleotides demonstrated that ureides were formed when IMP and XMP were supplied, but only weakly or not at all from added GMP and AMP, respectively (Atkins, 1981). In cell free extracts of soybean nodules supplied with XMP, IMP and different downstream products, the addition of hypoxanthine, inosine and IMP resulted in the highest allantoate production (Triplett *et al.*, 1980). In short, *in vitro* feeding experiments indicated that IMP and also XMP dephosphorylation are likely involved in ureide production. Interestingly, treatment of nodulated soybeans with the XDH inhibitor allopurinol caused a strong reduction of allantoin and allantoate concentrations coinciding with a strong increase of xanthine but not of hypoxanthine amounts (Fujihara and Yamaguchi, 1978). This argues against an involvement of IMP dephosphorylation in ureide biosynthesis in soybean nodules. In line with this, tracer studies with ¹⁴C-labelled glycine and IMP in cell-free extracts of cowpea nodules indicated that XMP rather than IMP dephosphorylation is the dominant route to ureide biosynthesis (Shelp and Atkins, 1983). In summary, it is not yet clear how xanthine is generated within ureide biosynthesis.

3.6 Current knowledge gaps

The enzymatic steps for biosynthesis of AMP and GMP are known although many plant enzymes have been merely postulated based on significant homology to enzymes from non-plant origin (Fig. 3). Also many aspects of the catabolic route of purine nucleotides with the ureides as intermediates are well-known by now. Nevertheless, blind spots exist which still need to be investigated. Two major classes are the unknown phosphatases and transporters. So far no phosphatase has been identified which catalyzes the dephosphorylation of purine NMPs (Fig. 3, genes #17, #19). Several factors complicate the identification of NMP phosphatases in general. First of all their substrates are central metabolites which are also substrates for other reactions. Thus, mutation of an NMP phosphatase would not necessarily result in a significant change in the size of the respective NMP pool, implying that identification of these phosphatases by random mutagenesis is unlikely. Moreover, NMP phosphatases often lack strong substrate specificity which makes the assignment of a specific physiological function based on *in vitro* activity measurements difficult, and which may also cause functional redundancy *in vivo*. Also the identification of transporters is especially difficult. The vast number of transporters and the biochemical difficulties to establish membrane systems with active transporters for measurements are substantial obstacles. The plastidic adenylate exporter *Brittle 1* (*BT1*, #13) and the *Ureide Permeases* (*UPS*) are the only known transporters involved in purine metabolism so far. *BT1* exports adenylates from the plastids to the cytosol (Kirchberger *et al.*, 2008). In tropical legumes, the *UPS* transporters are required for the long distance transport of the ureides from nodules to developing organs (Tegeger, 2014). The role of *UPS* transporters in non-legumes is however not clear. Possible roles as ureide and uracil transporters were previously discussed (Schmidt *et al.*, 2004; Soltabayeva *et al.*, 2018).

There are several transport processes for which the corresponding genes have not yet been identified:

- I. Ribose import into the plastids (#30): Ribose released by nucleoside hydrolysis needs to be reimported into the plastids where RBSK phosphorylates ribose to R5P.
- II. Uric acid import into the peroxisome (#22).
- III. Allantoin transport from peroxisomes to the endoplasmic reticulum (#25): This may be mediated by transporters in the organelle membranes, but also by a vesicle transport.

In context of the ureide production and export from nodules there are additional transport processes which have not yet been described:

- IV. Cellular transport from infected to uninfected nodule cells: Ureide biosynthesis is initiated in the plastids of infected nodule cells and is at some unknown point of the process shifted to the uninfected cells. This relocation is necessary to spatially separate the oxygen-sensitive nitrogenase from the oxygen-requiring urate oxidase (#23). Many reports on the cellular localization of enzymes participating in the ureide biosynthesis exist (Vaughn *et al.*, 1982; Bergmann *et al.*, 1983; Hanks *et al.*, 1983; Shelp *et al.*, 1983; Triplett, 1985; Nguyen *et al.*, 1986; van den Bosch and Newcomb, 1986; Webb and Newcomb, 1987; Raychaudhuri and Tipton, 2002). Their partly contradictory results however do not allow to draw any conclusion about which metabolite is transported from the infected to the uninfected cells.

- V. Transport of the ureides to the shoot: The transport of allantoin and allantoate to the shoot is likely comprising several transport processes and is still elusive. Tegeder (2014) proposed that allantoin and allantoate are exported from uninfected nodule cells in the infection zone to the apoplasm by an unknown transporter and that they move towards the vascular bundles by diffusion. To pass the Casparian strip they are reimported to the cytoplasm by Ureide Permease 1 (UPS1). Ureides are then diffusing through plasmodesmata to the vascular bundles, where they are loaded by another unknown transport process into the xylem or by UPS1 into the phloem for nitrogen supply of the shoot or developing roots, respectively.
- VI. Transport processes for unloading of ureides from the xylem to leaf parenchyma or from the phloem to the root parenchyma. It has been suggested that UPS1 imports ureides into the leaf symplasm after they have been exported from the xylem to the apoplasm by an unknown transporter (Tegeder, 2014).
- VII. Transport processes to supply reproductive organs, seeds in particular: After the xylem transport to the shoot ureides need to be loaded to the phloem to reach reproductive organs. This transport is still elusive. Partly it takes place in the symplasm, but it can also occur in the apoplasm of the leaf. Transporters that export the ureides to the apoplasm before they are loaded into the phloem have not yet been identified. It was proposed that the UPS transporters, which localize in the leaf sieve element companion cells of the phloem, are involved in phloem loading (Tegeder, 2014). Finally transporters are required to unload the ureides from the phloem from where they can be allocated to the sink cells.

The elucidation of these unknown transport processes and the identification of the involved transporters are of special interest. Perchlik and Tegeder (2017) investigated how the modulation of amino acid partitioning by the overexpression of the Amino Acid Permease 1 (AAP1) increased NUE, biomass production and seed yield of Arabidopsis. The authors outlined that the source-to-sink partitioning of amino acids can limit nitrogen uptake, assimilation and translocation by feedback control mechanisms. Accordingly, Carter and Tegeder (2016) found that the expression of common bean *UPS1* in soybean nodule cortex and endodermis increased nitrogen fixation, allocation to the shoot and increased seed yield. As transport processes seem to be more likely rate limiting than catalytic processes, they are promising targets for the improvement of NUE, symbiotic nitrogen fixation and plant growth and yield by genetic engineering.

3.7 Aim of this study

This study aimed to identify enzymes and transporters involved in soybean ureide biosynthesis from a comparative data set based on publicly accessible RNA sequencing data of amide- and ureide-exporting legumes. The establishment of a procedure to generate transgenic soybean nodules mutated in selected candidate genes using CRISPR-Cas9 and their metabolic analysis by liquid chromatography coupled to mass spectrometry (LC-MS) was planned to create a pipeline for the characterization of candidates. The Arabidopsis orthologs of the candidates should be characterized to shed light on their function in purine metabolism.

4 Results

4.1 Candidate list for the identification of enzymes and transporters involved in ureide biosynthesis

Tropical legumes export nitrogen in form of ureides from nodules to the shoot. For the identification of enzymes and transporters involved in ureide biosynthesis, a bioinformatic approach compiling online accessible RNA sequencing (RNAseq) data was set up by Prof. Dr. Claus-Peter Witte and Dr. Marco Herde. Considering that the ureide production takes place in nodules, expression of genes involved in ureide biosynthesis is expected to be upregulated in nodules compared to roots of tropical legumes, like soybean and common bean. In contrast, temperate legumes like *Medicago truncatula* and *Lotus japonicus* do not form ureides, but export nitrogen in form of amides like glutamine and asparagine. Therefore, an induced expression of genes involved in the ureide biosynthesis in nodules compared to roots is not expected for *M. truncatula* or *L. japonicus*.

A data set joining root and nodule RNAseq data of the four mentioned legumes was compiled by Dr. Marco Herde. Common bean was the starting point which comprises about 37 000 protein-coding transcripts of which 6964 transcripts were at least 1.5x more abundant in nodules compared to roots. The amino acid sequences of the corresponding proteins of this set of transcripts were used to assign orthologs of the other legume species by sequence similarity. Fold changes of gene expression in nodules *versus* roots were calculated for each legume ortholog. Assuming that the expression of genes involved in the ureide biosynthesis is at least 1.5x upregulated in nodules compared to roots of the ureide exporting legumes, but not of their orthologs of the amide exporting legumes, the data set was reduced to a list of 1376 transcripts. Corresponding genes built a candidate list which likely contains yet unidentified genes coding for enzymes and transporters involved in ureide biosynthesis. The validity of this candidate list was supported by the fact that it included all genes which are known to be involved in ureide biosynthesis.

For the overall evaluation of the candidate list, the expression pattern of orthologs across the four legumes species was checked. If the expression of a common bean gene and its soybean ortholog was upregulated in nodules compared to roots by at least 1.5x, and the expression of the corresponding orthologs of the amide-exporting legumes was not regulated like this, the ortholog was called “regulated in the expected fashion” (tab. 1, fig. 4). As expected all nine genes involved in IMP biosynthesis from PRPP as well as all six genes involved in the ureide production from xanthosine to allantoate were regulated in the expected fashion with nodule *versus* root fold changes of at least four-fold. Interestingly, neither the *Adenylosuccinate Synthase*, any of the *Adenylate Kinases*, the adenylate exporter *Brittle1* nor the *AMP Deaminase*, which are involved in adenylate nucleotide production, export and deamination, were regulated in the expected fashion. The involvement of the route through AMP in ureide biosynthesis seems thus unlikely. The direct export of IMP uncoupled from adenylate production and facilitated by an IMP exporter which is similarly regulated in the comparative data set as upstream and downstream located genes seems more reasonable and energy-efficient (Fig. 3, 4). Assuming that the IMP exporter shows a similar regulation pattern across the legumes, the gene coding for it should be found in the candidate list. IMP is oxidized in the cytosol by IMP Dehydrogenases to XMP, one of which is regulated in the expected fashion. Surprisingly, *GMP Synthetase* did not show the expected regulation pattern also questioning the involvement of the GMP – guanosine route to xanthosine in ureide biosynthesis.

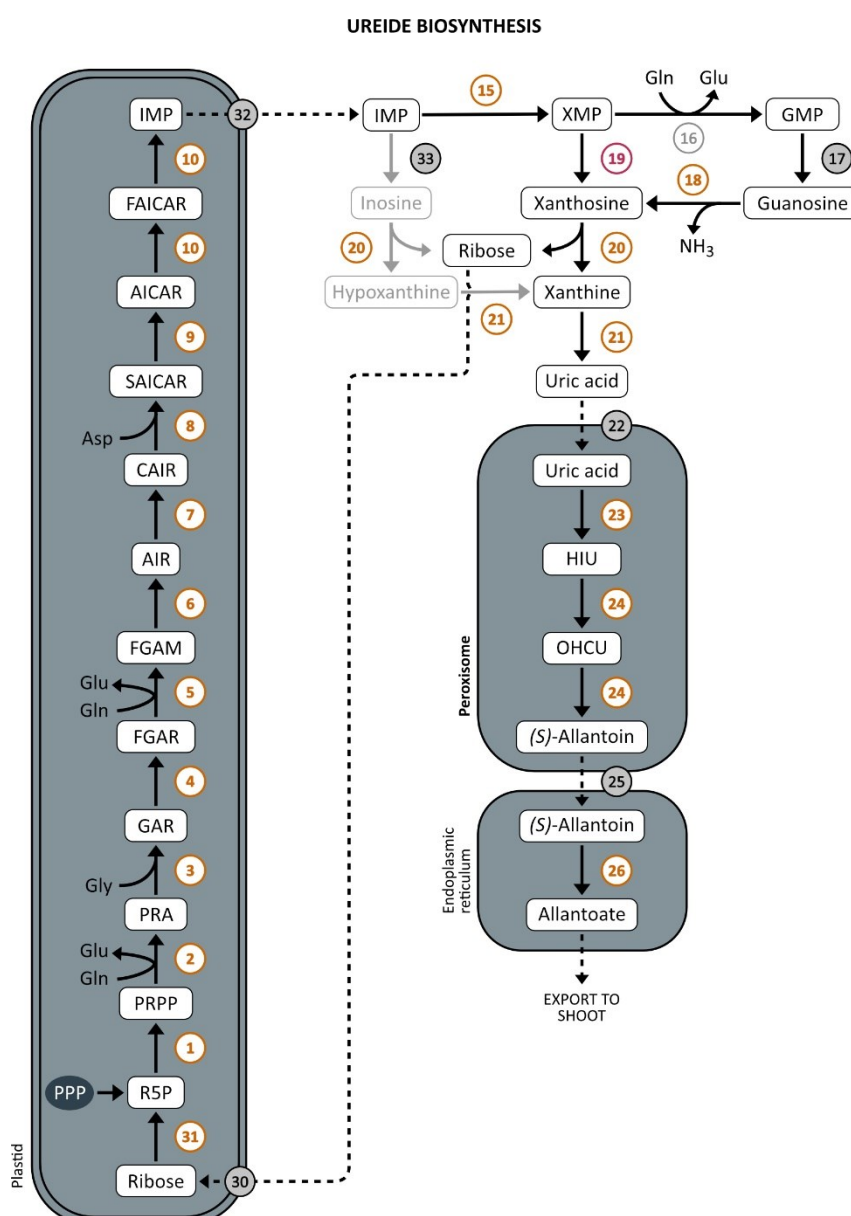


Figure 4 Ureide Biosynthesis. The purine metabolism is used in nodules of tropical legumes to produce ureides for nitrogen export from nodules. The map of figure 3 was adapted to the findings of the comparative data set and current knowledge (Tab. 1). IMP is likely directly exported into the cytosol and ureides are not degraded in the nodules but are exported to the shoot. In contrast, to purine catabolism in *Arabidopsis*, earlier studies reported that IMP dephosphorylation could play a role for ureide production in nodules of tropical legumes. The route is colored grey because it is shown in this work that it is not part of the ureide biosynthesis *in vivo*. Orange color indicates that the expression of the orthologs of ureide exporting legumes is induced in nodules compared to roots but not of their orthologs of amide exporting legumes. The *XMPP* candidate is colored in red. Grey color of *GMPS* (16) indicates that the corresponding orthologs were not regulated in the described fashion. Black numbers marked in grey indicate unidentified genes. Dashed lines symbolize transport processes. For gene identities see caption of figure 3. Additional genes here: 32, unknown IMP exporter; 33, unknown IMP phosphatase.

Results

Table 1 Extract of the candidate list from the comparative transcriptome analysis. List of genes shown in figure 3 and 4 including the corresponding Arabidopsis gene locus numbers and the nodule *versus* roots fold changes of the corresponding orthologs of soybean (*Glycine max*, *G. m.*), common bean (*P. vulgaris*, *P. v.*), *M. truncatula* (*M. t.*) and *L. japonicus* (*L. j.*). If fold changes are -1.5 to 1.5 cells are marked by “-”. Positive values indicate an induced expression in nodules *versus* roots.

Gene	Arabidopsis accession	Fold change (nodules vs. roots)				
		<i>P. v.</i>	<i>G. m.</i>	<i>M. t.</i>	<i>L. j.</i>	
1 <i>PRPP Synthase 1</i>	<i>PRS1</i>	At2G35390	16.9	52.2	-	4.6 ^a
2 <i>PRPP Amidotransferase</i>	<i>ATase</i>	At2g16570	19.3	509.0	-	-
3 <i>GAR Synthase</i>	<i>GARS</i>	At1g09830	7.4	13.6	-	-
4 <i>GAR Formyltransferase</i>	<i>GART</i>	At1g31220	8.7	21.7	-	-
5 <i>FGAM Synthase</i>	<i>FGAMS</i>	At1g74260	8.4	15.5	-	-
6 <i>AIR Synthase</i>	<i>AIRS</i>	At3g55010	10.9	5.0	-	-
7 <i>AIR Carboxylase</i>	<i>AIRC</i>	At2g37690	6.9	9.9	-	-
8 <i>SAICAR Synthase</i>	<i>SAICARS</i>	At3g21110	6.8	31.1	-	-
9 <i>Adenylosuccinate Lyase</i>	<i>ASL</i>	At1g36280	10.7	15.7	-	-
10 <i>AICAR Transformylase/IMP Cyclohydrolase</i>	<i>ATIC</i>	At2g35040	8.2	10.0	-	-
11 <i>Adenylosuccinate Synthase</i>	<i>ASS</i>	At3g57610	Not included in candidate list			
12 <i>Adenylate Kinase 1</i>	<i>AMK1</i>	At2g37250	Not included in candidate list			
12 <i>Adenylate Kinase 2</i>	<i>AMK2</i>	At5g47840	Not included in candidate list			
12 <i>Adenylate Kinase 3</i>	<i>AMK3</i>	At5g50370	Not included in candidate list			
12 <i>Adenylate Kinase 4</i>	<i>AMK4</i>	At5g63400	Not included in candidate list			
12 <i>Adenylate Kinase 5</i>	<i>AMK5</i>	At5g35170	Not included in candidate list			
12 <i>Adenylate Kinase 6</i>	<i>AMK6</i>	At2g39270	Not included in candidate list			
12 <i>Adenylate Kinase 7</i>	<i>AMK7</i>	At3g01820	Not included in candidate list			
13 <i>Brittle 1</i>	<i>BT1</i>	At4g32400	Not included in candidate list			
14 <i>AMP Deaminase</i>	<i>AMPD</i>	At2g38280	Not included in candidate list			
15 <i>IMP Dehydrogenase 1 or 2^b</i>	<i>IMPDH1 or IMPDH2</i>	At1g79470 or At1g16350	19.4	13.6	-2.3	-
16 <i>GMP Synthetase</i>	<i>GMPS</i>	At1g63660	Not included in candidate list			
17 Unknown GMP Phosphatase	?	?	?	?	?	?
18 <i>Guanosine Deaminase</i>	<i>GSDA</i>	At5g28050	2.8	7.0	-	-
19 <i>XMP Phosphatase candidate</i>	<i>XMPP</i>	At2g32150	16.5	60.7	1.8^a	-
20 <i>Complex of</i>						
<i>Nucleoside Hydrolase 1</i>	<i>NSH1</i>	At2g36310	6.8	12.7	-	-
<i>Nucleoside Hydrolase 2</i>	<i>NSH2</i>	At1g05620	3.8	7.5		
21 <i>Xanthine Dehydrogenase</i>	<i>XDH</i>	At4G34890	6.7	4.4		
22 Unknown uric acid transporter	?	?	?	?	?	?
23 <i>Urate Oxidase</i>	<i>UOX</i>	At2g26230	26.4	14.5	4.3 ^a	-
24 <i>Allantoin Synthase</i>	<i>ALNS</i>	At5g58220	8.3	11.0	-	-
25 Unknown allantoin transport process	?	?	?	?	?	?
26 <i>Allantoinase</i>	<i>ALN</i>	At4g04955	40.9	18.3	-	-
27 <i>Allantoate Amidohydrolase</i>	<i>AAH</i>	At4g20070	Not included in candidate list			
28 <i>Ureidoglycine Aminohydrolase</i>	<i>UGlyAH</i>	At4g17050	Not included in candidate list			
29 <i>Ureidoglycolate Amidohydrolase</i>	<i>UAH</i>	At5g43600	Not included in candidate list			
30 Unknown ribose importer	?	?	?	?	?	?
31 <i>Ribokinase</i>	<i>RBSK</i>	At1g17160	3.3	1.5	-	-
32 Potential IMP exporter	?	?	?	?	?	?
33 Unknown IMP Phosphatase	?	?	?	?	?	?

^a The candidate list includes genes induced in nodules of amide-exporting legumes when this induction is at least three times smaller than the induction of the corresponding orthologs in ureide-exporting legumes.

^b It was not possible to distinguish between *IMPDH1* and *IMPDH2* because of the high similarity of the corresponding amino acid sequences.

Triplett *et al.* (1980) and Atkins (1981) concluded according to their feeding experiments using cell-free extracts of soybean and cowpea nodules that ureide biosynthesis involves XMP dephosphorylation. A promising XMPP candidate was found in the candidate list when a group of potential purine and pyrimidine mononucleotide phosphatase genes were compiled in a project characterizing Arabidopsis orthologs of yeast mononucleotide phosphatases *Suppressor of Disruption of TFIS 1 (SDT1)* and *Phosphate Metabolism Gene 8 (PHM8)*; Zhu, 2016). One of these genes showed the expected regulation pattern in legumes with nodule *versus* root fold changes of 16x and 60x in common bean and soybean, respectively. The cDNA of the corresponding Arabidopsis ortholog was transiently expressed in *N. benthamiana* coding for a C-terminally Strep-tagged variant. After subsequent affinity purification, activity of the Arabidopsis XMPP candidate with XMP could be demonstrated by Dr. Marina Varbanova-Herde (not shown). C-terminally Strep-tagged soybean XMPP was produced the same way to assess its activity with XMP. An activity with XMP was observed and the kinetic constants were determined ($K_M = 10.4 \pm 1.5 \mu\text{M}$ and $k_{\text{cat}} = 14 \pm 0.5 \text{ s}^{-1}$, Fig. 5). Following these exciting results, the characterization of the XMPP candidate encoded at the genetic locus Glyma20g144800 in soybean and at locus At2g32150 in Arabidopsis became the focus of this thesis.

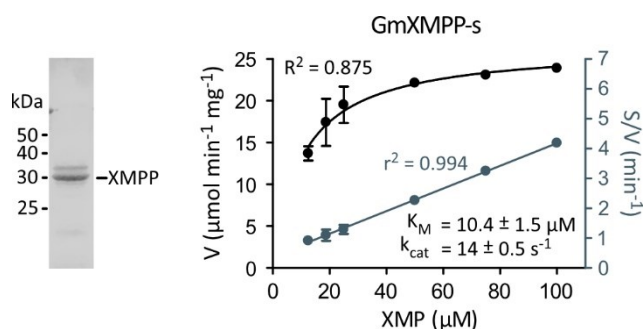


Figure 5 Determination of kinetic constants of the XMPP candidate from soybean. Soybean XMPP with C-terminal hemagglutinin (HA)- and Strep-tags was affinity purified from leaf extracts of *N. benthamiana* after transient expression. Left panel, Coomassie-stained SDS gel with the purified enzyme. Right panel, determination of the kinetic constants with the data fitted according to Michaelis Menten (left axis) or Hanes (right axis). Error bars are SD, $n_t = 3$.

4.2 Establishment of a workflow to examine candidates in soybean root nodules

To characterize the XMPP candidate and for future analysis of other candidates the aim was to establish a system in our laboratory which allowed the production of respective knockout nodules which could be analyzed regarding metabolic changes using liquid chromatography coupled to mass spectrometry (LC-MS). The system developed by Kereszt *et al.* (2007) was adopted to produce *Agrobacterium rhizogenes*-induced transgenic soybean hairy roots. The transfer of bacterial DNA to the plant genome thereby allowed to express genes of interest. Here, genes for the CRISPR-Cas9 machinery and DNA for guide RNAs (gRNAs) were transferred to the plant genome to create null mutants of candidate genes. A *Green Fluorescent Protein (GFP)* expression cassette was also transferred to trace and select successfully transformed hairy roots using fluorescence microscopy.

The overall procedure comprised five steps. First, soybean seeds were germinated under high humidity. Second, five days after sowing, seedlings were infected with *Agrobacterium rhizogenes* by pricking the hypocotyl below the cotyledons with a needle covered with bacteria to induce the

Results

formation of hairy roots. Third, after three weeks the development of transgenic hairy roots was assessed using fluorescence microscopy. Non-fluorescent hairy roots were removed assuming that roots which did not express GFP were not transgenic and did not carry genes encoding the CRISPR-Cas9 machinery. If green-fluorescent roots were developing in close proximity to each other, their number was reduced to ensure that roots could be kept separated. Because each of the hairy root represented an independent transformation event, it was important to keep the roots separated to avoid mixing genetically distinct roots. After the first hairy root selection, plants were inoculated with *Bradyrhizobium japonicus* to produce nodules. Fourth, after additional 2.5 weeks the hairy root development was inspected again to ensure that different transgenic roots were well separated. Fifth, nodules of independent hairy roots were harvested approximately nine weeks after sowing. Also the hairy roots were harvested. The procedure was established and optimized in our laboratory in a total number of 14 experiments to produce transgenic soybean nodules.

4.2.1 Choice of nutrient solution

At first, different commonly known nutrient solutions were tested for the cultivation of soybean cultivar Williams 82. According to previous work with soybean in our laboratory, the plants were grown in Lecaton which allowed to easily access roots for the selection of green-fluorescent roots and for later harvesting. Plants were grown under short-day conditions (12 h day/ 12 h night, 28°C/ 25°C). Six plants per treatment were fertilized weekly with either 200 mL of Broughton and Dilworth (B&D) solution, or modified Hoagland solution adjusted for *Vicia faba* cultivation or Mohammadi nutrient solutions (Tab. 2). The inoculation with *B. japonicus* was performed three weeks after sowing to produce nodules. By then all plants started showing leaf chlorosis likely caused by nitrogen

Table 2 Molar composition of nutrient solutions tested for cultivation of soybean cultivar Williams 82. Mohammadi 1 solution was used before and Mohammadi 2 solution after inoculation with rhizobia.

Element	Concentration (μM)				
	Mohammadi 1 ^a	Mohammadi 2 ^a	Hoagland ^b	B&D ^c	Adjusted B&D
N	2000	0	0	2000 (0) ^d	2000 (0) ^d
Mg	500	500	1000	250	2000
K	550	550	20	3000 (1000) ^d	10250 (8250) ^d
S	518	505	1002	504	3718
P	250	250	20	500	5000
Cl	750	750	3142	2000	201
Na	4	1	0.2	0.2	401
Fe	100	25	5	10	40
Ca	250	250	3140	1000	600
Mn	8	2	2	1	8
Zn	8	2	1	0.5	8
Cu	2	0.5	0.5	2	2
Mo	2	0.5	0.2	0.1	0.4
Co	0	0	0.2	0.1	0.4
Ni	0	0	0.2	0	0.4
B	45	11.5	1	2	8

^a Mohammadi-Dehcheshmeh *et al.* (2014)

^b Thal (2017) adapted from Hoagland and Arnon (1950)

^c Broughton and Dilworth (1971)

^d Nitrogen fertilization with 2 mM KNO₃ was stopped after three weeks when rhizobia were added.



Figure 6 Different nutrient solutions were tested for the cultivation of soybean cultivar Williams 82. Plants were grown under short-day conditions (12 h day/ 12 h night, 28°C/ 25°C) and were fertilized weekly with 200 mL of Broughton and Dilworth (B&D) solution, modified Hoagland solution adjusted for *Vicia faba* cultivation or Mohammadi nutrient solutions for each six plants (Tab. 2). *B. japonicus* were given three weeks after soybeans have been sowed to produce nodules.

Results

deficiency (Fig. 6). The chlorotic phenotype was no longer observed when nitrogen was being produced by symbiotic nitrogen fixation. Soybeans fertilized with the Mohammadi solution took longer to recover from nitrogen deficiency, possibly indicating impaired nodulation or nitrogen fixation. The absence of cobalt and nickel, two micronutrients which are important for soybean growth and nitrogen fixation could be the reason. Cobalt is the essential metal ion for vitamin B12 which is synthesized by rhizobia and which is required to produce leghemoglobin (Reisenhauer, 1960; Evans and Kliewer, 1964). Leghemoglobin is crucial to maintain a low oxygen concentration in infected nodule cells where the oxygen-sensitive dinitrogenase is catalyzing the fixation of atmospheric nitrogen. Nickel is important for the function of Urease and was shown to be beneficial for nitrogen metabolism and nitrogen fixation efficiency although it is not directly required for nitrogen fixation and the metabolism of ureides (Carter *et al.*, 2009; Witte, 2011; Freitas *et al.*, 2019).

Although plants fertilized with modified Hoagland solution performed best five weeks after sowing, being greenest and tallest, the picture was different after seven weeks, when these plants developed severe chlorosis and necrosis at the leaf margins. A comparison of molar concentrations of individual elements in the different nutrient solutions showed that the modified Hoagland solution contained relatively low amounts of potassium (Tab. 2). This might have been the reason for the observed necrosis at the leaf margins, which is a typical potassium deficiency symptom of soybeans. Based on this growth experiment, the B&D solution was chosen for fertilizing soybeans in the following experiments because plants fertilized with the B&D solution showed the best plant performance throughout the seven weeks.

4.2.2 Choice of plant substrate and nutrient concentration

Following the choice of nutrient solution, different substrates were tested for soybean cultivation. The Lecaton used so far is burnt expanded clay which promotes evaporation and has only low water holding capacity due to its porous but rigid nature. These characteristics led to low nutrient availability for the plant and required a high level of maintenance to prevent the roots from drying out. As Lecaton appeared to be unsuitable for soybean cultivation *Nullerde* and Seramis were tested as alternative substrates. *Nullerde* was a 70% white peat and 30% turf mix which was not fertilized by the manufacturer. It was chosen because of its higher water holding capacity and its texture which gives greater support to the roots than the loose Lecaton stones. Seramis is fired clay and its granules are like Lecaton small and rigid. Because of these qualities, it can be easily removed from roots. Unlike Lecaton, Seramis has greater water-holding capacity, which could benefit plants and reduce cultivation effort.

Soybean were grown under short-day conditions (12 h day/ 12 h night, 28°C/ 25°C) and were fertilized weekly with 15 mL of B&D solution per plant. Different concentrations of B&D solution were tested (1x, 2x, 4x, 10x). Five days after sowing seedlings were infected with *A. rhizogenes* carrying the empty control vector lacking gRNAs. After 19 days seedling roots were inoculated with *B. japonicus* to produce nodules. The comparison of substrates showed that Lecaton was especially prone to water loss as water quickly ran off the pots and evaporated from the granules. In comparison to the other substrates, plants in Lecaton were exposed to high fluctuations in wetting with the nutrient solution. These unstable conditions reduced plant performance which was characterized by limp and chlorotic leaves (Fig. 7). Plants grown in *Nullerde* also showed leaf chlorosis especially affecting the old leaves. With the 4x fertilizer concentration, these symptoms were alleviated indicating that nutrients of the

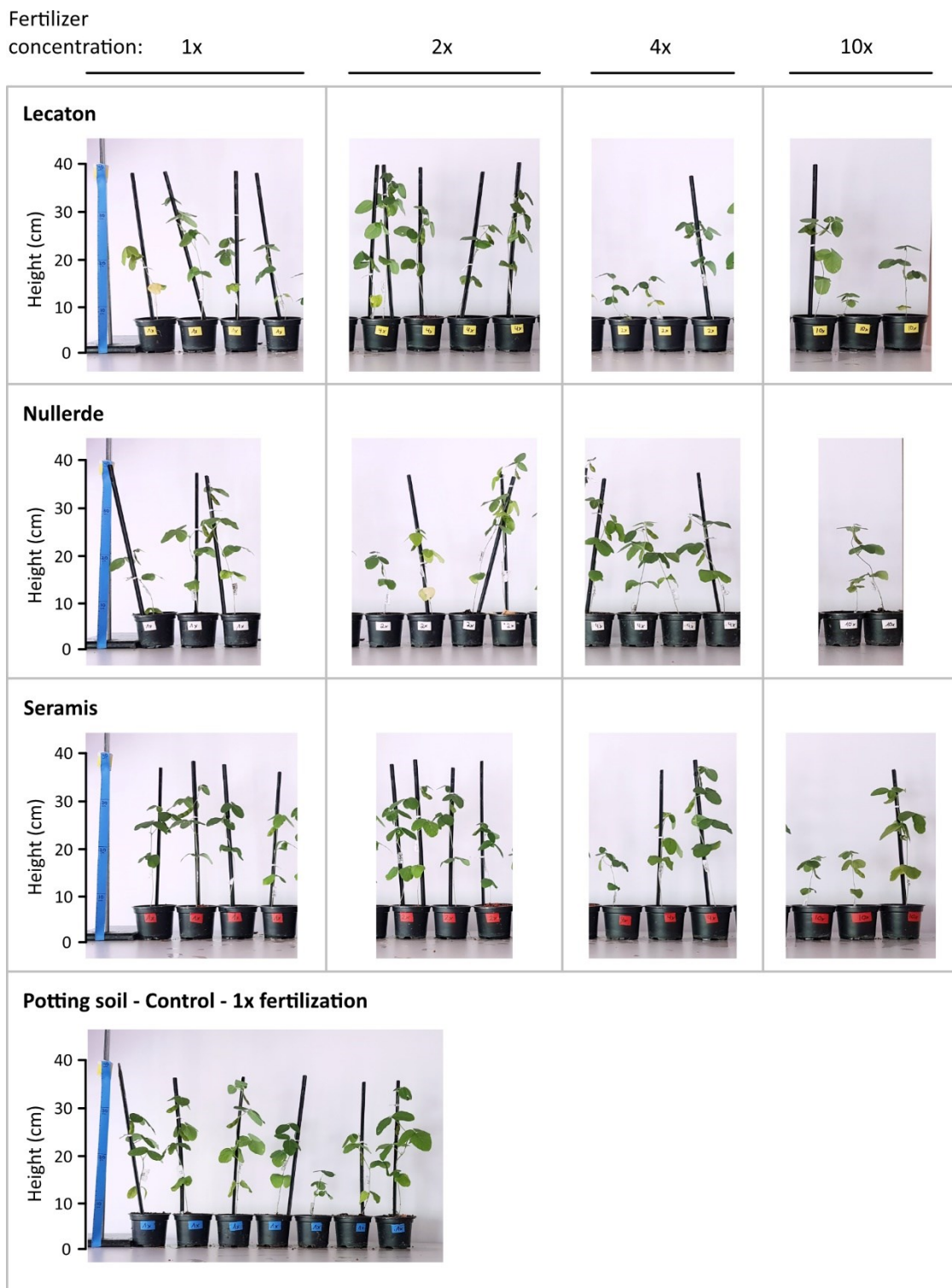


Figure 7 Lecaton, Seramis and Nullerde were tested for their suitability to grow soybean for the production of transgenic nodules. Potting soil was included for comparison. Different concentrations of B&D solutions were tested (1x, 2x, 4x, 10x). Plants were grown under short-day conditions (12h day/ 12h night, 28°C/ 25°C) and were fertilized weekly with 15 mL of B&D solution per plant. Five days after sowing seedlings were infected with *A. rhizogenes* carrying the empty control vector to produce hairy roots. After 19 days seedling roots were inoculated with *B. japonicus* to produce nodules.

fertilizer solution may have been adsorbed by soil particles. The plants grown in *Nullerde* and fertilized with 4x B&D solution performed similar to the control plants in potting soil. However, due to two major drawbacks, *Nullerde* was excluded as growth substrate. First, *Nullerde* may vary significantly in nutrient concentration and soil composition depending on the lot which can affect nutrient availability and negatively affect reproducibility of experiments. Second, the older the plants were the harder it became to remove the *Nullerde* from the roots. As the root development was assessed twice before the hairy roots were finally harvested, they needed to be easily accessible and cleanable.

Seramis combined the two most important aspects. It could be easily removed from roots and showed high water holding capacity. Plants grown in Seramis and fertilized by 2x B&D nutrient solution were the biggest and apparently greenest and strongest plants and performed similar to control plants in potting soil. Thus, Seramis and 2x nutrient solution were chosen for further experiments.

4.2.3 Further improvements were made for the production of transgenic nodules

In the course of multiple experiments conducted using Seramis and B&D solution, adjustments regarding several aspects of plant cultivation were made. An adaption regarding the light regime was to extend the day length. Soybeans are short day plants and increased day length was shown to delay flowering and extend the plant life cycle (Cao *et al.*, 2017). Because the production of transgenic nodules required about nine weeks, it was beneficial to extend the life cycle of the plant, thus delaying the late life cycle-dependent reduction in nitrogen fixation rate and nodule senescence (Nelson *et al.*, 1984). The light regime was changed from 12 h day/ 12 h night to 14 h day/ 10 h night.

Also the infection process of soybean seedlings with *A. rhizogenes* was optimized. One aspect was that the hypocotyl of the five days old seedlings was completely pierced. Hairy roots emerging on both sides of the hypocotyl could be kept separated easily. A crucial factor for successful hairy root development was how seedlings were cultivated after infection with *A. rhizogenes*. For this two procedures were described by Kereszt *et al.* (2007). According to the first one, the infection site was kept above the substrate before plants were separated to individual pots. For this, seedlings were grown in a mini-greenhouse under a sealed lid to ensure high humidity. The high humidity however favored fungal growth so that soybean batches were sometimes severely affected by fungal contaminations. Moreover, the plants exhibited fast and elongated growth under these conditions so that their leaves had touched the lid even before the hairy roots started emerging. When the hairy roots were about 1 cm in length, the high humidity was gradually decreased to separate the plants in individual pots. Although the humidity was slowly reduced over days, the unifoliate leaves suffered severely from the reduced humidity and developed necrosis and eventually died. Because of these problems, the second approach was tested which excluded the high humidity phase by directly moving the infection site below the Seramis surface. After the infection, plants were directly transferred to single pots and the seedlings were moved so deep into the substrate that only the tips of the cotyledons reached the surface. The cotyledons with their thick wax layer were tolerant towards the drastic humidity loss. Over the next days, plants were controlled twice a day and more Seramis was added to the pots when infection sites had moved out of the substrate by plant growth. Hairy roots developed well in the substrate and especially the unifoliate leaves benefitted from the stable humidity after the infection.

Another change concerned the original soybean roots. In the first experiments, original roots were removed to grow plants on hairy roots only. This was thought to avoid nodule development at the

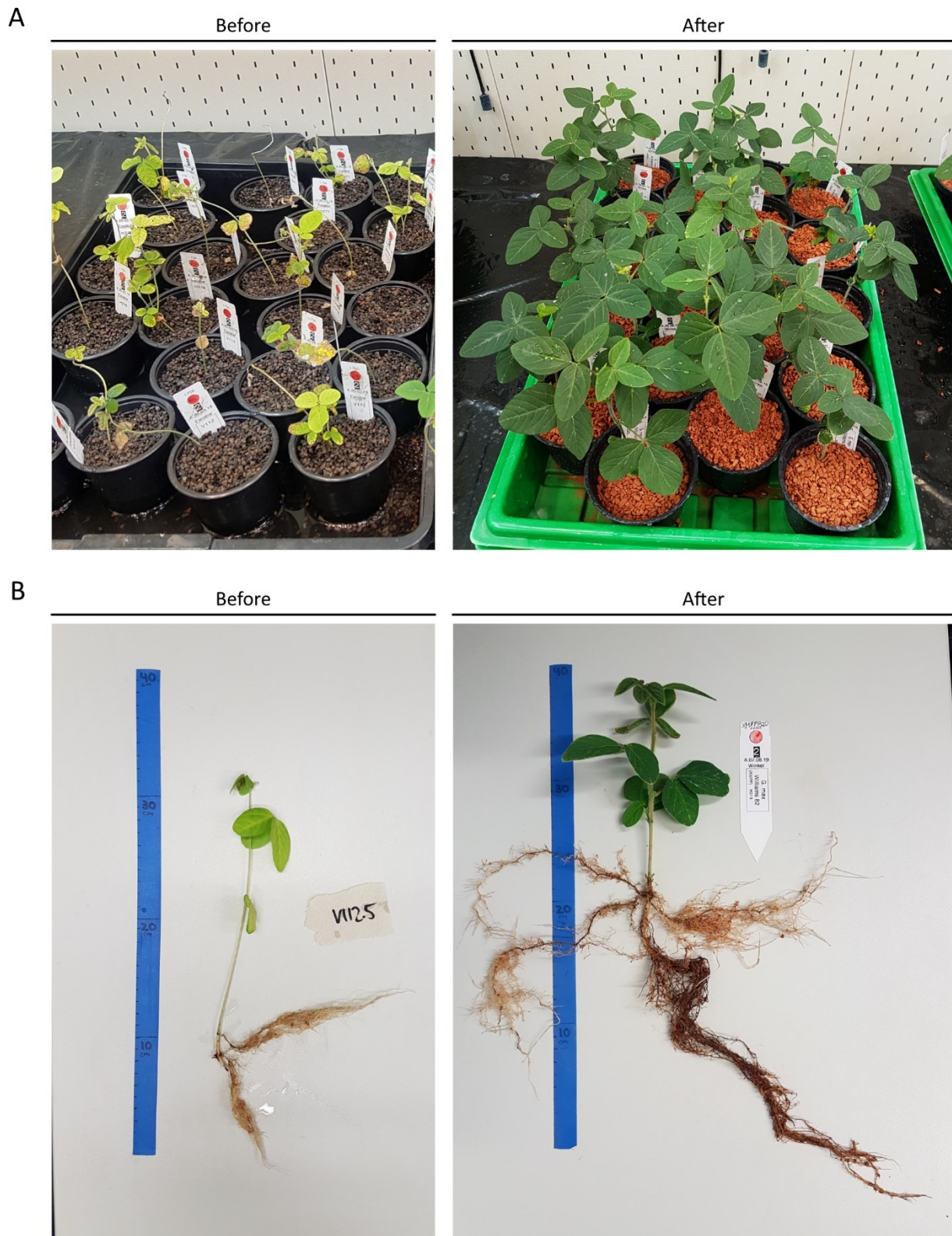


Figure 8 Illustration of the optimization success in soybean cultivation. Exemplary pictures of soybean plants before and after the optimization. **A**, Seven weeks after sowing. **B**, Ten (left) and eleven (right) weeks after sowing. Details on the changes of the cultivation parameters can be found in the text. Five days after sowing, seedlings were infected with *A. rhizogenes* carrying the empty control vector to produce hairy roots. After three weeks, seedlings were inoculated with *B. japonicus* to produce nodules.

Results

original roots which might have hampered nodulation of the transgenic roots (Kereszt *et al.*, 2007). The sudden cut in water and nutrient uptake and possibly also wounding-related stress responses however adversely affected plant performance. Plants quickly turned yellow and limp. In experiments in which original roots were retained, plant growth proceeded undisturbed and enough nodules formed at the transgenic hairy roots. Also flowering was further delayed by retaining the original roots. Removal of the original roots accelerated flowering, possibly caused by a stress response.

Due to the increase of day length, the optimization of the infection process and the decision to keep the original roots, plant growth was considerably improved. The increased growth however required again an adaption of the fertilizer (Tab. 2, 4). Besides the composition of the nutrient solution also application intervals were changed. Instead of fertilizing once a week, plants were fertilized three times a week with B&D solution to stabilize nutrient availability. Soybeans were watered from above before the application of the nutrient solution to avoid drainage of the nutrients. At the end of each week, trays were flushed with water to remove excess nutrients to prevent potentially toxic nutrient accumulations. In summary, the cultivation of soybean hairy roots and nodule development could be considerably improved by the described experiments (Fig. 8).

4.3 Characterization of the XMPP candidate, GSDA and XDH in nodules

To assess the possible biological function of the XMPP candidate in XMP degradation in nodules, *XMPP* knockout nodules needed to be generated. Such nodules should show an accumulation of XMP and a reduction of ureide production, if the XMPP candidate is indeed involved in their biosynthesis. The comparative transcriptome analysis showed that *GMP Synthetase (GMPS)* expression is not induced in nodules compared to roots of ureide exporting legumes suggesting that GMP biosynthesis and degradation are likely not involved in ureide biosynthesis. To also test this hypothesis, the generation of *GSDA* knockout nodules was intended. If *GSDA* knockout nodules would still produce ureides and would only accumulate minor amounts of guanosine, the involvement of the route via GMPS could be excluded. As positive control, *XDH* was also targeted for knockout. *XDH* is located downstream of *GSDA* and *XMPP* in the linear section of the ureide biosynthesis pathway and Arabidopsis *XDH* mutants and common bean *XDH* RNA interference nodules were shown to be impaired in ureide biosynthesis (Brychkova *et al.*, 2008; Coletto *et al.*, 2019). Thus, a successful knockout of *XDH* in soybean nodules was expected to cause the breakdown of ureide production (Fig. 4).

The CRISPR constructs used in this thesis were based on CRISPR-Cas9 technology and differed only in the gRNA sequences. For the generation of CRISPR constructs, it had to be considered that soybean is an ancient polyploid. Its genome underwent two duplications approximately 59 and 13 million years ago and was subjected to differentiations and losses of genes over time (Schmutz *et al.*, 2010). These duplications are the reason for the occurrence of two paralogs of *XMPP* and *XDH* each and even five of *GSDA* in the soybean genome. For the production of *XMPP*, *GSDA* and *XDH* knockout nodules, three CRISPR constructs were generated. With the *XMPP* CRISPR construct both *XMPP* paralogs were targeted. The transcriptionally regulated *XMPP* candidate retrieved from the candidate list and its non-regulated paralog were named *XMPP2* and *XMPP1* according to their location on the 20th and 10th chromosome, respectively. During the work with the RNAseq data, it was found that the 5' end of *XMPP1* was not covered by RNAseq reads which was caused by a gap in the genome sequence. This region was cloned and sequenced, revealing a new ATG codon and a potential splicing site. The combination of both new gene features resulted in a 5' coding sequence that was similar to that of the

regulated paralog *XMPP2* (Fig. A - 1). RNAseq reads were mapped against the corrected genome sequence validating the expression of the corrected *XMPP1* in its full length. The CRISPR construct generated to target *XMPP* encoded three gRNAs of which one was specific for *XMPP1*, one was specific for *XMPP2* and one was targeting both paralogs. The CRISPR construct directed against the *XDH* encoded four gRNAs, of which two targeted each one paralog. Although the expression of only each one of the two *XMPP* and *XDH* paralogs were regulated in the expected fashion, both paralogs were targeted to avoid that the not regulated gene may compensate the loss of the regulated one. Two of the five *GSDA* paralogs were not considered in the *GSDA*-specific CRISPR approach because according to the RNAseq data they were not transcribed in roots or nodules. The CRISPR construct directed against *GSDA* comprised five gRNAs so that each of the three considered paralogs was targeted by two gRNAs each. The binary vector without the coding region for gRNAs was used for the production of control nodules.

Because a method to detect CRISPR mutations in the hairy root system had not yet been established in our laboratory, nodule morphology and changes in metabolite concentrations corresponding to the aimed gene knockouts were initially assessed without knowing whether the nodules carried a mutation or not. Cross sections of nodules from 24, 14, 55 and 19 independent control, *XMPP* CRISPR, *GSDA* CRISPR and *XDH* CRISPR hairy roots were prepared, respectively. All *XMPP* CRISPR and *GSDA* CRISPR nodules were similar to the control nodules, whereas many *XDH* CRISPR nodules showed a compromised nodule morphology (Fig. 9A). Many *XDH* CRISPR nodules were smaller in size and had a soft texture (Fig. 9B). When these nodules were cut open they showed a green colored infection zone which is normally red due to the leghemoglobin (Fig. 9C). In cross sections many *XDH* CRISPR nodules showed elongated and misshaped vascular bundles (Fig. 9A). Curiously, black spots were observed in non-infected cells of the infection zone and the inner nodule cortex. *XDH* mutant nodules probably accumulate xanthine, thus it was suspected that the optically dense deposits might represent xanthine crystals. Such crystals were detected in *XDH* mutants of *Arabidopsis* and were shown to emit fluorescence upon excitement Ma *et al.* (2016). Consistently, the objects observed here were fluorescent (Fig. 9E). To exclude that the fluorescence was caused by the co-expressed GFP, the crystals were excited with light of 551 nm wavelength using a confocal laser scanning microscope. Light of this wavelength has too little energy to excite GFP with an excitation maximum at 488 nm. Eventually, the appearance of the crystals could be correlated with the accumulation of xanthine in the corresponding nodules (Fig. 9D).

Interestingly, xanthine crystals were primarily observed in uninfected cells of the infection zone and in the inner cortex. This strongly suggests that xanthine is either formed in or exported into the uninfected cells challenging the long-standing assumption that uric acid is the exported intermediate (Vaughn *et al.*, 1982; Shelp *et al.*, 1983; Smith and Atkins, 2002). Metabolite analysis was performed with 45 *XDH* CRISPR nodule pools which could be divided into three groups. Group I showed xanthine accumulation with coinciding block of ureide biosynthesis, group II showed xanthine accumulation while ureide production was partially compromised, and group III did not accumulate xanthine and produced ureides (Fig. 10). It is interesting to note that the average xanthine accumulation of group I *XDH* CRISPR nodules was $46 \mu\text{mol g}^{-1} \text{DW}$, whereas the corresponding average hypoxanthine concentration was only $0.022 \mu\text{mol g}^{-1} \text{DW}$ (not shown). Hypoxanthine and xanthine are both substrates of *XDH*. The fact that only xanthine is accumulating to high amounts demonstrates that the IMP – inosine – hypoxanthine route is not involved in ureide biosynthesis which is in contrast to some earlier reports postulating that IMP dephosphorylation is involved (Chapter 3.5). Based on the metabolite data, conclusions were drawn about the efficiency of the *XDH* CRISPR approach. Assuming that xanthine accumulation coinciding with a complete block of ureide biosynthesis is indicating that all alleles of both *XDH* paralogs were successfully mutated, the metabolite data suggest a frequency of

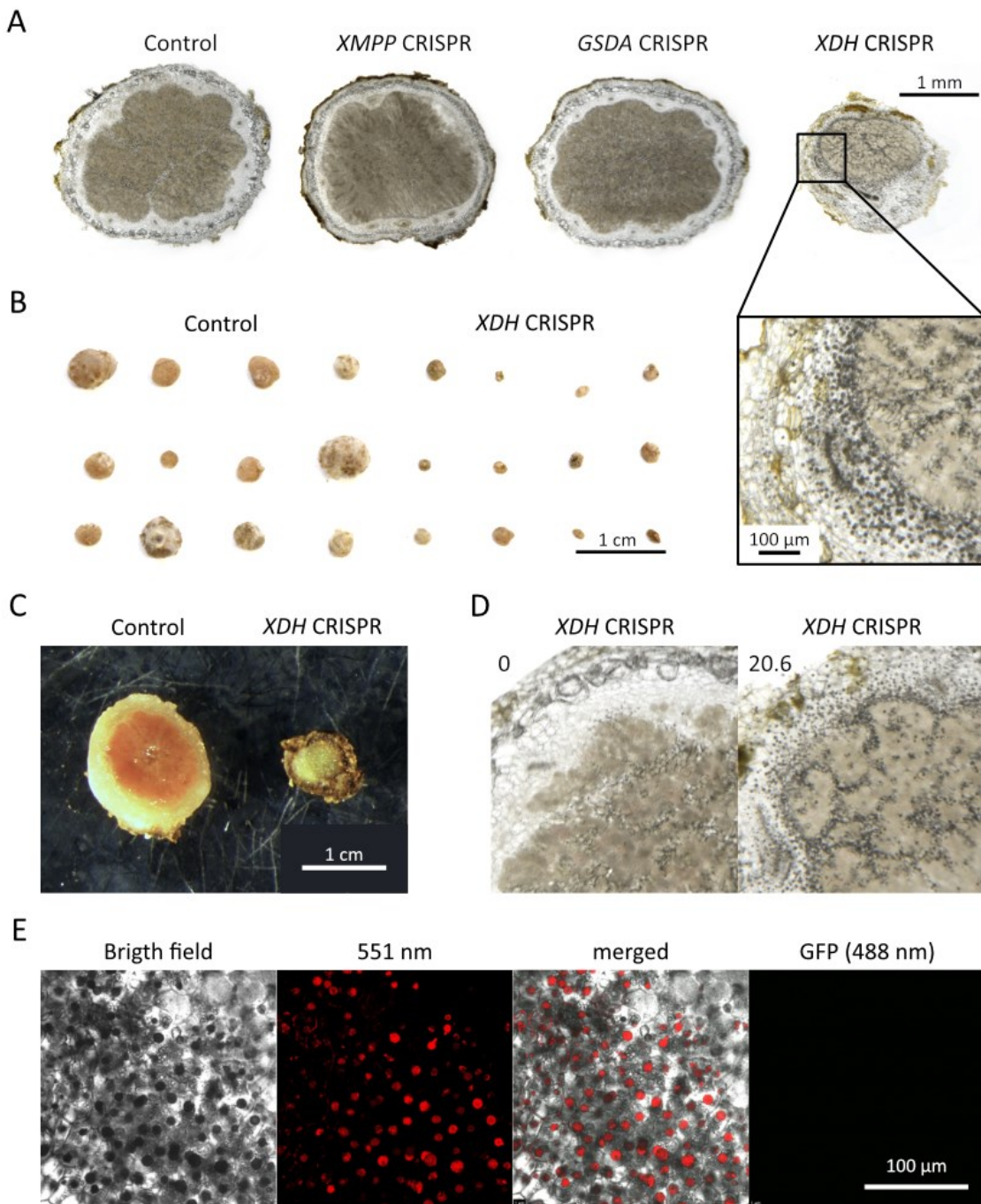


Figure 9 Assessment of the morphology of *XMPP* CRISPR, *GSDA* CRISPR and *XDH* CRISPR nodules. **A**, Representative nodule sections. **B**, Size comparison of control and *XDH* CRISPR nodules. **C**, Representative picture of control and *XDH* CRISPR nodules cut open. **D**, Black spots correlate with xanthine accumulation of *XDH* CRISPR nodules shown in upper left corner in $\mu\text{mol g}^{-1}$ DW. **E**, Optically dense objects can emit fluorescence which is not caused by the co-expressed GFP.

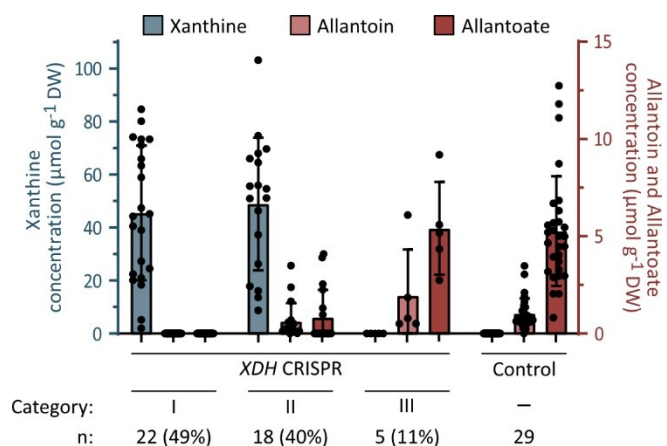


Figure 10 Quantification of xanthine, allantoin and allantoate concentrations in *XDH* CRISPR and control nodules. Nodule pools used for metabolite analysis were categorized according to their metabolite profile: I) Xanthine accumulation and breakdown of ureide production, II) Xanthine accumulation and remaining ureide production, III) No xanthine accumulation and ureide concentrations similar to control nodules. Control nodules were harvested from hairy roots transformed with the empty CRISPR vector. Error bars are SD, numbers of analyzed independent nodule pools are stated below the category in absolute numbers and relative to the total number of nodule pools in parentheses.

49% for this event. This indicates that a CRISPR mutation approach can be successfully used in hairy roots of soybean. Only for about 11% of the nodules the *XDH* CRISPR approach was not effective at all as they did not accumulate xanthine and showed ureide concentrations similar to the control. The genetic evaluation of CRISPR events by fragment length analysis (FLA) was established in parallel but due to time limitations it could not be used for the genetic characterization of these nodule pools.

GSDA CRISPR nodules showed neither an altered nodule morphology nor altered metabolite concentrations. The 63 analyzed *GSDA* CRISPR nodule pools were not different from the control nodules and neither accumulated guanosine nor showed a reduction of ureide content (not shown). Also here no genetic information was available to judge whether the mutation of the *GSDAs* was successful. Thus it could not be clarified whether the absence of guanosine accumulation was observed because the GMP – guanosine route is not part of ureide biosynthesis or because the *GSDA* CRISPR mutations were not successful.

The main focus of this study lay on the functional characterization of the XMPP candidate. Fourteen nodules of independent hairy roots were sectioned to assess their morphology. None of the nodules showed any morphological changes. In the metabolite analysis a total of 58 nodule pools of independent *XMPP* CRISPR hairy roots were analyzed. Interestingly, three nodule pools accumulated 17.4, 23.6 and 148.8 nmol g⁻¹ DW XMP indicating that the dephosphorylation of XMP by the XMPP candidate is part of the ureide biosynthesis (not shown). However, these nodule pools did not show any reduction of the ureide pool sizes. Preliminary data from the establishment of a detection method for CRISPR-mediated gene knockouts by FLA indicated that *CRISPR* efficiency was very low for the regulated paralog *XMPP2*. The three XMP-accumulating nodule pools may have thus been rare cases in which at least some but maybe not all alleles of *XMPP2* were knocked out.

The FLA using a capillary sequencer was established for the detection of small length alterations in the *XMPP1* and *XMPP2* genes. This approach is based on the fact that CRISPR-*Cas9*-mediated double strand breaks are repaired by an error-prone mechanism called non-homologous end joining (NHEJ). During the process of NHEJ, base pairs are deleted or inserted which alter the original DNA sequence. By the amplification of the corresponding DNA fragment with primers spanning the editing site, the number of nucleotides that are deleted or inserted in this DNA fragment can be determined in

Results

comparison with a fragment of wild-type size (Fig. A - 2). For this, dye-labelled PCR fragments of about 200 - 250 bp covering the gRNA binding sites can be amplified from control and *XMPP* CRISPR nodule DNA. The same homogenized freeze-dried nodule pools that were used for metabolite analysis could be used for FLA. Due to the laborious generation of nodule material, hairy roots were used instead of nodules to establish FLA. PCR fragments from control DNA were labelled with a different dye so that PCR fragments from control and *XMPP* CRISPR nodule pools could be analyzed in the same capillary electrophoresis run. If a peak derived from the *XMPP* CRISPR nodule overlapped with the wild-type peak in the chromatogram, at least one wild-type allele must have been present in the *XMPP* CRISPR sample. If in contrast peaks from *XMPP* CRISPR samples were not overlapping with the wild-type peak of the control sample, a successful CRISPR knockout of the respective gene across all four alleles was detected. The number of nucleotides which were inserted or deleted by NHEJ had to be different to three or a multiple of three to be sure that a frame shift had occurred preventing the expression of a functional protein. This approach allowed the identification of hairy roots with successful gene knockouts which was so far not possible for tetraploid soybean.

For the detection of *XMPP* CRISPR knockout mutations four primer sets were used, which were designed to amplify fragments including each one gRNA binding sites in a paralog-specific manner (Fig. 11). This specificity allowed to detect potential CRISPR events for each paralog and binding site individually and excluded the risk that wild-type sequences of the not targeted paralog would lead to false negative results. In an initial attempt to estimate the CRISPR efficiency of the *XMPP* CRISPR guides, 18 hairy roots were analyzed. Unfortunately, neither for gRNA 1 targeting *XMPP1* nor for gRNA 2 targeting *XMPP2* mutation was efficient. *XMPP1* gRNA 1 led to CRISPR events in two hairy roots that resulted in fragments with altered size in addition to the wild-type fragment that was still present. For gRNA 2 targeting *XMPP2* no CRISPR events could be detected. By contrast, gRNA 3 which was binding to both paralogs, led in 28% of samples to a complete tetra-allelic knockout of *XMPP1* by frame shifts. Despite the high efficiency for targeting *XMPP1*, the shared gRNA 3 did surprisingly not lead to any size alterations of the corresponding *XMPP2* fragment, although the sequences of the two paralogs surrounding the gRNA binding sites are almost identical (Fig. A - 1). Possible reasons for the different

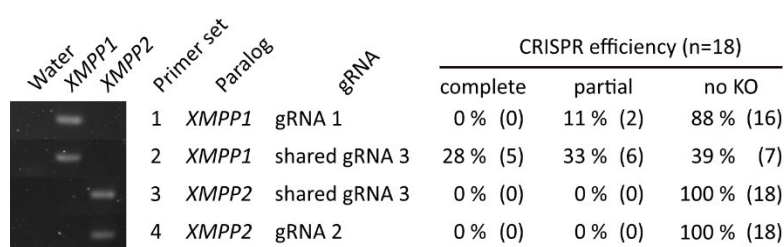


Figure 11 Assessment of knockout rates in *XMPP* CRISPR nodules. Fragment length analysis was used to identify hairy roots with knockout mutations in *XMPP2* from the candidate list and its paralog *XMPP1*. Each paralog was targeted by each one individual gRNA and one gRNA that targeted both paralogs. Left panel, Primers were designed to amplify fragments which were specific for each gRNA binding site and paralog. Right panel, CRISPR efficiency was evaluated for each gRNA binding site by comparing the length of fragments amplified from *XMPP* CRISPR hairy root and wild-type DNA. Differences in fragment sizes were determined in the same capillary sequencing run (Fig. A - 2). If the *XMPP* CRISPR sample showed no fragment of wild-type size but one or more additional peaks the sample was counted as complete knockout of all alleles. If the *XMPP* CRISPR sample showed the same peak in the size chromatogram as the control fragment and showed one or more additional peaks, it was counted as “partial” knockout. If the *XMPP* CRISPR sample showed only the peak of wild-type size, the sample was count as “no KO” (KO = knockout).

knockout rates of 28% for *XMPP1* and 0% for *XMPP2* could be genome features. Cis- and trans-elements regulating *XMPP2* transcription may impair the accessibility of the CRISPR machinery to the gene. Another often discussed factor is the packaging of a gene in heterochromatin. However, the expression of both paralogs is similarly high in roots which makes a packaging of *XMPP2* in tightly packed heterochromatin unlikely. The reason for the different knockout rates induced by the shared gRNA 3 remains unknown. The genetic complexity of soybean complicated the generation of CRISPR-Cas9-induced knockouts and their detection. This together with the complexity of the pathway under investigation, led to the conclusion that an easier biological system would be required to address the open questions. Therefore, work on common bean was initiated, which is only diploid facilitating genetic manipulation.

4.3.1 Characterization of the XMPP candidate and XDH in nodules of common bean

The lower ploidy compared to soybean was expected to increase the number of CRISPR-mediated complete knockouts as only two instead of four alleles per gene needed to be mutated. Additionally, common bean possesses only one copy each of *XMPP* and *XDH*. For these reasons, it was also simpler to detect CRISPR mutations which could be assessed by FLA or even commercial sequencing. Furthermore, an *in vitro* test system for gRNAs had been established at that time in our laboratory. This allowed to select gRNAs, that function *in vitro*, thereby increasing the chance to successfully knockout *XMPP* and *XDH* in common bean (Foresti, 2020). *XMPP* and *XDH* CRISPR constructs were designed to target the respective genes with one gRNA. It was found that the common bean *XMPP* was not correctly annotated in the Phytozome database. The RNAseq data showed that most of the first annotated exon was not covered by reads at the 5' end, whereas the 3' region was. The correct start codon was located, which was in frame with the wrongly annotated start codon further upstream. The corrected coding sequence (Fig. A - 3) is similar to the ones of the soybean and Arabidopsis homologs.

Based on soybean expertise gained here, Luisa Voß established the cultivation of common bean. Guide RNAs were selected and tested by William Foresti and Luisa Voß. Transgenic hairy roots and nodules were produced as previously described for soybean. Using FLA performed by Luisa Voß, it was shown that of the 13 *XMPP* CRISPR nodule pools, nodules of four pools (31%) carried biallelic knockouts due to frame shifts or deletions of at least 24 bp (Fig. 12C). Nodules of five pools (38 %) showed CRISPR events but still contained a fragment of wild-type size or showed in-frame deletions of 3 bp or 6 bp. Nodules of four pools (31%) were not affected by CRISPR targeting and showed only fragments of wild-type size. Ten nodule pools were analyzed to evaluate the mutation success in the *XDH* CRISPR nodules. Nodules of five pools (50 %) did not show any CRISPR event, whereas nodules of three (30 %) and two (20 %) pools carried a complete biallelic or only a monoallelic knockout, respectively.

Extracts of nodule pools of the control group and confirmed *xdh* and *xmpp* nodules were analyzed by LC-MS. As observed for the putative soybean *xdh* nodules, also common bean *xdh* nodules accumulated xanthine and showed a breakdown of ureide production (Fig. 12A). The absence of hypoxanthine accumulation in *xdh* nodules could be reproduced as well. The average xanthine concentration was 21 $\mu\text{mol g}^{-1}$ DW, whereas the average hypoxanthine concentration was 0.011 $\mu\text{mol g}^{-1}$ DW (not shown). Similar to the three XMP-accumulating soybean *XMPP* CRISPR nodule pools, common bean *xmpp* nodules showed XMP accumulation, which also did not coincide with a complete breakdown of ureide biosynthesis. However, in comparison with the control nodules, average allantoin and allantoate concentrations of *xmpp* nodules were reduced by about 51% and 57%, respectively. The statistical analysis showed that due to the low replicate number and the high concentration

Results

variability, only for the allantoin concentration the difference between the wild type and the *XMPP* mutant reached a p value below 0.05.

Interestingly, guanosine concentration was increased in *xmpp* nodules although there was no genetic block of *GSDA*. This indicates, that XMP, which cannot be directly dephosphorylated due to the lack of XMPP activity, is converted via GMP to guanosine and in such amounts that the guanosine pool is increased threefold in comparison to the wild type. As a consequence also the guanine concentration is elevated in this situation (Fig. 12B). This overflow to GMP and guanosine is a plausible explanation for the only moderate effect of the loss of XMPP on the ureide pools because *GSDA* deaminates guanosine to xanthosine from which ureides can be synthesized. The data indicate that the GMP –

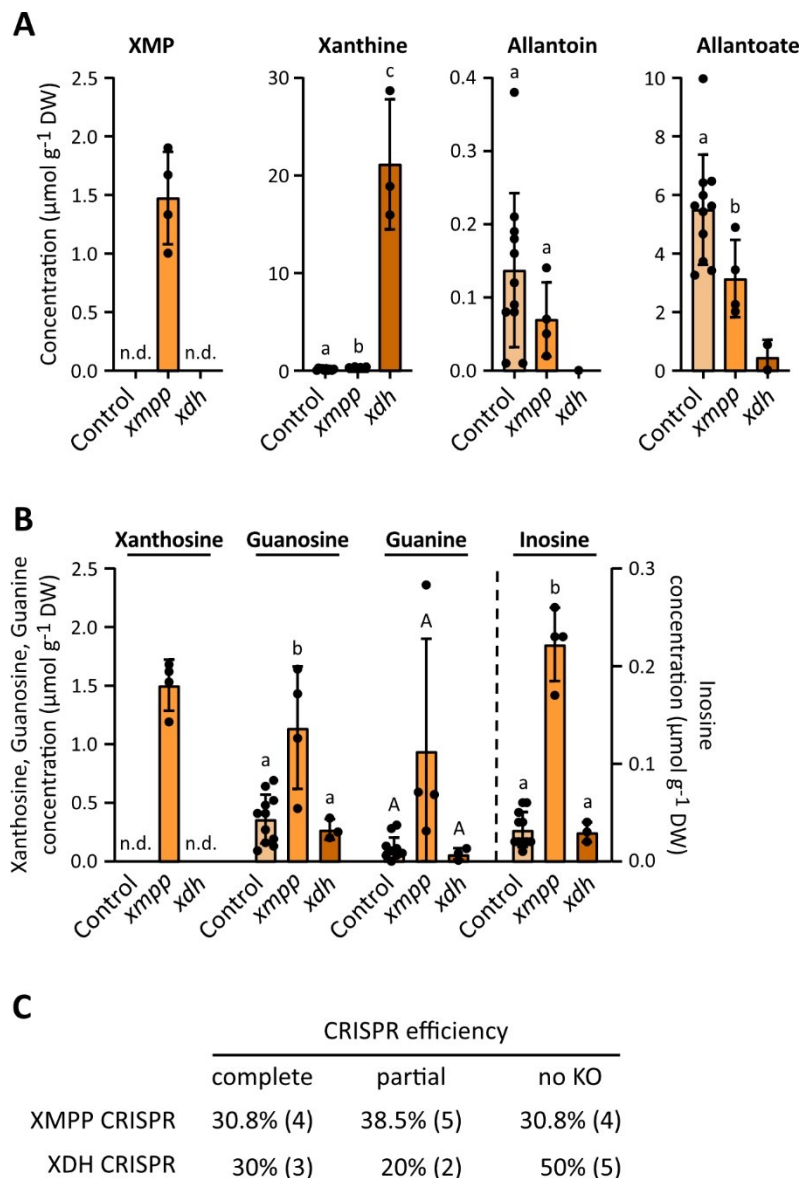


Figure 12 Analysis of *xmpp* and *xdh* nodules of common bean. **A**, Quantification of XMP, xanthine, allantoin and allantoate in extracts of control, *xmpp* and *xdh* nodules. **B**, Quantification of xanthosine, guanosine, guanine and inosine in extracts of control, *xmpp* and *xdh* nodules. For A and B, error bars are SD, n = 11 for control, n = 4 for *xmpp* and n = 3 for *xdh* nodules. Measurements not matching quality criteria (Chapter 7.8) were called not detected (“n.d”) and are not shown. Only groups with at least three valid measurements were included in statistical analysis. Different letters indicate p values < 0.05. For statistical analysis two-sided Tukey’s pairwise comparisons using the sandwich variance estimator were performed for each metabolite individually, indicated by big and small letters. **C**, Evaluation of CRISPR efficiency. Each gene was targeted by one gRNA. Categories “complete”, “partial” and “no KO” are described in Fig. 11. Generation of plant material and fragment length analysis for the identification of nodule pools with successful gene knockouts were performed by Luisa Voß.

guanosine – xanthosine route has not enough capacity to fully maintain ureide biosynthesis when XMPP activity is compromised. This is further underpinned by the observation that the XMP backlog in *xmpp* nodules led to more inosine. Inosine was likely derived from IMP, which was however not quantified. Note, inosine accumulation is relatively small in comparison to guanosine concentration suggesting that the GMP – guanosine route is the major route compensating the loss of XMPP. In summary, these findings demonstrate that the dephosphorylation of XMP by XMPP is an important reaction for ureide biosynthesis. Surprisingly, also xanthosine increased in *xmpp* nodules to a similar concentration as XMP. It is unexpected that the product of an enzyme accumulates when its expression has been genetically blocked. A possible explanation is the partial inhibition of the NSH1/2 heterocomplex in *xmpp* nodules. This could be mediated by XMP, guanosine or inosine, which all accumulate in this genetic background.

Finally, I would like to summarize the achievements of the work with soybean and common bean and the conclusions that were drawn.

Regarding the production of transgenic nodules:

- I) The cultivation of soybean was optimized.
- II) Key factors for the production of transgenic nodules were identified.
- III) It was demonstrated that FLA can be used for the identification of knockout nodules.
- IV) The metabolite analysis of *XDH* CRISPR nodules demonstrated that the soybean pipeline can in principle be successfully used.
- V) Because of the high ploidy level of soybean the generation and detection of complete knockouts was difficult. The analysis was further complicated by compensatory reactions reducing the metabolic effects of the introduced genetic defects. Therefore, it was not possible to conclusively show the roles of XMPP and GSDA in soybean nodules.
- VI) Diploid common bean poses a genetically simpler alternative.

Regarding the analysis of transgenic nodules from soybean and common bean:

- I) The knockout of *XDH* completely abolishes ureide production and causes xanthine accumulation.
- II) Soybean *XDH* CRISPR nodules form xanthine crystals that occur exclusively in uninfected cells.
- III) The knockout of *XDH* does not lead to hypoxanthine accumulation showing that the IMP – inosine – hypoxanthine route is not involved in ureide biosynthesis.
- IV) Loss of XMPP can partly be compensated by the GMP – guanosine route.

In vitro substrate screens revealed that SDTL2 to 4 are pyrimidine-specific phosphatases (Zhu, 2016). For SDTL1, the XMPP candidate, activity with various purine and pyrimidine mononucleotides was tested at that time but no activity was observed. However, XMP dephosphorylation was not tested because direct xanthosine production from XMP was considered to be irrelevant *in vivo*, based on previous work that had demonstrated that purine catabolism exclusively proceeds through GMP biosynthesis and degradation in *Arabidopsis* (Dahncke and Witte, 2013). This view was strengthened by metabolite analysis of the corresponding *XMPP* mutant, in which no effects on XMP or xanthosine concentrations *in vivo* were observed. Nevertheless, in the course of the work with the SDTL proteins also XMPP was partially characterized. The subcellular protein localization of XMPP-YFP fusion protein was determined by fluorescence microscopy after transient expression in *N. benthamiana* (Zhu, 2016). XMPP-YFP was shown to localize in the nucleus and the cytosol. IMP Dehydrogenases (IMPDHs), that generate XMP and GMP Synthetase (GMPS) that uses XMP as substrate to produce GMP are also located in the cytosol as are Guanosine Deaminase (GSDA), and the Nucleoside Hydrolase Heterocomplex (NSH1/2; Witte and Herde, 2020).

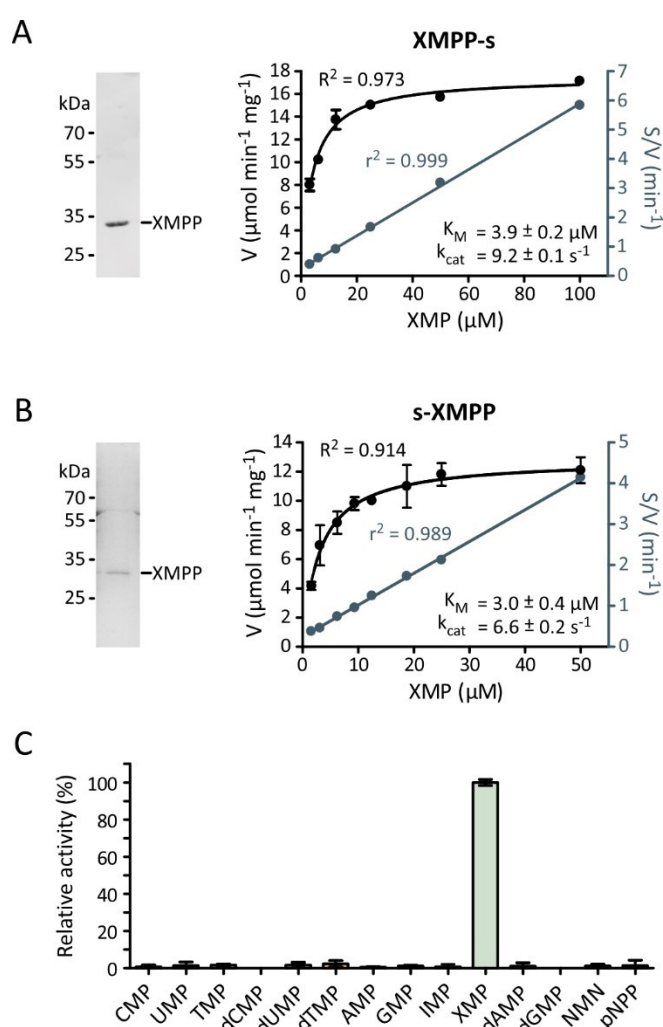


Figure 14 Determination of kinetic constants and substrate specificity of XMPP. **A**, XMPP-HASTrep (XMPP-s) affinity purified from leaf extracts of *N. benthamiana* after transient expression. Left panel, Coomassie-stained SDS-gel with the purified enzyme. Right panel, determination of the kinetic constants with the data fitted according to Michaelis Menten (left axis) or Hanes (right axis). Error bars are SD, $n_t = 3$. **B**, as **A** but with Strep-XMPP (s-XMPP) protein. **C**, Relative enzymatic activity of XMPP-s with 100 μM (deoxy)mononucleotides including nicotinamide mononucleotide (NMN) and the general phosphatase substrate paranitrophenyl phosphate (pNPP). Error bars are SD, $n_t = 3$. An XMP conversion rate of $12.1 \pm 0.2 \mu\text{mol mg}^{-1} \text{ min}^{-1}$ was set to 100%.

Results

In the course of this thesis, cDNAs of Arabidopsis *XMPP* were transiently expressed in *N. benthamiana* leaves to produce C- or N-terminally Strep-tagged variants. Upon Strep-Tactin-based affinity purification, enzyme kinetic constants with XMP as substrate were determined. Both *XMPP* variants showed similar kinetic behavior with a K_M of 3.9 μM and 3.0 μM and k_{cat} of 9.2 s^{-1} and 6.6 s^{-1} for the C- and N-terminally tagged variants, respectively (Fig. 14A, B). The C-terminally tagged *XMPP* was used in a substrate screen including common phosphatase substrates and purine and pyrimidine ribo- and deoxyribomononucleotides (Fig. 14C). The screen demonstrated that *XMPP* has a high substrate specificity for XMP, which is unlike *STDL2* to 4 which show activity for three to four substrates (Zhu, 2016). Generally, many phosphatases have a broader substrate spectrum.

For the characterization of *XMPP* in Arabidopsis its expression profile in various tissues was assessed online (Klepikova *et al.*, 2016 at bar.utoronto.ca; Winter *et al.*, 2007). *XMPP* transcript amount is especially high in flowers, seeds and senescent leaves. It is interesting to note that *XMPP* showed overall considerably higher transcript levels than *SDTL2* to 4 in qPCR analysis (Zhu, 2016). Also in comparison with other genes involved in purine nucleotide catabolism, the abundance of *XMPP* transcript is relatively high (Fig. 15A; Klepikova *et al.*, 2016 at bar.utoronto.ca; Winter *et al.*, 2007).

For the detection of the native *XMPP* a polyclonal antibody was produced against the untagged *XMPP* protein. Curiously, although the expression in *N. benthamiana* yielded high amounts of stable protein and the transcript is abundant in Arabidopsis, the *XMPP* protein could not be detected with this antibody in young and old rosette leaves, cauline leaves, flowers or in roots of six-week-old plants (Christel Schmiechen, not shown). The matured antibody reached a detection sensitivity of 250 pg *XMPP* per dot, which in practice gave a detection limit of about 1 ng considering the background noise of plant samples (Fig. 15B). The antibody quality would thus be sufficient to detect *XMPP*, if it was similarly abundant as other proteins of purine catabolism like *GSDA* or *NSH1*. *GSDA* could be detected in young and old rosette leaves, roots and flowers of four-week-old plants (Dahncke, 2014). *NSH1* could be detected in young and old rosette leaves, cauline leaves, roots and flowers of four-week-old plants with amounts of 3 ng to over 10 ng of protein in similar volumes of plant crude extract as tested for the *XMPP* detection (Baccolini, 2019). It is striking that although the *XMPP* transcript is five times more abundant in 4-week-old rosette leaves than the *NSH1* transcript, *NSH1* was clearly detectable with about 3 ng of protein in 12 μL crude extract, while *XMPP* was not detectable in 15 μL of crude extract and an antibody sensitivity limit of 1 ng (Fig. 15). This suggests the existence of a regulatory mechanism, which is either restraining the translation of *XMPP* transcript or maybe affecting protein stability.

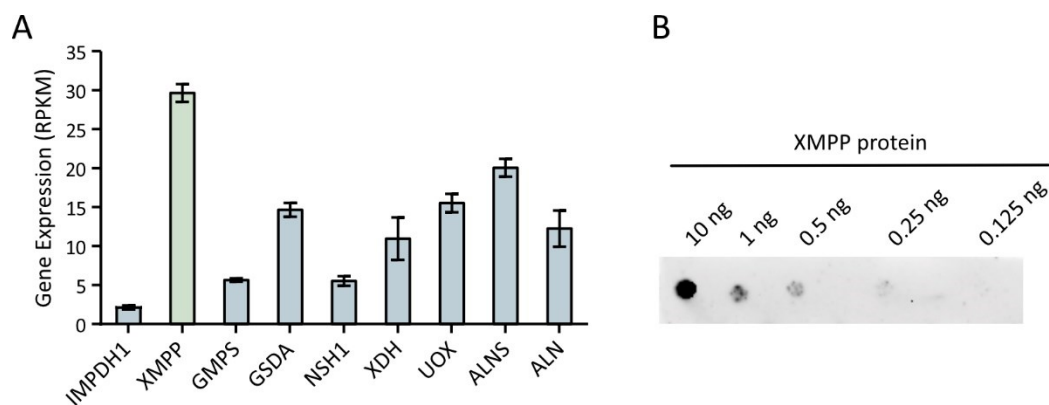


Figure 15 *XMPP* is highly transcribed but its protein could not be detected despite a sensitive anti-*XMPP* antibody. **A**, Gene expression data of Arabidopsis rosette leaves at the time of first flower anthesis extracted from RNAseq data accessible at Arabidopsis EFP browser (AT-00794; Klepikova *et al.* (2016) at Winter *et al.* (2007)). Error bars are SD, $n_b = 2$. **B**, Determination of anti-*XMPP* antibody sensitivity using purified *XMPP*-HAStrep (performed by Christel Schmiechen).

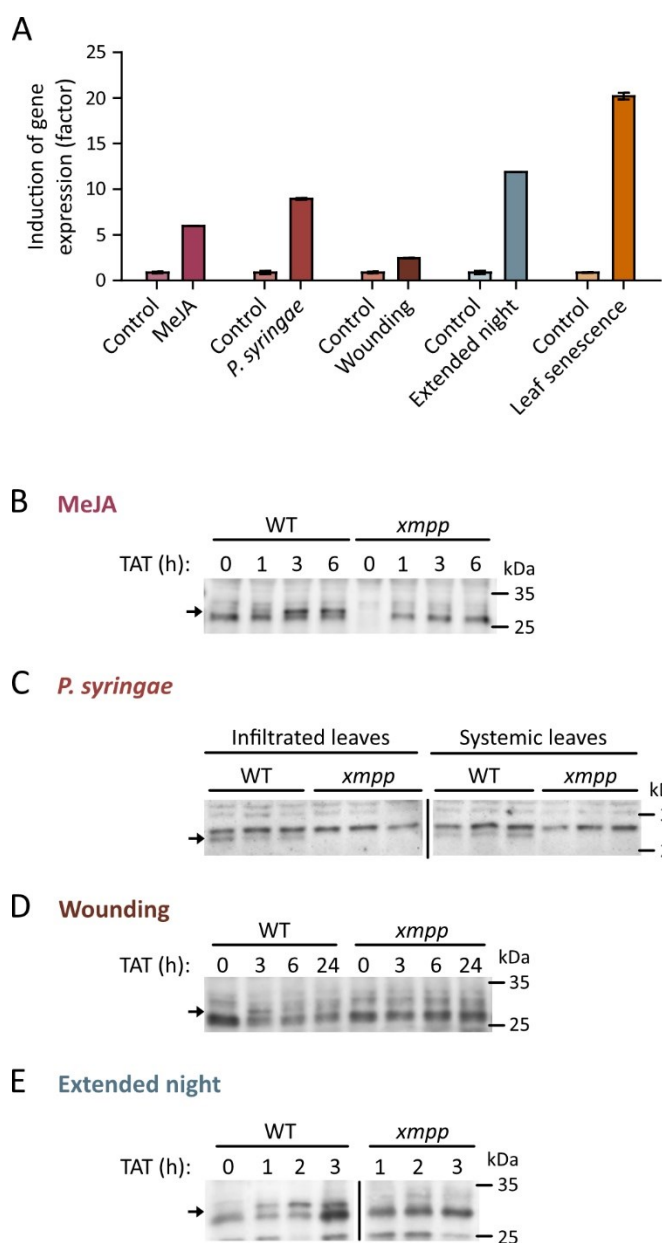


Figure 16 Detection of XMPP protein under conditions which induce XMPP gene expression. **A**, Induction of XMPP expression in response to various stimuli extracted from gene expression data accessible at Genevestigator (data sets AT-00281, AT-00794, AT-00110, AT-00406, AT-00654 at Hruz *et al.*, 2008; Usadel *et al.*, 2008; Klepikova *et al.*, 2016; Goda *et al.*, 2015; Mitra, 2018; Suzuki *et al.*, 2013). Error bars are SD, $n_i = 2 - 3$. **B**, Formation of the XMPP protein after treatment with methyl jasmonate (MeJA). Four-week-old Arabidopsis rosettes were sprayed with 500 μ L of 500 μ M MeJA. **C**, Formation of the XMPP protein five hours after infiltration with *P. syringae* ES4326. One leaf of four-week-old Arabidopsis rosettes was infiltrated by Björn Heinemann. Infiltrated and non-infiltrated systemic leaves were harvested separately. Three biological replicates were prepared, each represented by one lane. **D**, Formation of the XMPP protein after wounding. One leaf of four-week-old Arabidopsis rosettes was carefully squeezed five times with plastic tweezers. **E**, Formation of the XMPP protein in the course of an extended night. Four-week-old Arabidopsis rosettes were kept in extended darkness at the end of night. **B - E**, TAT = Time after treatment. The plants were grown under long-day conditions (16 h day/ 8 h night, 22°C/ 20°C). XMPP protein was detected using custom-made anti-XMPP antibody. The XMPP protein bands are marked with arrows. Immunoblots B, C and E were prepared by Christel Schmiechen.

Results

To find the conditions under which XMPP is required *in vivo* and under which the protein might therefore be detectable, publicly available gene expression data were searched with the expectation that induced gene transcription might be associated with increased protein amount. It was found that the *XMPP* transcript amount is increased under several stress conditions, like the infection with *Pseudomonas syringae* ES4326, wounding, the extension of the night and related to the two former stimuli also by the treatment with the stress hormone methyl jasmonate (MeJA; Fig. 16A; Hruz *et al.*, 2008; Usadel *et al.*, 2008; Suzuki *et al.*, 2013; Goda *et al.*, 2015; Mitra, 2018). Four-week-old *Arabidopsis* plants were exposed to these four stimuli to test whether XMPP protein would become detectable. XMPP was successfully detected one hour after MeJA treatment, and was showing the strongest signal after three and six hours (Fig. 16B). It was detected five hours after infiltration with *P. syringae* in the infiltrated leaves, and with similar signal strength also in the neighboring non-infiltrated systemic leaves (Fig. 16C). Upon wounding XMPP was detected three hours after the stimulus (Fig. 16D). The increase of XMPP protein upon MeJA treatment, *P. syringae* infiltration and wounding points to an involvement of XMPP in defense mechanisms. XMPP was also detected when plants were kept in prolonged darkness after the end of the night (Fig. 16E). XMPP was not yet detectable at the end of the night, whereas it was detected after one hour and with the highest signal after three hours. An induction of XMPP protein amount by extended darkness fits previous results by Brychkova *et al.* (2008) who demonstrated that purine nucleotide catabolism is dark-induced and proposed that it contributes in ROS quenching and to nutrient remobilization by the formation of the ureides allantoin and allantoate. Accordingly, XMPP might also be induced in senescence, which is supported by the expression data retrieved from the Klepikova expression atlas (Fig. 16A).

Conclusions from the enzyme biochemistry, gene expression analysis and immunoblots:

- I) XMPP has a high catalytic activity for XMP and is very specific for this substrate.
- II) Although the *XMPP* transcript is relatively abundant, the XMPP protein could not be detected under non-stress conditions.
- III) Transcript and protein amounts are both under the control of regulatory mechanisms.
- IV) The detection of the protein under the tested conditions suggests that XMPP plays a role in plant defense, prolonged darkness, and probably senescence too.

4.4.2 XMPP in *Arabidopsis* seed development

4.4.2.1 Metabolite analysis

To examine whether XMPP facilitates the XMP dephosphorylation *in vivo*, related metabolites were quantified in seed extracts of *XMPP* genetic variants in the context of other mutants of purine catabolism. The complementation line *xmpp nsh1 gsdA::sX* was included which expressed N-terminally TwinStrep-tagged XMPP under the control of its native promoter (Fig. A - 4). Seeds were the tissue of choice as results obtained by Baccolini and Witte (2019) suggested the involvement of XMP dephosphorylation in seeds. Xanthosine, guanosine, guanine, inosine and allantoin were quantified. Moreover, guanylates, adenylates and XMP concentrations were determined by Henryk Straube according to Straube *et al.* (2021). This new method for nucleotide quantification allowed to analyze the low XMP concentrations in the context of *XMPP* mutation for the first time.

XMP was not detectable in wild-type seeds but accumulated in *xmpp* seeds which confirmed the involvement of XMPP in *Arabidopsis* purine catabolism. Surprisingly, XMP could also be measured in

nsh1 seeds and its concentration was highest in *xmpp nsh1* seeds (Fig. 17). The XMP accumulation in *nsh1* seeds is likely caused by the high xanthosine concentration in this background, which is presumably biochemically blocking both XMP consuming enzymes, XMPP and GMPS (Fig. 3, 18). The inhibition of XMPP by xanthosine could be confirmed *in vitro* (Fig. 19). The biochemical inhibition of XMPP by xanthosine in *nsh1* seeds is however not complete, as the additional genetic block of XMPP in *xmpp nsh1* seeds led to a considerably increased XMP concentration (Fig. 17). The absence of such high levels of XMP in the *xmpp nsh1 gsdA* seeds, which is coinciding with the suppression of the xanthosine accumulation by the GSDA mutation, compared to the XMPP NSH1 double mutant, supports the notion that xanthosine inhibits GMPS (Fig. 17, 18).

The observation of Baccolini and Witte (2019) that the xanthosine accumulation in *nsh1 gsdA* was 30% of the xanthosine accumulation present in *nsh1* could be reproduced (Fig. 18). The further decreased xanthosine concentration of *xmpp nsh1 gsdA* seeds, which was restored in the corresponding complementation line to *nsh1 gsdA* level, also confirmed the role of XMPP in XMP dephosphorylation in seeds. The presence of residual 7% of xanthosine in the triple mutant compared to *nsh1* may have resulted from chemical deamination of the highly accumulated guanosine. Interestingly, only with the XMPP NSH1 GSDA triple mutant it was possible to demonstrate the effect of XMPP mutation on xanthosine level, while this was not possible with *xmpp nsh1* seeds. In order to be able to explain this, it is first necessary to note that guanosine and guanine concentrations were higher in *xmpp gsdA* seeds compared to *gsdA* seeds (Fig. 18). This shows, as postulated for common bean nodules, that XMP which cannot be processed by the missing XMPP is probably aminated at a higher rate by GMPS to GMP, which is dephosphorylated to guanosine. This shows that the GMP – guanosine route compensates the missing XMPP reaction, which is the reason why xanthosine concentration in *xmpp nsh1* seeds was not different than in *nsh1* seeds.

Guanine is not involved in purine nucleotide catabolism in wild-type seeds but was accumulating in *gsdA* background by hydrolysis of the highly accumulating guanosine. Therefore, the mutation of XMPP led to increased guanosine and guanine concentrations in *xmpp gsdA* seeds compared to *gsdA* seeds and in tendency also in *xmpp nsh1 gsdA* seeds compared to *nsh1 gsdA* seeds. Accordingly, guanosine and guanine concentrations in seeds of the *xmpp nsh1 gsdA::sX* complementation line were in tendency restored to *nsh1 gsdA* levels. Interestingly, the GTP pool size, but not the GMP or GDP pool sizes, was also greater in genotypes that over-accumulated guanosine (Fig. 17, 18). Also it is interesting to note that the increase of guanosine and GTP by XMPP mutation was only observed in seeds with *gsdA* background, but not in *xmpp* seeds. These observations allow two conclusions: I) The unidentified GMP Phosphatase (GMPP; Fig. 3, #17) and GSDA (#18) can maintain GMP and guanosine homeostasis in seeds when there is surplus metabolic flux from XMP to GMP caused by XMPP mutation. II) The guanylate pool sizes are under the control of regulatory mechanisms.

The guanosine and guanine concentrations in the higher order mutants with *gsdA* background were also affected by the mutation of NSH1. This caused increased guanosine accumulations, but decreased guanine concentrations comparing *nsh1 gsdA* with *gsdA* and *xmpp nsh1 gsdA* with *xmpp gsdA*. NSH1 is not considered to hydrolyze guanosine *in vivo* (Jung *et al.*, 2009; Jung *et al.*, 2011; Baccolini and Witte, 2019). The guanosine hydrolysis by NSH1 in *gsdA* background is likely an artefact of the high accumulation of guanosine. It is important to note that the occupation of the NSH1 capacity by guanosine hydrolysis and potentially its inhibition by guanosine is probably the cause for the accumulation of xanthosine and inosine in seeds with *gsdA* background (Fig. 18, A - 6). Guanosine pool sizes were increased to 160% in *xmpp gsdA* and to 153% in *nsh1 gsdA* compared to *gsdA* seeds. In the XMPP NSH1 GSDA triple mutant, the mutation of XMPP and NSH1 caused the highest increase in guanosine concentration to 184% from the guanosine concentration measured in *gsdA* seeds. The concentration profile of guanosine across the different mutants was similarly observed for GTP but not

Results

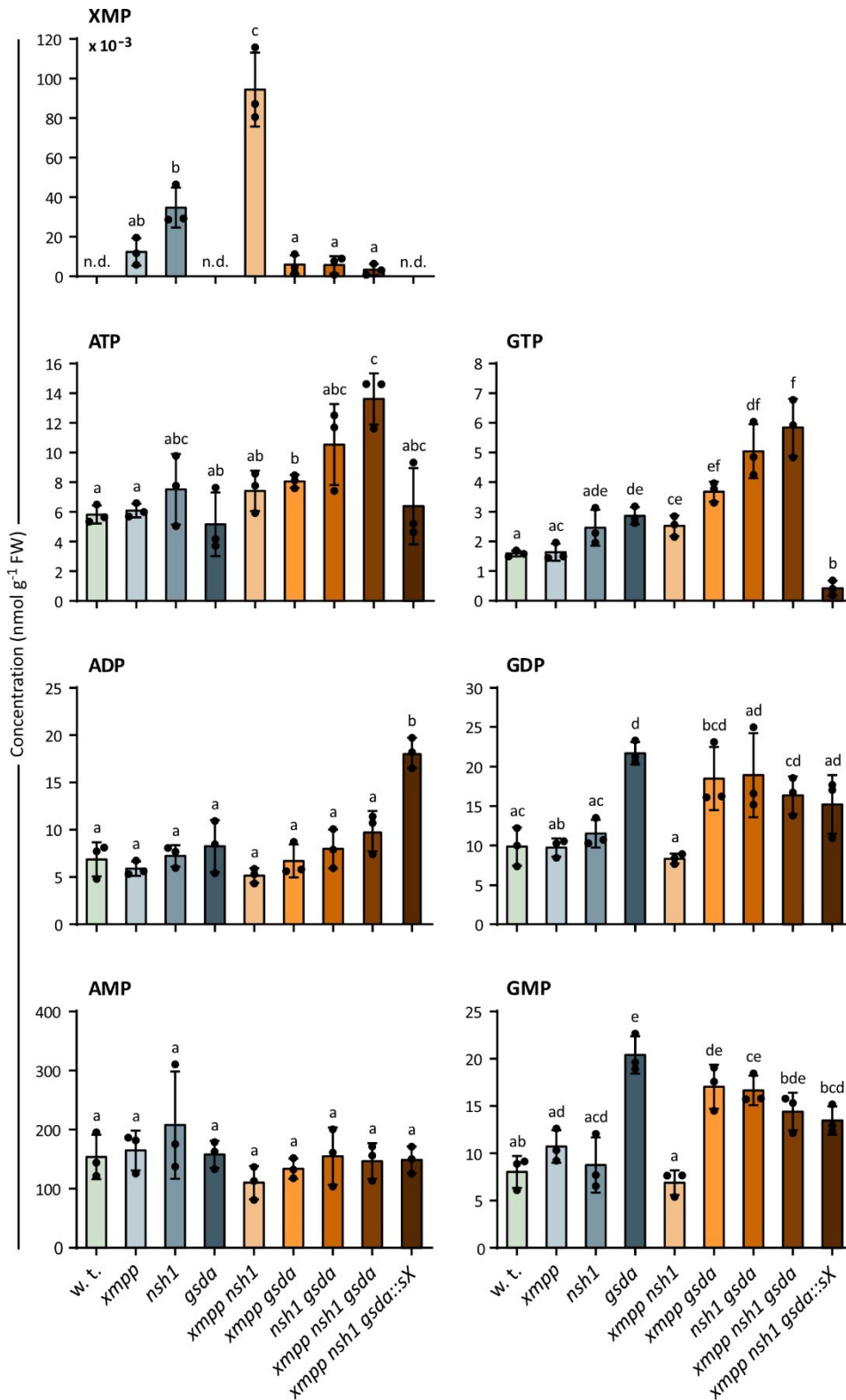


Figure 17 Quantification of XMP, adenylates and guanylates in seed extracts of *XMPP* genetic variants in the context of other mutants of purine catabolism. The complementation line *xmpp nsh1 gsda::sX* contained a transgene encoding an N-terminally TwinStrep-tagged XMPP under the control of the native promoter. Error bars are SD, $n_b = 3$. A biological replicate (n_b) is a seed sample from an independent mother plant grown in parallel with all other plants of the experiment (16 h day/ 8 h night, 22°C/ 20°C). For statistical analysis two-sided Tukey's pairwise comparisons using the sandwich variance estimator were performed. Different letters indicate p values < 0.05. Measurements not matching quality criteria (Chapter 7.8) were called not detected ("n.d."). Nucleotide quantification was performed by Henryk Straube according to Straube *et al.* (2021).

for GDP or GMP, indicating that the guanylate concentrations are subject to some metabolic control (Fig. 17). The most striking example is the drastically reduced GTP concentration in *xmpp nsh1 gsdA::sX* seeds, whereas GDP and GMP as well as guanosine and guanine are not affected. The reduction was thus more than just a simple deprivation of XMP, which is required for guanylate production but which is dephosphorylated by the abundant XMPP of the complement line. This is another indication that guanylate homeostasis is subject to unknown control mechanisms. The profile of guanylate concentrations across the genotypes were in tendency reflected in the adenylate pools as described by Straube *et al.* (2021). The reduction of GTP in the complementation line, was mirrored in a reduced ATP concentration. The elevated ADP concentration in the complementation line may be the consequence of such an adaptation to a lower ATP concentration to maintain ATP and GTP balance. In summary, the absence of XMPP in the *xmpp* seeds, with the exception of XMP accumulation, had no effect on the measured metabolites, but the presence of the *XMPP* transgene caused a reduction in ATP and GTP concentrations in the complementation line.

A contribution to purine nucleotide catabolism by IMP dephosphorylation via inosine, hypoxanthine to xanthine was excluded due to the relative low concentrations of inosine and hypoxanthine in *NSH1* and *XDH* mutants, respectively (Baccolini and Witte, 2019; Fig. A - 6).

Although the allantoin pool size was captured in steady state, and was not blocked by *ALN* mutation, differences in the allantoin pool sizes between mutants were observed, matching the model for the metabolic placement of XMPP so far developed (Fig. 18). Interestingly, allantoin concentration was extraordinary high in comparison with other metabolites quantified in wild-type seeds. This may indicate that allantoin is a seed storage compound, presumably for nitrogen, which can later be degraded to recycle nitrogen. In accordance with observations for xanthosine, the bypass of the XMPP reaction in *xmpp* background through GMP and guanosine did not cause any reduction of allantoin concentration in the *XMPP* mutant compared to wild-type seeds. The *XMPP GSDA* double mutant was required to demonstrate that XMPP is operative in seeds. The allantoin concentration in *gsda* was almost 50% lower than in the wild type and allantoin was not detectable in *xmpp gsdA* seeds. It is important to note that it is not possible to draw quantitative conclusions from the metabolite analyses of mutants. Mutants accumulate highly unphysiological metabolite amounts that can lead to side effects, like the inhibition of *NSH1* by guanosine or the inhibition of XMPP and GMPS by xanthosine. Therefore, this type of metabolite analysis can give insights into the hardwiring of metabolic pathways, but can be misleading for the estimation of metabolic flow rates.

Main conclusions from the seed metabolite analysis:

- I) *XMPP* is operative in Arabidopsis seed development.
- II) XMP accumulates slightly in *xmpp* seeds.
- III) Mutation of *XMPP* does not alter other related metabolites in *xmpp* seeds.
- IV) The XMPP reaction can be bypassed through GMP and guanosine to xanthosine.
- V) GMPP and GSDA can maintain guanylate and guanosine homeostasis despite increased metabolic flux from XMP to GMP in *xmpp* seeds.
- VI) The absence of XMPP does not affect ATP and GTP concentrations, the presence of an *XMPP* transgene however leads to a strong reduction of these nucleotides.
- VII) XMPP and GMPS are inhibited by high xanthosine concentrations.
- VIII) *NSH1* is inhibited by high guanosine concentrations.
- IX) Seeds accumulate high amounts of allantoin.

Results

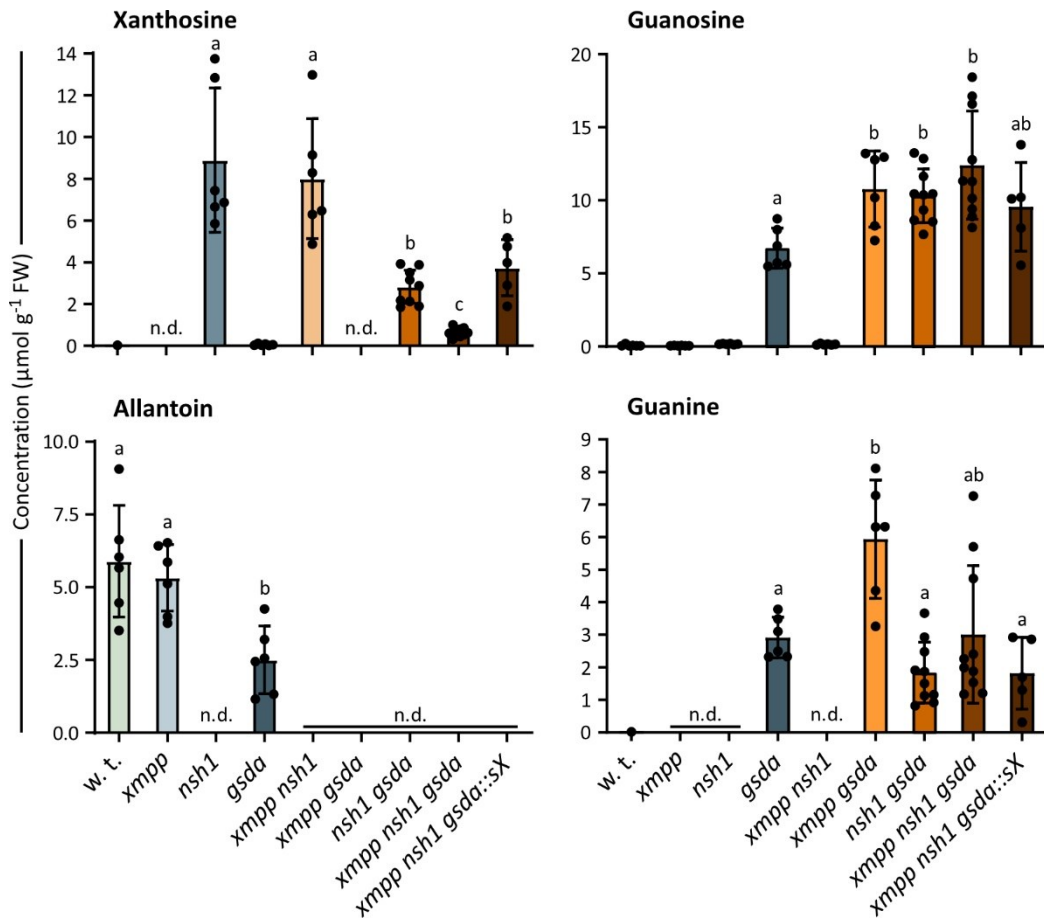


Figure 18 Quantification of intermediates downstream of XMP in seed extracts of XMPP genetic variants in the context of other mutants of purine catabolism genes. The complementation line *xmpp nsh1 gsda::sX* contained a transgene encoding an N-terminally TwinStrep-tagged XMPP under the control of the native promoter. Error bars are SD, $n_b = 5 - 6$ for all but *nsh1 gsda* and *xmpp nsh1 gsda* with $n_b = 10$. A biological replicate (n_b) is a seed sample from an independent mother plant grown in parallel with all other plants of the experiment (16 h day/ 8 h night, 22°C/ 20°C). Measurements not matching quality criteria (Chapter 7.8) were called not detected (“n.d.”) and are not shown. For statistical analysis two-sided Tukey’s pairwise comparisons using the sandwich variance estimator were performed. Different letters indicate p values < 0.05.

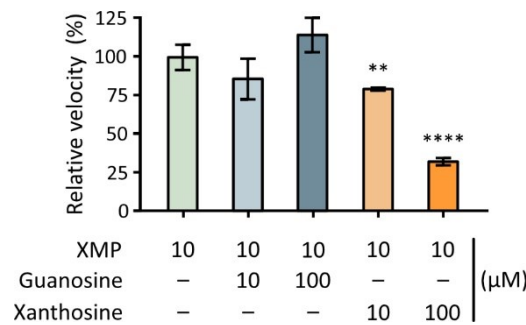


Figure 19 Inhibitory effect of guanosine or xanthosine on XMPP activity. The enzymatic velocity of XMPP was assessed with 10 μM XMP setting an activity of $14.0 \pm 1.0 \mu\text{mol mg}^{-1} \text{min}^{-1}$ to 100%. Whether guanosine or xanthosine had an inhibitory effect on XMPP activity was tested in the additional presence of 10 or 100 μM guanosine or xanthosine. Error bars are SD, $n_t = 4 - 5$. For statistical analysis, two-sided Dunnett’s comparisons using the sandwich variance estimator were performed. The assay without nucleoside additions served as reference group. **, $p < 0.01$; ****, $p < 0.0001$.

4.4.2.2 Seed yield and appearance

For the metabolite analysis described in the previous chapter, seeds were harvested from mother plants which were grown in parallel. The weight of the harvested seeds per plant was determined showing significantly smaller seed weights for the *XMPP*, *NSH1* and *GSDA* mutants. The reduced seed weight was likely caused by reduced seed numbers, because the longest seed diameter and appearance were not affected (Fig. 20). Especially *gsda* and also higher mutants with *gsda* background showed a strong reduction in seed yield. The reduction in *gsda* was significantly stronger than in *nsh1*, which indicates that it is more likely due to pleiotropic effects caused by the strong guanosine accumulation in *gsda* than due to a block of purine nucleotide catabolism. The reduced seed yield of *xmpp* was partly restored in the complementation line. Curiously, the mutation of *XMPP* showed an effect on seed yield although the metabolite analysis did not show any changes in metabolite concentrations. Possible reasons could be an involvement of XMPP in tissue-specific or development-specific processes, which do not alter the overall seed metabolite concentrations.

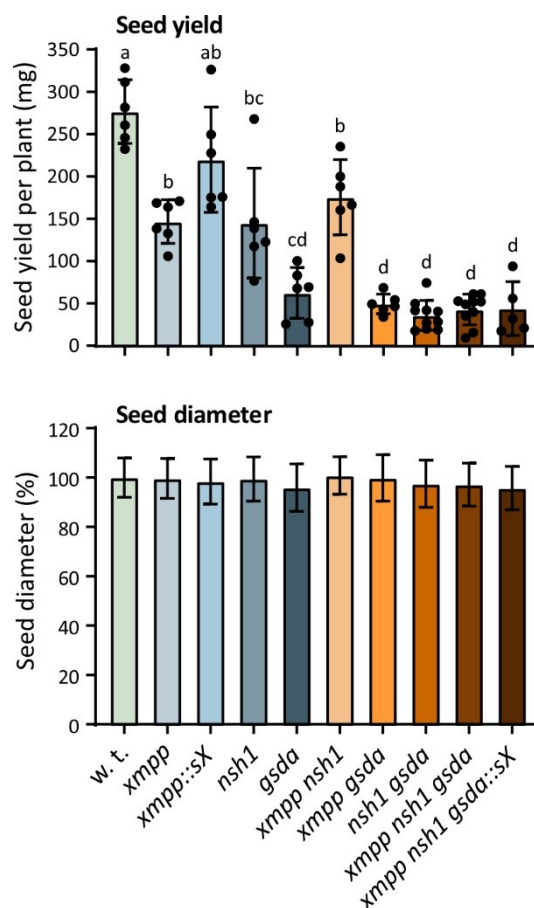


Figure 20 Quantification of seed yield and seed diameter of *XMPP* genetic variants in the context of other mutants of purine catabolism genes. **A**, The complementation lines *xmpp::sX* and *xmpp nsh1 gsda::sX* contained a transgene encoding an N-terminally TwinStrep-tagged XMPP under the control of the native promoter (Fig. A - 4). Error bars are SD, $n_b = 5 - 6$ for all but *nsh1 gsda* and *xmpp nsh1 gsda* with $n_b = 10$. A biological replicate (n_b) is a seed sample from an independent mother plant grown in parallel with all other plants of the experiment (16 h day/ 8 h night, 22°C/ 20°C). Samples from the same seed pools were used for metabolite analysis (Fig. 17, 18). For statistical analysis two-sided Tukey's pairwise comparisons using the sandwich variance estimator were performed. Different letters indicate p values < 0.05. **B**, Relative seed diameter of the longest side. The average of wild-type seed diameter was set to 100%. Error bars are SD, $n_t = 95$ from $n_b = 5$.

Results

4.4.2.3 Test for *uox* phenotype suppression by *XMPP* mutation

The mutation of *UOX* causes a detrimental accumulation of uric acid in the cotyledons of the mature embryo (Hauck *et al.*, 2014). Uric acid disturbs glyoxysome function impairing β -oxidation of fatty acids and remobilization of energy from the lipid bodies meant to nourish the young seedling. As the β -oxidation is also required for the induction of germination *UOX* mutants show two germination-related phenotypes. One is the inhibition of seed germination and the other the inhibition of the seedling establishment. The latter is caused by the unavailability of energy from the lipid bodies and can thus be complemented by the supplementation with exogenous sucrose (Hauck *et al.*, 2014). Mutations that suppress the accumulation of uric acid in the *uox* background will improve seed germination and seedling establishment. Such mutations will for example lie in genes that code for enzymes acting upstream of *UOX* in purine nucleotide catabolism. An *uox* suppressor test was performed to assess whether the mutation of *XMPP* in addition to the *UOX* mutation would suppress or mitigate the *uox* phenotypes, thereby further supporting the biological function of *XMPP* in seed development. The following genotypes were included: wild type, *XMPP*, *GSDA* and *UOX* single mutants, and *XMPP UOX* and *GSDA UOX* double mutants. Mutation of *GSDA* in the *uox* background is known to almost completely suppress the *uox* phenotypes (Baccolini and Witte, 2019). According to the seed metabolite data (Fig. 18), a suppression of the *uox* phenotypes by an additional *XMPP* mutation was not expected, since the absence of *XMPP* can be compensated via a bypass reaction through GMP and guanosine resulting in a similarly high uric acid concentration. Since the reduced seed yield of the *xmpp* plants had already indicated a role for *XMPP* in seed development, it was still considered useful to perform the *uox* suppressor test (Fig. 21).

As expected uric acid accumulation of *xmpp uox* seeds was as high as in the *UOX* single mutant, whereas it was strongly reduced in *gsda uox* seeds (Fig. 21A). The germination rate of *gsda uox* seeds was recovered from 27% to 99% (Fig. 21B). Surprisingly, also *xmpp uox* showed a significantly improved germination rate of 45%, although uric acid concentration was unchanged. Similar to the reduced seed yield of *XMPP* mutants, the increased germination rate of *xmpp uox* seeds suggest that *XMPP* may play a role in seed development or germination. A tissue- or development-specific function of *XMPP* in seeds may explain why the mutation of *XMPP* led to reduced seed yield and increased *xmpp uox* germination without overall showing altered concentrations of the quantified metabolites. Note, that *xmpp* seeds did not show an impairment of germination or seedlings establishment. Although the germination rate of *xmpp uox* seeds was higher than that of *uox* seeds, the seedlings failed to establish and seedlings development arrested shortly after the emergence of the radicle (Fig. 21C). As the uric acid concentration in *xmpp uox* seeds was equally high as in *uox* seeds, it can be assumed that the growth arrest was here also caused by the lack of energy due to the impaired β -oxidation in the cotyledons. *XMPP* is thus a suppressor of the germination phenotype but not of the seedling establishment phenotype. The latter could be suppressed by sucrose supplementation so that *xmpp uox* seeds which germinated on plates including 1% sucrose could establish seedlings. When the segregating *xmpp uox* population was grown on sucrose supplemented plates, some of the seedlings developed purple or transparent cotyledons with green globular spots. These phenotypes were exclusively observed for *xmpp uox* but neither for *uox*, *xmpp*, *gsda* nor *gsda uox* seedlings. These phenotypes are not further discussed because they are highly artificial, caused by the *UOX* and *XMPP* mutation and the rescue of the germinated seedlings by the addition of sucrose. Nevertheless, they indicate that *XMPP* is involved in seedling development.

Main conclusions from the seed yield experiment and the *uox* suppressor test:

- I) Although *xmpp* seeds do not show any changes in metabolite concentrations other than the XMP accumulation, this mutant is impaired in seed production
- II) The *XMPP* mutation can partially suppress the *uox* germination phenotype, however not the *uox* seedlings establishment phenotype.
- III) Some seedlings of the segregating *xmpp uox* population supplemented with sucrose developed purple or transparent cotyledons supporting a role of XMPP in seedling development.

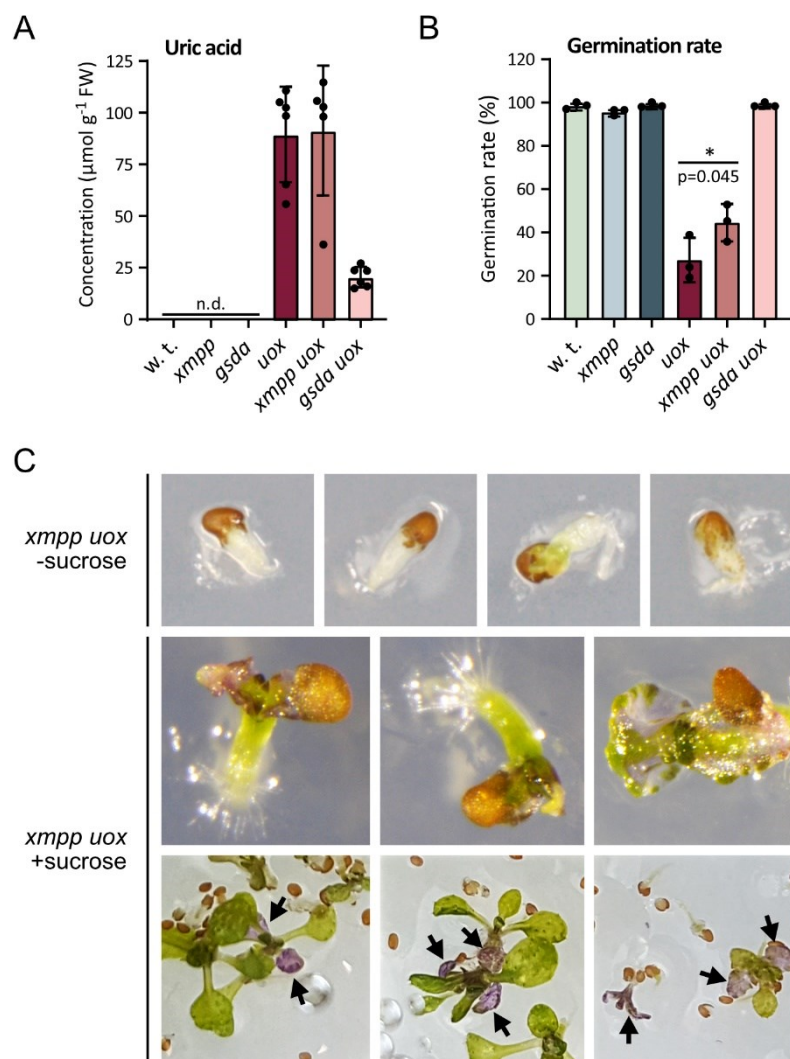


Figure 21 Partial genetic suppression of the *uox* seed germination phenotype by the *XMPP* mutation. **A**, Quantification of uric acid in seed extracts. Error bars are SD, $n_b = 5 - 6$. Measurements not matching quality criteria (Chapter 7.8) were called not detected (“n.d.”) and are not shown. **B**, Germination test on half-strength MS plates with fresh seeds. Error bars are SD, $n_b = 3$. A biological replicate (n_b) is a seed sample from an independent mother plant grown in parallel with all other plants of the experiment. The average germination rate of wild-type seeds was set to 100%. The asterisk indicates a p value < 0.05 using one-sided Student’s t-test assuming variance homogeneity for the comparison of *xmpp uox* with *uox* seeds. **C**, Top panel, Exemplary pictures of germinated *xmpp uox* seeds which did not establish a seedling on half-strength MS plates without supplementation with sucrose. Middle panel, On plates supplemented with 1% sucrose seedlings could establish. Most cotyledons were only rudimentary structures but some cotyledons developed showing transparent leaves including green spherical structures. Bottom panel, From a segregating *xmpp uox* seed batch multiple plants developed purple cotyledons in the four-leaf stage grown with sucrose supplementation. The development of some completely purple plants was arrested in the two-leaf stage. Arrows mark purple leaves.

4.4.3 XMPP in Arabidopsis seedlings

When the onset of light is delayed (prolonged darkness) the activity of purine catabolism rises and the amount of XMPP protein increases (Baccolini and Witte, 2019, Fig. 16E). To assess whether XMPP is operative in extended darkness, metabolite analysis was performed with wild-type, *xmpp*, *gsda* and *xmpp gsda* seedlings, which were either exposed to 48 h of darkness prolonging the fifth night after germination or which continued to grow under long-day conditions. In addition to the XMPP mutant line which was generally used, a second independent mutant line was included in this experiment. The lines are referred to as *xmpp-1* and *xmpp-2* (new line). Allopurinol was applied at the beginning of the extended darkness to block XDH biochemically. Similar to the xanthosine accumulation caused by the *NSH1* mutation, which was measured in the seed metabolite analysis, XDH was inhibited to create a xanthine accumulation with which the involvement of upstream genes could be investigated. The advantage of allopurinol is that xanthine accumulates only in a short, selected period after application and not constitutively in high amounts as it is the case with genetically engineered *xdh* plants. Like this changes of metabolite concentrations caused by the prolonged night could be assessed. Allopurinol has a similar structure as hypoxanthine, a substrate of XDH. After the hydrolysis of allopurinol by XDH, the product oxipurinol binds strongly to the reduced molybdenum cofactor of XDH inhibiting the enzyme (Montalbini and Della Torre, 1995).

Xanthine accumulation increased twofold when plants were exposed to prolonged darkness (Fig. 22A). Interestingly, no xanthine was detected in *gsda* seedlings kept in long day cycle conditions, whereas xanthine accumulated in dark-stressed *gsda* seedlings reaching 9% of the xanthine concentration measured in wild-type seedlings. The additional mutation of XMPP in *xmpp gsda* seedlings prevented this xanthine accumulation showing that XMPP acts in dark-stressed seedlings.

In a parallel experiment, seedlings were not treated with allopurinol and several metabolites were monitored (Fig. 22B). The differences in guanosine concentrations are very informative revealing several aspects. I) In long-day conditions guanosine accumulated in *gsda* seedlings suggesting that the route through GMP and guanosine was active. II) In dark conditions guanosine content in *gsda* seedlings increased over sixfold compared to long-day conditions indicating that the flux through the GMP route was significantly elevated in extended darkness. III) The additional mutation of XMPP in *gsda* background caused a 68% increase in guanosine accumulation in the dark suggesting that more XMP is aminated to GMP overflowing into the guanosine pool – similar to what has been observed in seeds. This explains the absence of changes in xanthine concentration in *xmpp* compared to wild-type seedlings (Fig. 22A). IV) This overflow was not observed in the long day regime comparing *gsda* and *xmpp gsda* seedlings supporting the assumption that the physiological importance of XMPP is greater in darkness which is reflected in higher transcript and protein amounts under these conditions (Fig. 16E). The elevated xanthosine concentration in dark-stressed *gsda* seedlings were likely caused by the inhibitory effect of the accumulating guanosine on NSH1/2 as described for seeds already (Fig. 18). Although this effect is similar as observed in seeds, it can be better visualized graphically in this experiment, because there is no comparison to *nsh1*, which accumulates xanthosine so strongly that smaller effects in other genotypes are difficult to display. Interestingly, in *xmpp gsda* seedlings no xanthosine accumulation is observed although they have even more guanosine. This demonstrates again that the XMPP reaction is a direct source of xanthosine in purine catabolism. Residual amounts of xanthosine in *xmpp gsda* seedlings may be derived from chemical decomposition of guanosine to xanthosine.

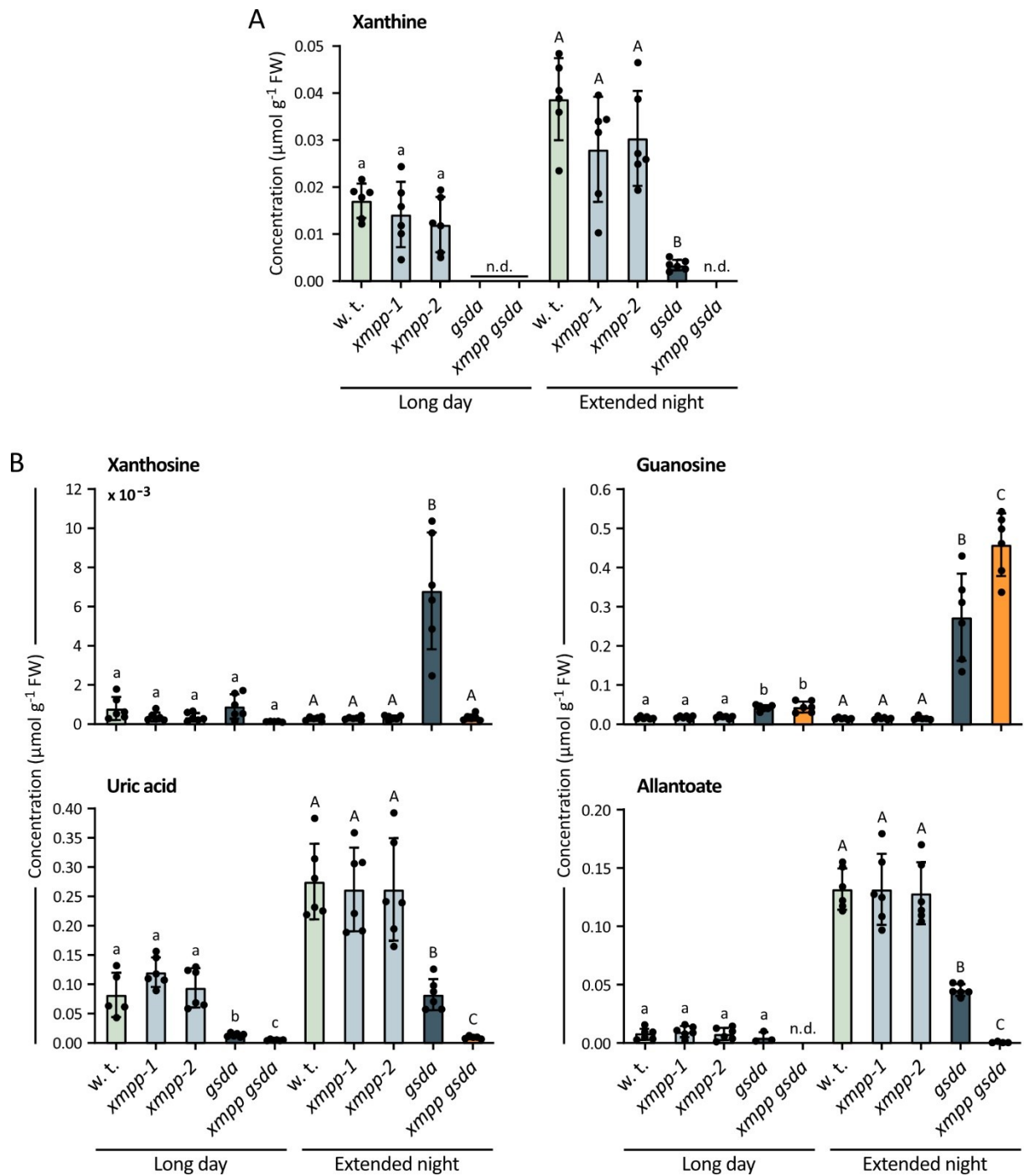


Figure 22 Quantification of intermediates downstream of XMP in *XMPP* genetic variants in the context of other mutants of purine catabolism genes in seedlings under long-day or extended-night conditions. Seedlings were grown under long-day conditions (16 h day/ 8 h night, 22°C/ 20°C). **A**, Quantification of xanthine. Seedlings were treated with 200 μM allopurinol at the end of the fifth night after germination. One half of the seedlings was kept under long-day conditions, whereas the other half was kept in the dark for 48 h. Error bars are SD, $n_b = 6$. **B**, Quantification of xanthosine, guanosine, uric acid and allantoate. Plant material was obtained as described in A but without allopurinol treatment. Error bars are SD, $n_b = 5 - 6$. **A - B**, Measurements not matching quality criteria (Chapter 7.8) were called not detected (“n.d.”) and are not shown. Two-sided Tukey’s pairwise comparisons using the sandwich variance estimator were employed for statistical analyses. Different letters indicate p values < 0.05 . Samples from long-day and extended-darkness conditions were independently analyzed indicated by small and capital letters.

Results

Allantoin concentrations in seedlings were too low to detect. Instead, uric acid and allantoate were quantified. Both steady state pools were higher in seedlings exposed to prolonged darkness and their concentrations showed the same pattern across the tested genotypes. Concentrations were highest in wild-type seedlings in the dark, unchanged in *xmpp-1* and *xmpp-2* seedlings, and were reduced to 30% in *gsda* seedlings and to 2% in *xmpp gsda* seedlings. The data show that the XMPP reaction contributes significantly to purine catabolism under conditions of prolonged darkness. However, an involvement of XMPP was also observed in seedlings grown under long-day conditions. Also here the uric acid concentration was highest in wild-type plants which was similar in *xmpp-1*, *xmpp-2*, but which was significantly reduced in *gsda* and lowest in *xmpp gsda* seedlings. Regarding allantoate concentrations tendencies across the genotypes were similar but less pronounced. The effects of the XMPP mutation on these metabolite pool sizes were only observed in *gsda* background again showing that the absence of XMPP is compensated by the GMP – guanosine route, as previously described in seeds and common bean nodules.

It was noticed, that seedlings treated with allopurinol contained surprisingly high concentrations of allantoate, although theoretically the inhibition of XDH should prevent the generation of allantoate (Fig. 3). The steady state allantoate pool size in allopurinol-treated wild-type seedlings was 65 - 68% of the pool size of untreated seedlings (not shown). Montalbini and Della Torre (1995) reported that XDH in gel activity with 2 mM hypoxanthine as substrate was inhibited by 81% by the addition of 200 μ M allopurinol to the *in vitro* reaction. Accordingly, an incomplete chemical inhibition of XDH by allopurinol was to be expected. However, the amount of allantoate was surprisingly high. Increasing the allopurinol concentration did not enhance the XDH inhibition as reflected in the allantoate pool, showing that the allopurinol amount was not the limiting factor (Fig. 23A). Another aspect which could reduce allopurinol efficiency may be the duration of the treatment. Limited allopurinol stability in the plant and the production of new XDH might reduce the inhibitory effect. In the study of Ma *et al.* (2016) 250 μ M allopurinol was given in half-strength MS medium and seedlings were grown for three weeks. The inhibitory effect was sufficient to lead to the formation of xanthine crystals. Therefore, a time-dependent instability of allopurinol in the 48 hours chosen here for the experiments is unlikely.

An allopurinol experiment was performed treating wild-type seedlings at the end of the fifth night after germination. The effect on the concentrations of xanthine and downstream metabolites was monitored in a time course during which seedlings were kept in prolonged darkness. Within the first 1.5 hours the xanthine concentration rose slowly followed by a strong increase in the following 4.5 hours (Fig. 23B). The increase was less pronounced up to six hours and xanthine concentration reached a steady state after nine hours until 48 h. In the first six hours uric acid and allantoate concentrations did not change but increased steadily afterwards showing that XDH activity was not completely inhibited. The data indicate that after nine hours, xanthine generation balanced xanthine oxidation by the remaining XDH activity. This activity level of XDH seemed to be stable up to 48 h indicating that the allopurinol inhibition of XDH is stable, but not complete until that time. Reasons to explain the incomplete blockage could be a localization of XDH in a protecting compartment or the reversibility of the allopurinol block. Allopurinol exerts its inhibiting effect by the hydrolysis product oxipurinol, which binds strongly to the reduced molybdenum cofactor of XDH. This inhibition is however not irreversible (Montalbini and Della Torre, 1995). In the experiment, allopurinol/ oxipurinol inhibits XDH, which leads to a rising concentration of xanthine and rising competition of xanthine *versus* oxipurinol for XDH binding. A biochemical equilibrium might be established allowing for a certain degree of XDH activity.

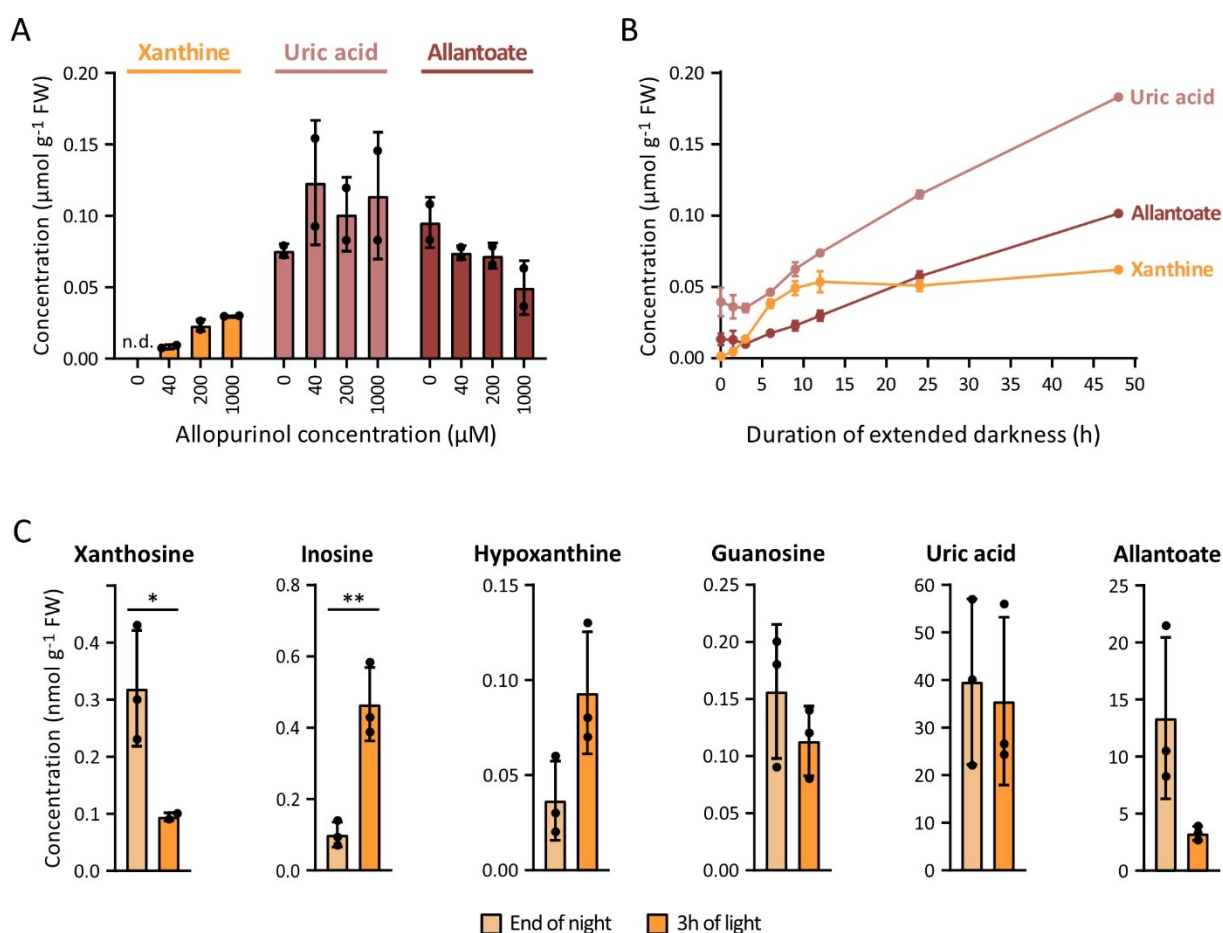


Figure 23 Effect of allopurinol on seedlings. Wild-type seedlings were grown and treated with allopurinol as described for figure 22A. **A**, Xanthine, uric acid and allantoate concentrations in extracts of seedlings which were treated with allopurinol of different concentrations and subjected to 48 h of darkness. Error bars are SD, $n_b = 2$. **B**, Xanthine, uric acid and allantoate concentrations in the course of extended night after the treatment with 200 µM allopurinol. Error bars are SD, $n_b = 2-3$. **C**, Concentrations of purine catabolism intermediates at the end of the night and after three hours of light. Plant material production was included in the time course experiment (B), but without allopurinol treatment. Error bars are SD, $n_b = 2-3$. Two-sided Student's *t*-tests assuming variance homogeneity was performed for statistical analyses. *, $p < 0.05$; **, $p < 0.01$.

The seedling experiment shown before (Fig. 22) already confirmed that purine nucleotide catabolism is boosted by 48 h of prolonged night. Data from this experiment demonstrate that the uric acid and allantoate concentrations are continuously rising during the prolonged night, although they are thought to be in a steady state of influx and efflux. It is also important to note that here XDH was partially inhibited. The rise of the uric acid and allantoate concentrations might thus be even more pronounced in a situation without XDH inhibition. This raises the question, whether their accumulation serves a physiological purpose.

Another interesting observations was that in seedlings which were not treated with allopurinol xanthosine, inosine and in tendency also hypoxanthine ($p = 0.065$) and allantoate ($p = 0.069$) pool sizes reacted to the onset of light after a normal night (Fig. 23C). The data points of metabolite concentrations at the end of the night were the same as used for the 0 h time point of the extended darkness time course (Figure 23B). Additional seedlings were grown in parallel which were not treated with allopurinol and which were harvested 3 h after the light period of the long day started. Light has apparently a marked impact on purine catabolism also in a continuous day and night rhythm.

Results

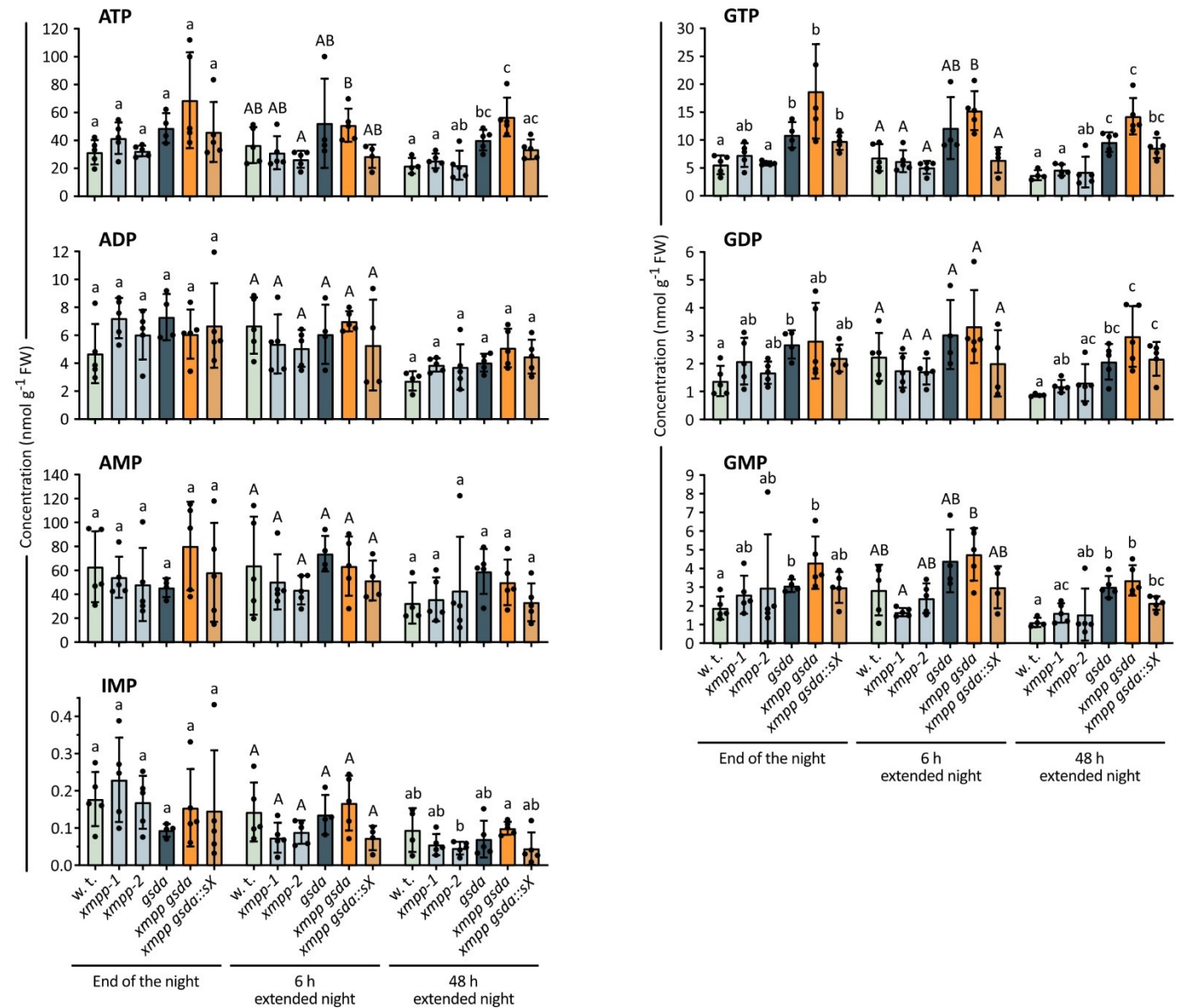
After the digression on the effects of allopurinol in the extended night, the metabolic analysis of dark-stressed seedlings was still of interest. New plant material was prepared as described for figure 22 to also determine purine nucleotide concentrations under these conditions. Five days-old seedlings were grown as before and were either exposed to 48 h of extended night or were kept under long-day conditions. Allopurinol was not used. Purine nucleotide concentrations were determined by Henryk Straube according to Straube *et al.* (2021). This time a third time point of six hours of extended darkness was included to cover also the early phase of extended darkness. XMP concentrations were too low to detect with an estimated limit of detection corresponding to $7.8 \text{ pmol g}^{-1} \text{ FW}$. The concentrations of guanylates, adenylates and IMP were unchanged in *xmpp* seedlings (Fig. 24). By contrast, high guanosine concentrations in seedlings with *gsda* background led to increased GTP, and in contrast to the seeds, also to increased GDP and GMP concentrations (Fig. 17, 24). This may indicate that different control mechanisms operate in seed and seedlings. Guanylate concentrations were in tendency further increased by the additional *XMPP* mutation because in the *xmpp gsda* line guanosine hyperaccumulates as discussed before. This effect was not observed when the *XMPP* mutation was complemented in the *xmpp gsda::sX* line. Also in contrast to the seeds, the complementation line *xmpp gsda::sX* did not show a strong reduction of GTP concentration below wild-type level. The metabolite profile across the genotypes with the highest concentration occurring in the *XMPP GSDA* double mutant is in tendency observed for all other nucleotides. Although statistical tests revealed that most concentration differences were observed by chance ($p > 0.05$), similar differences were repeatedly observed for all metabolites. The repetitiveness of differences across all metabolites and the consistency with the results of the seed metabolite analysis support their veracity. It is important to bear in mind that the high guanosine concentration of the *gsda* background is causing the inhibition of NSH1 which results in increased xanthosine (Fig. 22), inosine (Fig. A - 7), and also adenosine concentrations (not shown). The accumulation of adenylates and IMP may thus also be caused by elevated adenosine and inosine levels and not or not only by active balancing of adenylate and guanylate ratios.

Interestingly, the metabolite profiles across the genotypes are becoming more pronounced after 48 h of extended darkness, although the nucleotide concentrations decreased in tendency (Fig. 24). Another interesting observation is that nucleotide concentrations in wild-type seedlings initially increased in tendency in the first six hours of extended darkness, which led to statistically significant ($p < 0.05$) concentration differences of ADP, GDP and GMP at 6 h and 48 h of darkness (Fig. 25).

Main conclusions from the metabolite analysis of seedlings exposed to an extended night:

- I) Again *XMPP* mutation alone did not show any effect on the concentrations of purine catabolic intermediates.
- II) In the *gsda* background, the involvement of *XMPP* in purine catabolism was demonstrated in non-stressed and more prominently in dark-stressed seedlings.
- III) The absence of an effect on guanylate levels in the complementation line may indicate that guanylate homeostasis in seedlings is regulated differently than in seeds.
- IV) Uric acid and allantoate continuously accumulate in the extended night.
- V) Xanthosine, inosine, hypoxanthine and allantoate concentrations and in tendency all purine nucleotide concentrations are influenced by light.
- VI) Purine nucleotide concentrations increase during the first six hours of extended darkness, but decrease overall in 48 hours.

Figure 24 Purine nucleotide concentrations in XMPP genetic variants in the context of other mutants of purine catabolism genes in seedlings under long-day or extended-night conditions. In an independent experiment plant material was generated as described in figure 22, but with different harvest time points. Seedlings were harvested at the end of the fifth night after germination, and after 6 h and 48 h of extended night. The complementation line *xmpp gsda::sX* contained a transgene encoding an N-terminally TwinStrep-tagged XMPP under the control of the native promoter (Fig. A - 4). Error bars are SD, $n_b = 4 - 5$. Two-sided Tukey's pairwise comparisons using the sandwich variance estimator were employed for statistical analyses. Different letters indicate p values < 0.05. Samples from long-day, 6 h and 48 h extended-darkness conditions were independently analyzed indicated by small and capital letters. Nucleotide quantification was performed by Henryk Straube according to Straube *et al.* (2021).



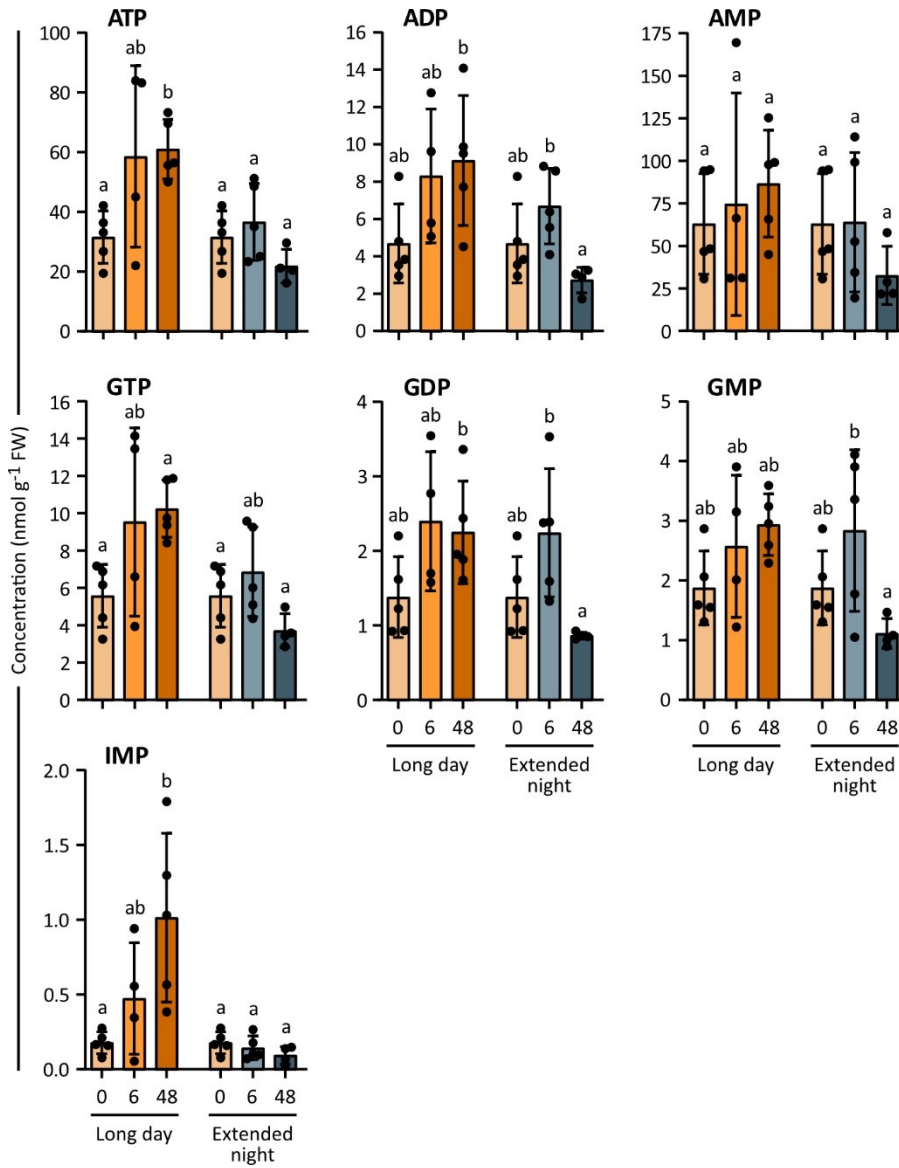


Figure 25 Purine nucleotide concentrations in wild-type seedlings under long-day or extended-night conditions. Metabolite data of wild-type seedlings exposed to extended darkness are the same as for figure 24. In parallel of this experiment, seedlings kept under long-day conditions for 6 h and 48 h after the end of the fifth night after germination were also analyzed. Bars representing nucleotide concentrations at the end of the night ("0") were duplicated for better comparability to the 6 h and 48 h bars. Error bars are SD, n_b = 4 - 5. Two-sided Tukey's pairwise comparisons using the sandwich variance estimator were employed for statistical analyses. Different letters indicate p values < 0.05. Nucleotide quantification was performed by Henryk Straube according to Straube *et al.* (2021).

4.4.4 XMPP in Arabidopsis rosette leaves

XMPP expression in leaves of four-week-old plants is relatively low compared to other tissues (Klepikova *et al.*, 2016). The absence of xanthosine in four-week-old *nsh1 gsdA* rosettes observed by Baccolini and Witte (2019) compared with the xanthosine concentrations in seeds and seedlings of the same mutant, indicate that XMPP is not operative in the vegetative rosette. Here, a comprehensive experiment was performed to investigate the role of XMPP in the vegetative rosette, to test its activation in extended darkness, and to assess whether XMPP plays a role in the reproductive rosette during seed development. The genotypes *xmpp*, *gsdA*, *nsh1*, *xmpp gsdA*, *xmpp gsdA::X*, *nsh1 gsdA* and wild-type Arabidopsis were included in this experiment. The complementation line *xmpp gsdA::X* contains a transgene encoding an untagged XMPP under the control of the 35S promoter. Arabidopsis were grown under long-day conditions for four weeks. Just before bolting one third of the plants was exposed to 48 h of darkness starting at the end of the night. Another third remained under long-day conditions for 48 h. The last third continued to grow under long-day conditions for three more weeks until they were producing seeds. At harvest, each rosette was divided into young and old leaves which were analyzed regarding their allantoate, xanthosine, guanosine, guanine and inosine contents. Because metabolite concentrations in rosette leaves were generally lower than in seedlings, no attempt was made to analyze allantoin concentrations in rosettes (Baccolini and Witte, 2019). From the same material, samples were taken to produce immunoblots with the aim to correlate metabolite data with the induction of the XMPP protein. Moreover, immunoblots for the detection of GSDA, NSH1 and XDH were supposed to give a broader view on how other enzymes of the purine catabolism are affected. For clarity, detailed results are only presented for young leaves. Figure A – 9 gives an impression of the metabolite concentrations in old leaves.

As expected, the mutation of *GSDA* in non-stressed vegetative rosettes was sufficient to prevent allantoate production in *gsdA* rosettes and to suppress xanthosine accumulation in *nsh1 gsdA* rosettes completely (Fig. 26A). Although this supports the notion that XMPP is not operative in non-stressed vegetative rosettes, the allantoate concentration was slightly but significantly reduced in *xmpp* compared to the wild type. This indicates that XMPP might also play a role in non-stressed vegetative rosettes. It is noteworthy that the overexpressed transgene of the complementation line *xmpp gsdA::X* was overcompensating the loss of XMPP leading to an allantoate concentration as in the wild type, whereas allantoate was generally not detectable in the *gsdA* background. The overcompensation of the complementation line may be attributed to its constitutively high XMPP protein amounts, which are normally so low that they cannot be detected in extracts of wild-type non-stressed vegetative rosette (Fig. 27B). Another interesting observation was that non-stressed vegetative rosettes of the *GSDA* mutant did not accumulate more guanosine than wild-type rosettes (Fig. 26A). Small increases of the guanosine concentration in such rosettes were observed for the *nsh1 gsdA* and in tendency for the *xmpp gsdA* lines. This agrees with the assumption that remobilization of nutrients and therefore also the purine catabolism are only weakly operative in non-stressed vegetative rosettes. Consistently, the concentrations of the purine metabolites in non-stressed vegetative rosettes are comparatively low (A - 9). Although metabolite data suggest that XMPP might be operative in non-stressed vegetative rosettes, XMPP protein could not be detected (Fig. 27A). By contrast, GSDA and also NSH1 and XDH proteins were clearly present. Despite the presence of GSDA, the enzyme does not appear to be required, as guanosine concentration in the *GSDA* mutant was similar as in the wild type (Fig. 26A).

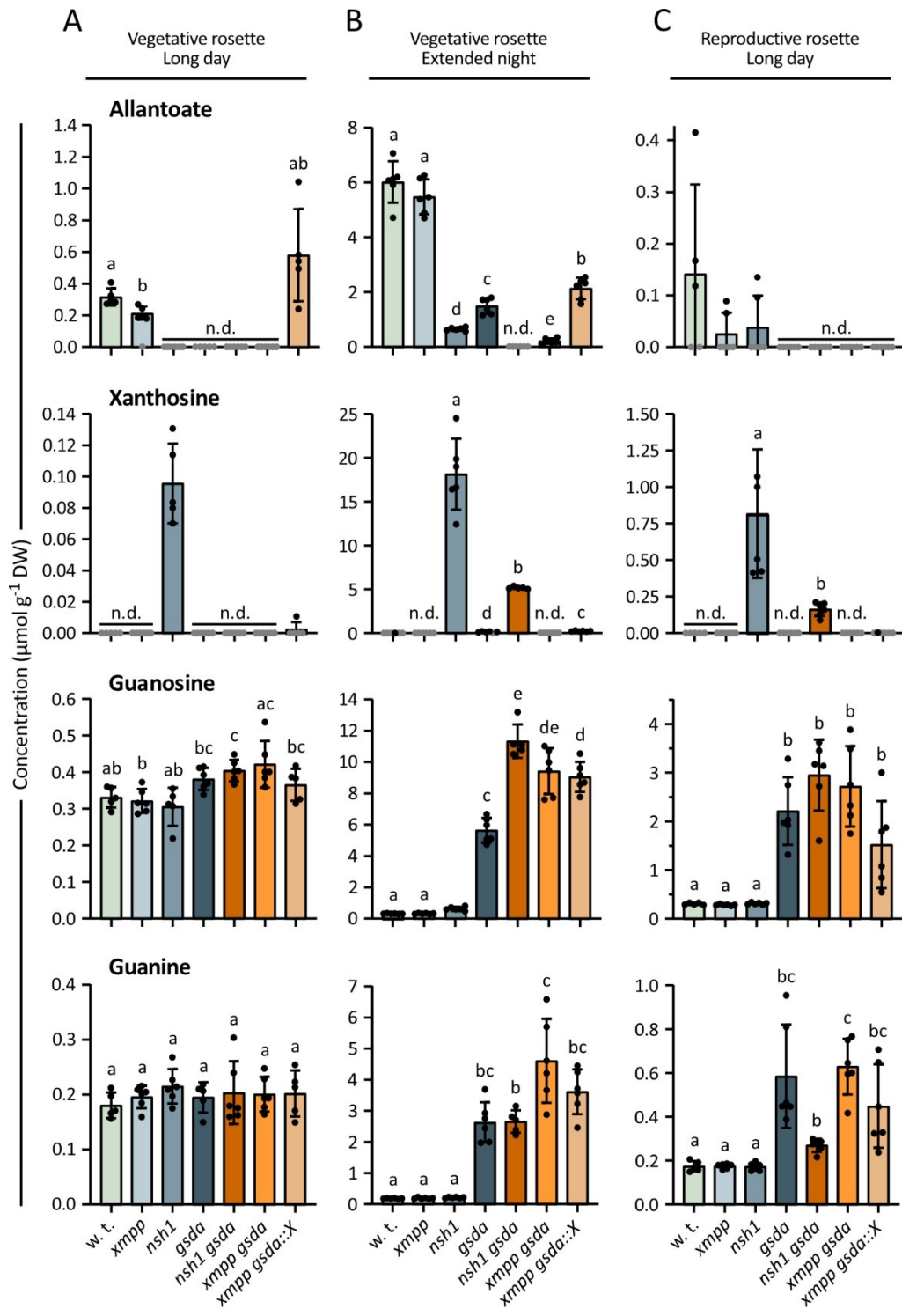


Figure 26 Quantification of intermediates downstream of XMP in XMPP genetic variants in the context of other mutants of purine catabolism genes in vegetative rosettes, dark-stressed vegetative rosettes and reproductive rosettes. Arabidopsis were grown under long-day conditions (16 h day/ 8 h night, 22°C/ 20°C). After four weeks, at the time before bolting, one third of the plants were subjected to 48 h of darkness beginning at the end of the night (A). Another third stayed for the same time under long-day conditions (B). Another third was grown three more weeks under long-day conditions until seeds were being produced (C). Rosettes were separated into young leaves and old leaves. Detailed results are only presented for young leaves. Figure A - 9 gives an impression of the metabolite concentrations in old leaves. Samples of plant material used for metabolite analysis was used to prepare immunoblots for the detection of XMPP, GSDA, NSH1 and XDH proteins (Fig. 27). The complementation line *xmpp gsda::X* contained a transgene encoding an untagged XMPP under the control of the 35S promoter (Fig. A - 4). Error bars are SD, $n_b = 5 - 6$. Measurements that failed quality criteria (Chapter 7.8) were called not detected (“n.d.”) are shown as grey data points set to 0. Statistical analysis was performed with groups that comprised at least three valid measurements. Two-sided Tukey’s pairwise comparisons using the sandwich variance estimator were employed for statistical analyses. Different letters indicate p values < 0.05 .

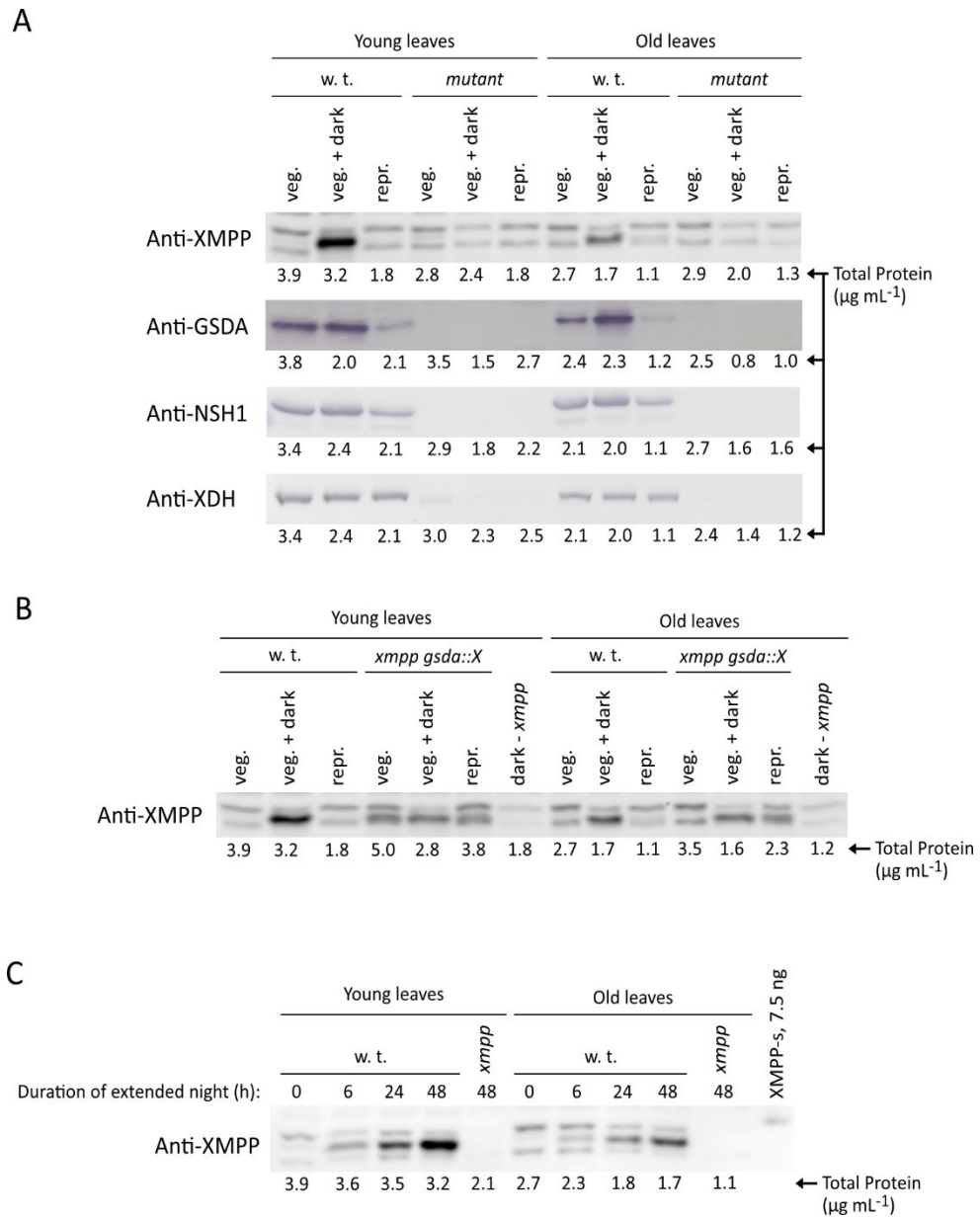


Figure 27 Immunoblots for XMPP, GSDA, NSH1 and XDH detection in extracts of vegetative rosettes, dark-stressed vegetative rosettes and reproductive rosettes. Immunoblots correspond to metabolite data of figure 26 for which experimental details are described. Bands corresponding to the proteins of interest were identified by comparison with the respective mutant (*xmpp*, *gsda*, *nsh1*, *xdh*) which lack this band. Equal sample volumes were used for each individual blot (15 μL for all but 40 μL for anti-XDH immunoblot). The total protein concentration for each sample is given. **A**, Detection of XMPP, GSDA, NSH1 and XDH proteins in rosette extracts. **B**, Comparison of detected XMPP protein in the wild type and the complementation line *xmpp gsda::X*. The complementation line contained a transgene encoding an untagged XMPP under the control of the 35S promoter. **C**, Time course monitoring the formation of XMPP protein in the extended night. For comparison 7.5 ng of purified XMPP-HAStrep (XMPP-s) was loaded.

Results

In extended darkness purine catabolism was strongly induced resulting in the increase of xanthosine in *nsh1*, guanosine in *gsda* and allantoate in wild-type young rosette leaves by factors 190x, 15x and 26x, respectively (Fig. A - 9). The effect was especially strong in young rosette leaves but was also observed in old rosette leaves. The dark-induced activation of purine catabolism was accompanied by the fact that the *GSDA* mutation was no longer sufficient to prevent allantoate production in *gsda* or xanthosine accumulation in *nsh1 gsda* vegetative rosettes (Fig. 26B). Note, small concentrations of xanthosine and allantoate observed in mutants with *xmpp gsda* or *nsh1* background, may derive from chemical decomposition of the accumulating nucleosides. In case of *NSH1* mutants, background nucleoside hydrolase activity independent of *NSH1* may also be responsible (Jung *et al.*, 2011; Riegler *et al.*, 2011). The additional *XMPP* mutation in *xmpp gsda* clearly reduced allantoate production which was complemented in *xmpp gsda::X*, demonstrating the involvement of *XMPP* in dark-stress induced purine catabolism (Fig. 26B). Note that the prolonged darkness caused the same allantoate accumulation in the *XMPP* mutant as in the wild type, although in the non-stressed rosette there was a slight difference between these two genotypes regarding the allantoate concentration (Fig. 26A, B).

In non-stressed vegetative rosettes, the guanosine concentrations in all genotypes were almost equal and quite low but increased strongly in the extended night, in particular in lines with *gsda* background (Fig. 26A, B). The additional mutation of *XMPP* or *NSH1* in the *gsda* background led to the hyperaccumulation of guanosine as already observed for seeds and seedlings. The strong dark-induced guanosine accumulation in *gsda* rosettes likely caused the inhibition of *NSH1* and thereby the accumulation of xanthosine and inosine, also as previously discussed for seeds and seedlings (Fig. 26B, A – 8). The inosine accumulation was increased in *xmpp gsda* compared to *gsda* rosettes possibly because the higher guanosine content of this double mutant has a stronger inhibitory effect on *NSH1/2*. The *NSH1 GSDA* double mutant exposed to prolonged darkness showed a strikingly high concentration of inosine in contrast to *nsh1*. This cannot be explained by the current model. Since dark-stressed rosettes with *gsda* background accumulate high levels of guanosine, guanine, and putatively guanylates, a feedback control mechanism might inhibit GMP biosynthesis maybe leading to an increased IMP concentration and increased IMP dephosphorylation. Quantification of nucleotides under these conditions could provide insights. Note, inosine concentrations in dark-stressed *nsh1* rosettes were more than two orders of magnitude lower than the corresponding xanthosine concentrations. Thus, the IMP – inosine – hypoxanthine route is not considered relevant to purine nucleotide catabolism in extended darkness. As inosine concentrations in the non-stressed vegetative rosettes and in the reproductive rosettes of the *NSH1* mutant were also one order of magnitude lower than the corresponding xanthosine concentrations, this route is apparently not relevant for purine nucleotide degradation in general.

Although metabolite data show that purine degradation is strongly induced in prolonged darkness, no correlating increase in protein amounts of *GSDA*, *NSH1*, and *XDH* relative to leaf weight was observed (Fig. 27A). Only the amount of *GSDA* increased in old leaves during the prolonged night. Total protein content became smaller in the 48 h of extended darkness, especially in young leaves, while the amount of purine catabolic enzymes remained constant or even increased, as observed for *XMPP* in general and for *GSDA* in old leaves. Two conclusions can be drawn so far. I) The relative protein concentration of purine catabolic enzymes to total protein concentration is increasing in the extended night – because total protein concentration decreases – supporting the view that purine catabolism plays an important role under these conditions. II) Protein amounts of *GSDA*, *NSH1* and *XDH* are constitutively high in vegetative rosettes. The fact that *GSDA*, *NSH1*, and *XDH* were able to cope with the increased flux through the metabolic pathway during prolonged darkness without increased protein levels suggests that their capacities in the non-stressed vegetative rosette are significantly

higher than would be required to meet metabolic demands. A reason that could explain the maintenance of such high unused protein levels could be the need for rapid activation of purine catabolism, as observed in the prolonged night. The large increase in XMPP protein under these conditions (Fig. 27C) combined with the metabolite data suggests that XMP dephosphorylation may represent a switchable entry reaction into purine catabolism.

Purine catabolism is not only induced in the extended night, but metabolite pool sizes also suggest that it is induced in the reproductive phase. Concentrations of xanthosine in *nsh1* and guanosine in *gsda* were fivefold higher in the reproductive rosette than in the non-stressed vegetative rosette (Fig. A - 9). A higher concentration was expected, as the seven-week-old reproductive rosettes had three more weeks to accumulate guanosine or xanthosine depending on their genotype. A fivefold increase was however significantly more than what would be expected just because of time. Although the purine catabolism is apparently induced in senescing leaves, the allantoate concentration in the wild-type reproductive rosette was lower than in the non-stressed vegetative rosette (Fig. 26A, C). Allantoate can be fully degraded to release ammonia, which can subsequently be reassimilated into amino acids and transported to the seeds (Werner and Witte, 2011). The allantoate that is produced in the reproductive phase is thus likely not accumulating because it is further degraded for nitrogen remobilization. This again raises the question about the purpose of the ureide accumulation in extended darkness.

Metabolite analysis in reproductive rosettes suggests that purine catabolism is induced and XMPP is operative in rosettes during seed production. Although XMPP protein could not be detected in reproductive rosettes, xanthosine accumulation in *gsda nsh1* supports the assumption that XMPP is operative (Fig. 26A, C). NSH1 and XDH protein amounts per leaf weight were almost unchanged in the reproductive rosettes compared with the non-stressed vegetative rosette despite a marked decrease in total protein concentration. A slight reduction in protein amount was observed for NSH1. GSDA protein amounts per leaf weight were considerably reduced. Nevertheless, the protein amount was sufficient to process the induced flux in leaf senescence without increasing guanosine concentration in the wild type.

Main conclusions from metabolite analyses and immunoblots of non-stressed vegetative, dark-stressed vegetative and reproductive rosettes:

- I) XMPP is involved in purine catabolism especially in dark-stressed vegetative rosettes and reproductive rosettes, but also plays a less pronounced role in non-stressed vegetative rosettes.
- II) Even XMPP protein amounts below the detection level in immunoblots contribute to purine catabolism.
- III) The XMPP protein amount is strongly increasing in the course of extended darkness.
- IV) Allantoate accumulates in rosettes exposed to extended darkness but not in reproductive rosettes.
- V) GSDA, NSH1 and XDH proteins are fairly stable under all conditions representing more metabolic capacity than required in most situations and potentially allowing for rapid flux changes through purine catabolism.

5 Discussion

5.1 Identification of enzymes and transporters involved in nodule ureide biosynthesis of tropical legumes

A comparative transcript dataset was compiled by Dr. Marco Herde to identify so far unknown enzymes and transporters which are involved in the ureide biosynthesis in nodules of tropical legumes. The condensed candidate list comprised genes which were induced in nodules compared to roots of the two ureide-exporting legumes common bean and soybean but which were not induced in nodules compared to roots of the amide-exporting legumes *M. truncatula* and *L. japonicus* (Tab. 1, Fig. 4). All genes known to be involved in the ureide biosynthesis were included in the candidate list, which validated the approach. For the *XMPP* candidate, which was highly induced in nodules of common bean and soybean, an involvement in ureide biosynthesis could be demonstrated (Fig. 12). The identification of *XMPP* shows that the candidate list can be used to identify genes involved in ureide biosynthesis, which includes yet unidentified genes for transport processes as described in chapter 3.6.

It is important to note, that the use of this candidate list requires background knowledge for the selection of candidates. The ureide biosynthesis is not the only process which is induced in nodule *versus* roots of ureide-exporting legumes but not in amide-exporting legumes. A multitude of genes participating in signaling, developmental and metabolic processes are regulated in the described fashion and make up the greatest part of the candidate list. In case of *XMPP*, the selection was based on the previous identification of the *SDTL* gene family in Arabidopsis which are homologs of known yeast NMP phosphatases *SDT1* and *PHM8* (Zhu, 2016). Accordingly, the candidate list could be used to search for homologs of already known metabolite transporters like monosaccharide transporters (Büttner, 2007) or the adenylate transporter *BT1* (Kirchberger et al., 2008) to identify the plastidic ribose importer or the potential plastidic IMP exporter, respectively (Fig. 4: #30 and #32).

5.2 Characterization of *XMPP*, *GSDA*, and *XDH* in nodule ureide biosynthesis

5.2.1 Production of mutant nodules

The procedure for the production of transgenic soybean nodules was successfully established in our laboratory (Fig. 8). For the production of knockout nodules, the CRISPR-Cas9 technology was used to induce nonsense mutations in target genes. A method for fragment length analysis (FLA) was established to identify roots and nodules with tetraallelic gene knockouts. In case of the soybean *XMPP* CRISPR hairy roots, the FLA was successfully used to estimate the mutation rate for each gRNA binding site (Fig. 11). In contrast to diploid plants like Arabidopsis, commercial sequencing to identify potential mutations was not an option here. Because soybean is tetraallelic, up to four different mutations can occur per gene, which can lead to the overlay of up to four different chromatograms in commercial sequencing. It is however not possible to unravel the overlay of more than two chromatographic tracks. Although the result of a FLA has a lower information content compared to sequencing, it can be used to identify nodules which lack wild-type alleles by assessing whether fragments of wild-type size are present in the samples. In the absence of such fragments and if the size difference of the generated other fragments is not 3 bp or a multiple of 3 bp compared to the wild-type fragment, the sample could be considered a tetraallelic gene knockout (Fig. A - 2). Some effective knockouts can be

missed by the method, for example when stop codons are generated while the fragment length does not change or changes by a multiple of 3 bp. The same applies to mutations which alter splicing sites and thereby disturb the proper processing of the transcript and to non-conservative missense mutations, which can cause proteins to lose their function by altering conserved amino acids. Note, in the two latter examples mutations may or may not necessarily lead to the loss of the functional protein. Even if the FLA cannot detect all knockouts, this method represents an important advance, because it offers the possibility to find successful knockouts in the first place, which was so far not possible for soybean. For this work FLA was not established beyond the proof of concept because the first *XMPP* CRISPR results indicated that the mutation rate was insufficient and further experiments in soybean were abandoned due to time reasons.

A method introduced in our laboratory that increased the chance of producing knockout nodules, was an *in vitro* test system for gRNAs. This test system allows to test different gRNAs and select the one that works best *in vitro* (Foresti, 2020). If this method had been already available when the gRNAs for the soybean *XMPP* were designed, other gRNA than the ineffective *XMPP1* gRNA 1 and *XMPP2* gRNA 2 might have been selected (Fig. 11). However, the curious case of the shared gRNA 3 which induced mutations in only one of the paralogs probably could not have been prevented. Nevertheless, any aspect that may increase knockout rates should be considered to be able to produce sufficient mutant nodules for metabolite analysis.

The metabolite data from the soybean *XDH* CRISPR nodules indicated that the knockout rate was 49% (Fig. 10). This shows that the characterization of genes with the established soybean pipeline can work. For the more complex cases like *GSDA* with its five paralogs or *XMPP* with its placement at a branch point of the pathway, it was not possible to elucidate their roles in soybean nodules. The investigation of *XMPP* in soybean nodules failed first of all because of the low mutation rate. Another obstacle was that the generation and detection of complete gene knockouts was difficult. For genetic characterization of one *GSDA* CRISPR nodule pool, six FLAs would have been required to analyze two gRNA binding sites in each of the three paralogs. Moreover, in such a complicated case, the probability of generating knockout nodules is also relatively low. With three *GSDA* paralogs and four alleles per paralog, twelve alleles would have had to be successfully knocked out simultaneously for the nodule pool to be considered successfully mutated. For the analysis of *XMPP* and *GSDA*, the use of diploid common bean could simplify the performance and analysis experiments to eventually obtain conclusive results. In a joint effort of several laboratory members combining gRNA tested *in vitro* provided by William Foresti, the transfer of the procedure for nodule generation from soybean to common bean and the FLA-based identification of knockout nodules by Luisa Voss, and the metabolite analysis performed by me eventually, allowed the generation, identification and full analysis of *xmpp* nodules from a tropical legume (Fig. 12).

5.2.2 XMP dephosphorylation is possibly the main route to ureide production

In vitro activity of purified soybean *XMPP2*-HASTrep with XMP was demonstrated and kinetic constants of $K_M = 10.4 \pm 1.5 \mu\text{M}$ and $k_{\text{cat}} = 14 \pm 0.5 \text{ s}^{-1}$ were determined (Fig. 5). The accumulation of XMP and the considerable reduction in allantoin and allantoate concentrations in common bean *xmpp* nodules showed that *XMPP* catalyzes dephosphorylation of XMP also *in vivo* (Fig. 12). It had been suggested before that XMP dephosphorylation might be involved in ureide biosynthesis in legume nodules. Triplett *et al.* (1980) showed that allantoate was formed in the cytosolic fraction isolated from soybean nodules with IMP, inosine, hypoxanthine, XMP, xanthosine and xanthine as substrates. Atkins (1981) reported that allantoate was similarly produced in cell-free extracts from cowpea nodules supplied

Discussion

with XMP and IMP. Shelp and Atkins (1983) investigated possible routes for the ureide production by supplying cell-free extracts of cowpea nodules with ^{14}C -labelled IMP and glycine, which is used in the purine nucleotide biosynthesis. The authors observed that there are likely two main routes in ureide biosynthesis, one is the IMP - inosine - hypoxanthine route and the other is the IMP - XMP - xanthosine - xanthine route. Interestingly, it was observed that when the amount of ^{14}C -IMP added to the extract was reduced, the proportion of the ureides contributed by the IMP - inosine - hypoxanthine route also decreased. This observation indicates that the IMP catabolic route is likely biochemically favored by the high ^{14}C -IMP concentration. When ^{14}C -glycine was applied, the XMP dephosphorylation was the dominant route indicating that it may be the main route for ureide biosynthesis *in vivo*. Data reported from Fujihara and Yamaguchi (1978), who treated nodulated soybeans with XDH inhibitor allopurinol, showed a strong reduction of allantoin and allantoate concentrations coinciding with a strong increase of xanthine however not of hypoxanthine, which suggests that IMP dephosphorylation is not part of ureide biosynthesis.

The impression obtained from Shelp and Atkins (1983) and Fujihara and Yamaguchi (1978) was supported by the findings presented here. Soybean *xdh* nodules accumulated $46 \mu\text{mol g}^{-1}$ DW xanthine and common bean *xdh* nodules $21 \mu\text{mol g}^{-1}$ DW xanthine, whereas hypoxanthine concentrations did not increase compared to control nodules and were only 0.022 and $0.011 \mu\text{mol g}^{-1}$ DW, respectively (Fig. 12, Chapter 4.3). Having ruled out the involvement of IMP dephosphorylation in ureide production in nodules and confirmed the involvement of XMP dephosphorylation, the role of GMP dephosphorylation remains to be clarified. The loss of XMPP resulted in a significant increase in guanosine concentration and a reduction of ureide content in common bean nodules, suggesting that the loss of XMPP is partially but not completely compensated by the GMP – guanosine – xanthosine route (Fig. 12). By contrast, in none of the tested *Arabidopsis* tissues and under none of the tested conditions the *XMPP* mutation caused an accumulation of guanosine or such a clear reduction of ureides (Fig. 18, 22, 26). The catalytic capacities of GMPS, GMPP and GSDA are sufficient in *Arabidopsis* to process the additional XMP, GMP and guanosine, respectively, originating from the lack of XMP degradation in *xmpp* background. However, the capacity of these enzymes seems to be insufficient in common bean *xmpp* nodules, maybe because the flux through purine catabolism is significantly higher in ureide-producing nodules. Although the *GSDA* expression was induced in nodules compared to roots of the ureide exporting legumes, the guanosine accumulation indicates that it is a rate-limiting step when the metabolic flux is diverted into the GMP catabolic route in *xmpp* nodules (Tab. 1, Fig. 12). This is in line with the observation of Atkins (1981) that GMP supplied to cell-free cowpea nodule extracts cannot be used as efficiently for ureide production as XMP. In summary, the findings indicate that the main route to ureide biosynthesis proceeds through XMP dephosphorylation. To question whether the route through GMP contributes to ureide biosynthesis or whether it is not involved can be assessed by the generation and metabolite analysis of *gsda* nodules. If guanosine and ureide concentrations were not affected in this genetic background, the involvement of the GMP catabolism could be excluded. However, it has to be considered that in *gsda* background potentially accumulating guanosine can have an inhibitory effect on NSH1/2 as described in the *Arabidopsis* seeds (Chapter 4.4.2). The occupation of NSH1/2 capacity by accumulated guanosine is likely the reason for the increased xanthosine and inosine concentrations in dry *Arabidopsis gsda* seeds (Fig. 18, A - 6). This is also a possible explanation for the increased xanthosine and inosine concentrations observed in *xmpp* nodules (Fig. 12). The increase of guanosine caused by the mutation of *XMPP* might also here partially inhibit NSH1/2, which is required for inosine and in context of ureide biosynthesis especially for xanthosine degradation.

Another interesting finding and possible starting point for more experiments is the observation that xanthine crystals in soybean *xdh* nodules exclusively occurred in the uninfected cells. This is

inconsistent with the current model in which the ureide biosynthesis pathway leaves the infected cells at the stage of uric acid by its export into the uninfected cells (Vaughn *et al.*, 1982; Shelp and Atkins, 1983; Smith and Atkins, 2002). It remains however unknown whether xanthine is produced in uninfected cells – in this case ureide biosynthesis would leave the infected cell already at the stage of xanthosine – or whether it is transported from the infected to the uninfected cells. Nguyen *et al.* (1986) suggested based on immunofluorescence experiments that XDH is located in uninfected cells, whereas the histochemical experiments by Triplett (1985) indicated that XDH activity is mainly restricted to the infected cells. To clarify the localization of proteins involved in ureide biosynthesis, nodules expressing respective reporter fusion proteins could be analyzed using confocal laser microscopy. Transgenic soybean hairy roots could be produced that express such fusion proteins. Inoculation with transgenic fluorescent rhizobia would allow the formation of nodules in which infected and uninfected cells can be easily distinguished (Ledermann *et al.*, 2015). Cross sections similar to the ones presented in figure 9A could be analyzed using confocal laser microscopy. Similarly, the cell type-specific expression of the respective genes could be analyzed by a promoter-reporter study. The localization of *XDH* promoter activity and the XDH fusion protein could be especially interesting. A localization of XDH only in uninfected cells would be another indication that IMP dephosphorylation is not part of ureide biosynthesis. Since IMP is formed in infected nodules, IMP degradation in these cells would end with hypoxanthine, because XDH would be required to generate xanthine from it.

5.3 Characterization of the XMP Phosphatase of Arabidopsis

5.3.1 XMP dephosphorylation is an entry point for purine nucleotide catabolism

In addition to characterizing XMPP in soybean and common bean nodules, this study also aimed to examine the function of its homolog in Arabidopsis. IMP derived from purine *de-novo* biosynthesis can flow into GMP biosynthesis (Fig. 3). In this process, IMP is oxidized by IMPDHs to XMP which is aminated by GMPS to GMP. XMP can also be dephosphorylated, as presented in this thesis. This reaction bifurcates from GMP biosynthesis in the cytosol and initiates the irreversible degradation of XMP. Accordingly, it has been shown previously that an XMPP-YFP fusion protein localized in the cytosol after transient expression in *N. benthamiana* leaves (Zhu, 2016). XMPP-HAStrep was transiently expressed from cDNA in *N. benthamiana* leaves and affinity purified. A substrate screen including common phosphatase substrates and purine and pyrimidine ribo- and deoxymononucleotides was performed which showed that XMPP is highly specific for XMP (Fig. 14C). This is unusual compared to many other phosphatases and also compared to its homologs SCTL2 to 4 which showed activity with three to four substrates (Zhu, 2016). The C-terminally and also an N-terminally Strep-tagged variant showed similar activity with XMP as substrate (Fig. 14A, B). Two conclusions were drawn. First, the tags at different ends of the protein did not cause differing enzyme activities. Second, the K_M values of the XMPP variants were comparatively low at 3 - 4 μM in contrast to K_M values of 60 and 264 μM of the NSH1/2 heterocomplex for xanthosine and GSDA for guanosine, respectively. The catalytic efficiencies of C- and N-terminally tagged XMPP variants were especially high with 2200 and 2359 $\text{s}^{-1} \text{mM}^{-1}$, respectively, in comparison with catalytic efficiencies of NSH1/2 heterocomplex with xanthosine and GSDA with guanosine of 388 and 6.6 $\text{s}^{-1} \text{mM}^{-1}$ (Dahncke and Witte, 2013; Baccolini and Witte, 2019). In summary, substrate specificity and catalytic efficiency suggest that XMPP may have a role requiring great specificity and high activity. There are two enzymes that can use the low-concentrated XMP in the cytosol, XMPP and GMPS. Since the XMPP protein concentration can moreover increase strongly, as was observed during the extended night, it can be assumed that the abundant XMPP, with its high

substrate affinity and catalytic efficiency, could deprive GMPS and thus GMP biosynthesis of XMP when it initiates purine catabolism under such conditions. The high substrate specificity could be important to prevent the abundant XMPP from causing unwanted dephosphorylation of other nucleotides.

Because of its localization in the pathway, XMPP can initiate purine catabolism independently of GMP biosynthesis. An initial assumption was therefore that XMPP may allow to reduce the adenylate content contributing to the adenylate-guanylate homeostasis. Mammals do not possess XMPP but express IMPDHs containing a so-called Bate domain (Buey *et al.*, 2015). The Bate domain comprises six nucleotide binding pockets which depending on the adenylate to guanylate ratio changes its conformation (Johnson and Kollman, 2020). When mainly guanylates are bound, IMPDHs form inactive monomers which can polymerize upon increased binding of adenylates to active IMPDH filaments directing the metabolic flux into GMP biosynthesis (Johnson and Kollman, 2020). Plant IMPDHs lack such a Bate domain and are thus unlikely to regulate the adenylate/guanylate ratio. Therefore, it seemed plausible to assume that XMPP might play such a role in plants. If this was true, the absence of XMPP under conditions that actually increase its protein amount should lead to an imbalance in adenylate and guanylate homeostasis. This however was not observed in the purine nucleotide analysis of dark-stressed seedlings (Fig. 24). Although the *XMPP* mutation caused increased flux via the catabolic GMP route, as indicated by the hyperaccumulation of guanosine in *xmpp gsda* seedlings, there was no increase in guanosine, guanylates or adenylates in the *XMPP* single mutant. This indicates that XMPP is not required for the maintenance of the adenylate/guanylate homeostasis and that GMPP and GSDA are sufficient to metabolize for the additional input into the GMP and guanosine pools in *xmpp seeds*. To clarify the function of XMPP in Arabidopsis, analyses of *XMPP* genetic variants in comparison with other mutants of purine catabolism were performed with seeds, seedlings in the context of an extended night, and in rosettes in the context of an extended night and during seed production.

5.3.2 XMPP in seed development

The involvement of XMPP in purine catabolism was demonstrated by the accumulation of XMP in *xmpp* seeds (Fig. 17). This was however the only detected metabolic change of *xmpp* seeds in comparison with wild-type seeds (Fig. 17, 18). The hyperaccumulation of guanosine in *xmpp gsda* seeds showed that the loss of XMPP can be compensated by the GMP catabolic route, which is why no change in other metabolite pools, was observed. The increased input to the catabolic GMP route did not cause changes in guanylate and guanosine pool sizes in *xmpp* seeds, which indicates that GMPP and GSDA are sufficient to maintain the GMP and guanosine homeostasis. Although the absence of XMPP in *xmpp* seeds did not have any other effect than the XMP accumulation, the presence of an *XMPP* transgene in the *xmpp nsh1 gsda::sX* complementation line caused a fourteen-fold reduction of the GTP concentration compared to the *nsh1 gsda* line. The complementation line expressed genomic DNA for an N-terminally TwinStrep-tagged XMPP variant under the control of the native promoter. The XMPP amount in this line seemed moderately elevated compared to the wild type in seedling extracts (Fig. A - 4). The more abundant XMPP protein concentration in the complementation line may have caused a decrease of the guanylate amounts by an elevated XMP dephosphorylation rate hindering the XMP to GMP conversion by GMPS. However, neither GDP, GMP nor guanosine concentrations were reduced in *xmpp nsh1 gsda::sX* compared to *nsh1 gsda* seeds (Fig. 17, 18). The reduction of GTP might be not only caused by the alteration of metabolic fluxes but possibly also by specific regulatory processes. It would be interesting to quantify the GTP concentration in *xmpp::sX* seeds to test whether

the strong reduction of GTP is caused by the *XMPP* transgene independently of the impact of the *NSH1* and *GSDA* mutations. Another interesting observation is that the decrease in GTP concentration was accompanied by a less pronounced but considerable decrease in ATP concentration and an increase in ADP concentration. It appears that the dephosphorylation of ATP may be a measure to adjust ATP to GTP concentrations. This suggests that ATP/GTP homeostasis can be regulated independently of *XMPP*. Nevertheless, the data also indicate that the unphysiological presence of *XMPP*, as in the complementation line, can disturb purine nucleotide homeostasis. This could be one reason why the enzyme itself is not constitutively present, but is produced only under certain conditions.

The quantification of uric acid in seeds used for the *uox* suppressor test showed again that the *XMPP* mutation alone does not alter pool sizes of the purine catabolic metabolites (Fig. 21). Nevertheless, *xmpp uox* seeds showed an 18% higher germination rate compared to *uox* seeds. Despite the increased germination rate viable seedlings were not established. This can be attributed to the unchanged high uric acid concentration in *xmpp uox* seeds, which is known to prevent seedling establishment. Uric acid disturbs glyoxysome function impairing the β -oxidation of fatty acids and the remobilization of energy from the lipid bodies (Hauck *et al.*, 2014). The lack of energy prevents the establishment of seedlings but can be compensated by application of sucrose. When *xmpp uox* seeds of a segregating population were germinated on agar plates supplemented with 1% sucrose some seedlings developed purple or transparent cotyledons. These seedlings could be homozygous double mutants, but this was not examined. The seedlings phenotype was only observed for the *XMPP UOX* but not for *GSDA UOX* double mutant. Hauck *et al.* observed that *UOX* mutants commonly fail to develop cotyledons, but the strength of the phenotype was dependent on the seed batch. Therefore the occurrence of purple and transparent cotyledons was likely caused by the additional *XMPP* mutation. A conclusive experiment with homogenous *xmpp uox* seeds in comparison with *uox*, *xmpp* and wild-type seeds also including other known *uox* suppressors germinated on sucrose supplemented agar plates could confirm this assumption. Reasons causing this phenotype were not further investigated because it is a highly artificial phenotype and probably no physiologically relevant conclusions could be drawn from them. The important aspect is that the phenotype indicates that *XMPP* might play a role in seedling development. The observation that the *XMPP* mutation partially inhibits the *uox* germination phenotype, although the total uric acid concentration remains unchanged, suggests that *XMPP* may be involved in tissue- or development-specific processes. Such an involvement might also explain why the seed yield of the *XMPP* mutant was considerably reduced although *xmpp* seeds did not show any altered metabolite pool sizes except for a small accumulation of XMP.

In non-legumes comparably little is known about the role of ureides in nitrogen metabolism. In perennial plants like comfrey and maple, ureides were shown to accumulate in dormant roots which supply the shoot with nitrogen in spring (Schubert and Boland, 1990). For the ureides allantoin and allantoate in *Arabidopsis*, it was proposed that they are used to transport nitrogen from old to young leaves under nitrogen-limited conditions (Soltabayeva *et al.*, 2018). Whether ureides can also be used for nitrogen storage in seeds was not considered so far. The metabolite analysis of *Arabidopsis* wild-type seeds showed that allantoin was present at $5.9 \mu\text{mol g}^{-1}$ which was exceptionally high in comparison to the concentrations of xanthosine and guanosine of 0.03 and $0.08 \mu\text{mol g}^{-1}$, respectively. Allantoin concentration was more similar to the xanthosine and guanosine concentrations in *nsh1* and *gsda* seeds which were 8.9 and $6.7 \mu\text{mol g}^{-1}$, respectively. This suggests that allantoin is not imported from the leaves into the seed during nitrogen remobilization but is formed in the seed. The purpose of the high allantoin concentration could be to store nitrogen, which could serve to supply the embryo during germination.

5.3.3 XMPP in seedlings and its role in the extended night

In dark-stressed seedlings the involvement of XMPP in purine catabolism was clearly demonstrated (Fig. 22). The wild-type steady state pools of uric acid and allantoate decreased to about 30% in *gsda* seedlings and to 2% in *xmpp gsda* seedlings. Similarly, in seedlings treated with the XDH inhibitor allopurinol before the start of the extended night, xanthine accumulation was significantly reduced in *gsda* seedlings compared to the wild type and not detectable anymore in *xmpp gsda* seedlings. The increase of xanthosine concentration caused by the partial inhibition of NSH1/2 due to the accumulated guanosine in *gsda* seedlings was suppressed in *xmpp gsda* seedlings indicating that XMPP is operative under these conditions. Similar to the observations in seeds, the additional XMPP mutation caused the hyperaccumulation of guanosine in *xmpp gsda* seedlings. This was also reflected in the purine nucleotide concentrations, especially in the guanylates, GTP in particular (Fig. 24). The general increase in purine nucleotide concentrations in seedlings with *gsda* background was less pronounced at the end of the normal night, possibly due to the lower guanosine concentrations under these conditions (Fig. 22). The absence of xanthosine accumulation in *gsda* seedlings at the end of the night can also be attributed to the lower guanosine concentration, which presumably had an accordingly smaller inhibitory effect on NHS1/2. On the basis of the increased guanosine, uric acid and allantoate concentrations, it can be assumed that the purine catabolism is induced in the extended night as previously described (Brychkova *et al.*, 2008; Baccolini, 2019). It is interesting to note that the guanosine hyperaccumulation of *xmpp gsda* seedlings in comparison to *gsda* seedlings was observed for the dark-stressed seedlings but not for the seedlings kept under long-day conditions (Fig. 22). Probably XMPP plays a minor role under long-day conditions. Nevertheless, the decrease of uric acid concentration in *xmpp gsda* seedlings compared to *gsda* seedlings suggested that XMPP might also be active under long-day conditions. Interestingly, uric acid and allantoate concentrations accumulate in the extended night although neither *UOX* nor *Allantoate Amidohydrolase (AAH)* were genetically blocked (Fig. 22, 23B). Brychkova *et al.* (2008) also observed the accumulation of ureides in dark-stressed rosettes and suggested that they act as ROS scavengers. In chapter 5.3.6 the role of XMPP and purine catabolism in extended darkness is discussed in detail.

5.3.4 XMPP in rosettes and in context of extended night and nutrient remobilization

A comprehensive experiment to assess the role of XMPP in purine nucleotide catabolism in *Arabidopsis* rosettes was performed. The focus laid on the inducibility of XMPP in the prolonged night and during seed development, as suggested by gene expression data (Fig. 16A). Plant material was split for metabolite analysis and generation of immunoblots to be able to relate metabolite data with relative XMPP, NSH1, GSDA and XDH protein amounts. Results presented by Baccolini and Witte (2019) showing that xanthosine accumulation in *nsh1* rosettes was fully suppressed in *nsh1 gsda* rosettes could be confirmed (Fig. 26A). This led to the assumption that XMPP is not operative in non-stressed vegetative rosettes. However, in this work a small reduction of the allantoate concentration was observed in the XMPP mutant, indicating that XMPP is to some extent operative in non-stressed vegetative rosettes. Although the XMPP protein could not be detected in the corresponding leaf extracts, it is possible that due to the high catalytic efficiency even low XMPP amounts can make a metabolic impact (Fig. 27A). In leaf extracts from seven-week-old rosettes, XMPP protein was not detected either, although xanthosine accumulation in the *nsh1 gsda* line can be attributed to XMPP function, based on similar results in seedlings (Fig. 22, 26C). The absence of XMPP protein in the

immunoblots does accordingly not exclude the participation of XMPP in purine catabolism. XMPP was clearly detected in extracts of dark-stressed rosettes and the signal was especially strong in extracts of young leaves (Fig. 27A). The immunoblot visualizing the XMPP amounts during the course of the extended night showed that XMPP protein could not be detected at the end of the night (Fig. 27C). However, it was detected already six hours later and the amounts continued to rise up to 48 h of extended darkness. An independently performed immunoblot produced with dark-stressed four-week-old rosettes showed that the XMPP protein could be clearly detected after only one hour of extended darkness (Fig. 16E).

Metabolite analysis of dark-stressed vegetative rosettes in comparison with non-stressed vegetative rosettes showed that the purine catabolism was strongly induced by prolonged darkness. This conclusion was deduced from the increased xanthosine and guanosine concentrations in the *nsh1* and *gsda* mutants in the dark (Fig. 26A, B). In dark-stressed rosettes, the hyperaccumulation of guanosine was observed in the *xmpp gsda* compared to the *gsda* mutant, which was only in tendency observed in non-stressed vegetative rosettes. This indicates that the XMP dephosphorylation may be more important in dark-stressed rosettes, which would also correlate with the strong induction of XMPP protein in extended darkness (Fig. 27C). However, non-stressed *xmpp* rosettes had a reduced allantoate content, which was not observed in dark-stressed *xmpp* rosettes. One possible explanation could be that prolonged darkness also induces vacuolar RNA degradation, which could attenuate the relative effect size of the *XMPP* mutation. Conclusions that can be drawn so far are: I) XMPP is operative in non-stressed vegetative rosettes. II) Purine catabolism is induced in the extended night. III) XMPP protein amounts strongly increase at the same time. IV) Xanthosine accumulation due to the lack of NSH1 is not fully suppressed by *GSDA* mutation anymore. These data demonstrate that XMPP plays a particularly important role in extended darkness. A quantitative statement is however not possible, because the *XMPP* mutation is compensated by the catabolic GMP route, the size of the contribution by vacuolar RNA degradation is unknown and the high accumulation of purine metabolites in mutants can have inhibitory side effects, like for example the observed inhibition of NSH1 due to guanosine or of XMPP and GMPS due to xanthosine accumulation. Interestingly, similar to the seedlings, the wild-type rosettes accumulated allantoate during the extended night and did so to a similar extent as the *NSH1* and *GSDA* mutants accumulated xanthosine and guanosine, respectively. The possible roles of ureides, the XMPP and the purine catabolism during prolonged darkness are discussed in detail in chapter 5.3.6.

In contrast to the strong accumulation of ureides in the extended night, allantoate was barely detectable in seven-week-old rosettes (Fig. 26C). It can be assumed that purine catabolism is induced in the reproductive rosette, because the xanthosine content in *nsh1* mutant and guanosine content in the *gsda* mutant were fivefold higher than in the non-stressed vegetative rosette (Fig. 26A, C). Although the reproductive rosette had three more weeks to accumulate more of these nucleosides, a fivefold increase can only be generated by an increased flux into the pathway. Nevertheless, the allantoate concentration was low (Fig. A - 9). Since these rosettes were already in the reproductive phase, the ureides are likely constantly degraded at this stage for the remobilization of nitrogen to support seed development.

Immunoblots corresponding to the metabolite analysis gave new insights regarding the control of purine catabolism (Fig. 27A). Relative protein amounts of XMPP, GSDA, NSH1 and XDH under the tested conditions were assessed for the first time. Especially interesting was the inducibility of XMPP in extended darkness with respect to the protein amounts of GSDA, NSH1 and XDH. These were similarly abundant in untreated and dark-stressed vegetative rosettes. Because the flux through the purine catabolism is increased during the extended night, but no increase in guanosine or xanthosine concentrations was observed in dark-stressed compared to untreated wild-type rosettes (Fig. 26A, B),

it can be concluded that the amounts of GSDA and NSH1 are sufficient to process the increased input into the pathway under these conditions. This indicates that the catalytic capacities of GSDA, NSH1 and likely also XDH are largely unused in the untreated vegetative rosette. If the flux through purine catabolism suddenly increases, for example in extended darkness, the amounts of these enzymes do not seem to be limiting. Strong dark-induced accumulation of XMPP protein (Fig. 27C) suggests that XMPP may represent a switch to channel such a strongly increased metabolic flux. The purpose of boosting purine catabolism, the source of nucleotides by which it is fueled and also possible explanations why the loss of XMPP has little effect on metabolism are discussed below.

5.3.5 XMPP represents a switch for the induction of purine catabolism

The parallel analysis of purine-derived metabolites and relative protein abundances of XMPP, GSDA, NSH1 and XDH in vegetative rosettes exposed to an extended night in contrast to the control plants showed that purine catabolism seems to be held in a stand-by state in the non-stressed vegetative rosette (Fig. 26, 27). GSDA, NSH1 and XDH amounts remained almost completely unchanged whether plants were exposed to extended darkness or kept under long-day conditions. In the extended night, only the amount of GSDA in old leaves rose slightly and the amount of XMPP in general increased strongly. These observations and the fact that in wild-type rosettes there was no increase in steady state xanthosine and guanosine pool sizes when purine catabolism was induced indicates that GSDA, NSH1 and likely also XDH amounts are more than sufficient to cope with the increased flux through the pathway under these conditions, whereas XMPP may represent a switch that is induced to channel the flux.

XMPP is highly transcribed in comparison to the homologous phosphatases *SDDL2* to *4* and other genes involved in purine catabolism (Zhu, 2016, fig. 15). In a pulse-labeling study, *XMPP* transcript was shown to be among the 5% most abundant transcripts in *Arabidopsis* seedlings (Szabo *et al.*, 2020). However, the protein could not be detected with the sensitive antibody developed in this work in seven days old seedlings or in any tissue of six weeks-old *Arabidopsis* (not shown, Christel Schmiechen). Interestingly, in several studies on transcript dynamics, *XMPP* transcript was consistently listed as highly unstable with half-life times of 18 to 60 min (Gutierrez *et al.*, 2002; Lu *et al.*, 2005; Kwasnik *et al.*, 2019; Szabo *et al.*, 2020). Unstable transcripts are generally considered to have important regulatory roles and are therefore themselves highly regulated. The constitutive generation and degradation of such transcripts allows to rapidly adjust transcript levels as needed. In the case of *XMPP*, the increased transcript amount in the extended night or in the context of plant defense (Fig. 16A) may be generated by inhibition of transcript turnover or also by an induction of the promoter activity. In four-week-old *Arabidopsis* plants carrying the native *XMPP* promoter driving a fluorescent mNeogreen-SKL reporter – the SKL tag served to concentrate the reporter in peroxisomes for better detectability – no reporter signal could be detected. After treatment with MeJA, NeonGreen fluorescence was observed, demonstrating that transcript amounts can be increased by the induction of promoter activity (Schmiechen, 2019). The reason why the plants did not initially show expression of the reporter, even though *XMPP* transcript amount and turnover are generally reported to be particularly high, could possibly be due to the absence of trans elements supporting promoter activity but which were not part of the 999 bp sequence upstream of the translational start codon that was cloned for the promoter-reporter construct.

Overall, the impression developed that the XMPP is strictly regulated. Apart from the control of transcript abundance, the control of translation and/or protein stability plays role, because despite

high transcript abundance, XMPP amounts are very low in non-stressed plants. Translation may be inhibited by binding of short RNAs to the transcript or by structural features such as hairpins in the 5'UTR (Merchante *et al.*, 2017). Some examples are known, however the mechanisms and trans-elements unblocking such translational suppression are not elucidated. Here, it was found that from genomic XMPP DNA including the native promoter XMPP could not be expressed in detectable amounts in *N. benthamiana*. When the genomic sequence was replaced with the cDNA some XMPP was detected indicating that the introns may play a role in the translational control of XMPP transcript (Schmiechen, 2019). It is unknown which influence the introns have in this process. It is possible that XMPP transcripts might be prepared by trans factors before they can be spliced and translated. Such trans factors might be absent during the expression in *N. benthamiana*. In *Arabidopsis*, such a mechanism could withhold protein production until required under certain conditions.

It is also conceivable that control mechanisms operate at the post-translational level. Using the PhosPhAt online database an *in vivo* phosphorylation site at S250 was identified (Heazlewood *et al.*, 2008). Point mutants encoding XMPP variants S250A and S250D were generated using XMPP cDNA and were cloned for the expression as C-terminally HASTrep-tagged proteins. The exchange of serine to alanine removed the possibility of phosphorylation, whereas the replacement with aspartate possessing a negative charge served as a phosphorylation mimic. When transiently expressed in *N. benthamiana*, none of the purified mutants appeared to be less stable than the wild-type protein. However, transient expression is not a suitable measure to assess this question. Regulatory mechanisms might be different in *N. benthamiana* than in *Arabidopsis*, and infiltration with agrobacteria might stimulate the plant defense which is known to increase transcript amounts and may also lead to the stabilization of the XMPP protein. The stability of phosphorylation site mutants has not been studied in *Arabidopsis*.

The mutants which were purified after transient expression were used to determine their kinetic constants. These were similar to the ones of C- and N-terminally tagged wild-type proteins (Fig. 14, A - 5). This is consistent with the study of the crystal structure showing that the C-terminus, which contains the phosphorylation site, plays no role in enzyme activity (Heinemann *et al.*, 2021). The phosphorylation state at S250 of XMPP has no effect on its *in vitro* activity, but it is not clear whether it has any effect on protein stability. Interestingly, in a large RNAseq study involving many *Arabidopsis* tissues, Mergner *et al.* (2020) identified a second phosphorylation site near the first at S248. Surprisingly, their study revealed that two phosphorylation variants of XMPP exist and that either S248 or S250 is phosphorylated. In a tissue screen, both or neither of the phosphorylation variants were detected in some tissues, whereas only one of the variants was detected in other tissues. These findings support the notion that the phosphorylation sites may be an important regulatory switch.

The phosphorylation of XMPP might influence protein stability, but it could also affect the formation of complexes with other proteins. Interestingly, it was recently shown by tracer studies in human cell line that the purine biosynthesis from PRPP to AMP and to GMP is highly channeled (Pareek *et al.*, 2020). It was already shown before that enzymes of the purine biosynthesis can dynamically assemble to a complex called purinosome which represents a form of metabolic control (Laursen *et al.*, 2015; Sweetlove and Fernie, 2018). The assembly of proteins can create a microenvironment in which locally high concentrations of metabolic intermediates can occur. The structure of such complexes can favor that intermediates at a metabolic branch point are utilized by one route while the utilization by another route is prevented. Such a complex formation can thus rapidly change the metabolic fate of branch point metabolites like possibly XMP. In view of these findings, it seems possible that XMPP also forms complexes with other proteins of the pathway to access and channel the small amounts of XMP. The XMP concentration in seedlings was below 7.8 pmol g⁻¹ FW, which corresponds to a cellular concentration of 260 nM assuming an average cytosol volume of about 30 µL

g^{-1} FW (Koffler *et al.*, 2013). Thus, the physiological XMP concentration is more than two orders of magnitude lower than the K_M determined *in vitro*. In addition, GMPS competes with XMPP for the XMP. From studies of GMP biosynthesis in humans, it is known that GMPS can assemble with IMPDH1 and also with IMPDH2 to channel XMP. If this was the case in plants, it might also be conceivable for XMPP to interact with IMPDHs to gain access to XMP. Under conditions that lead to the stable formation of XMPP protein, a mechanism like a phosphorylation could control the interaction with the IMPDHs. Analysis of *in vitro* enzyme activity already showed that the XMPP has high affinity for XMP and catalytic activity. Once the XMPP has access to XMP, it could likely divert the flux to GMP biosynthesis for degradation. To date, no studies have been published investigating the occurrence of metabolite channeling in the plant purine metabolism (Zhang and Fernie, 2021). Our efforts to show the interaction of Arabidopsis GMPS with IMPDH1 or 2 by co-immunoprecipitation after co-expression in *N. benthamiana* were not successful. Experiments including XMPP as a possible interaction partner also failed. However, this does not exclude the possibility that protein interactions could occur *in vivo*. It would certainly be interesting to pursue this investigation in the context of XMPP characterization.

It is noteworthy that in the crystal structure of XMPP (Heinemann *et al.*, 2021) a conserved stretch of amino acids in an alpha helix exposed to the outside of the protein was found. Such a potential interaction site could allow XMPP to bind to IMPDH 1 or 2. It is also possible that the potential interaction site serves to bind the kinase that phosphorylates XMPP to possibly modulate protein stability.

In summary, XMPP is apparently under tight control. However, not much is known about the details of the regulatory mechanisms and how stable XMPP protein is produced upon exposure to extended darkness, in leaf senescence, upon wounding, infiltration with *P. syringae* and by MeJA treatment (Fig. 16A - E). Collectively the data suggest that purine catabolism is maintained mostly in a stand-by status using only a minor fraction of its catalytic capacity in an unchallenged plant. Upon a stimulus the flux through the pathway can be increased probably mediated by an increased activity of XMPP. In the following, possible roles of XMPP and purine catabolism will be discussed in context of the extended night and pathogen response.

5.3.6 The role of XMPP and purine catabolism in plant energy metabolism

XMPP transcript and protein abundance were strongly increased in extended darkness (Fig. 16, 27). Metabolite analysis of non-stressed and dark-stressed vegetative rosettes showed that this coincided with an induction of purine catabolism in extended darkness (Fig. 26A, B). A role of purine catabolism in extended darkness was already suggested in previous studies. The most striking examples are the darkness-induced phenotypes of *GSDA*, *NSH1* and *XDH* mutants exhibiting chlorosis primarily affecting old leaves and impaired recovery rates after re-exposure to long-day conditions (Brychkova *et al.*, 2008; Jung *et al.*, 2011; Dahncke, 2014; Schröder *et al.*, 2018). It should be mentioned that the strong dark-induced phenotypes of *nsh1* and *xdh* mutants could not be reproduced in our laboratory. As it will be discussed in the following chapter, purine metabolism is intertwined with energy metabolism, so it could be hypothesized that differing conditions and methods of plant cultivation may cause the appearance or absence of a dark-induced phenotype.

Plants use light to drive photosynthesis which enables them to fix carbon dioxide to form sugar and starch. Usadel *et al.* (2008) showed that 90% of the starch reservoir built up during the day is depleted by the end of the night to fuel plant metabolism in the absence of light. The strong reduction of the starch pool by the end of the night indicates that extended darkness quickly leads to an energy

shortage. In a study with yeast growing under carbon limitation, it was shown that nucleotides were catabolized to release the ribose moiety serving as energy reserve (Xu *et al.*, 2013). Carbon starvation caused increasing concentrations of purine and pyrimidine catabolic intermediates and interestingly also sedoheptulose-7-phosphate (S7P). Xu *et al.* concluded that the flux through the nucleotide catabolism was enhanced and that recycling of the ribose moieties through the non-oxidative branch of the pentose phosphate pathway (PPP) enabled yeast to survive under carbon starvation. S7P thereby represented the actual energy reservoir. This is why the inhibition of nucleotide catabolism by the mutation of the yeast main nucleotidase *PHM8* reduced the yeast viability under carbon starvation by 90% (Xu *et al.*, 2013).

This observation led to the assumption that ribose recycling from plant nucleotides in extended darkness may accordingly release carbon for energy metabolism during the extended night. In line with this, *GSDA* expression was found to be induced in extended darkness and carbon starvation and was repressed by carbon supply in form of sugar (Dahncke, 2014). However, results from the inhibition of ribose recycling by the mutation of *RBSK* led to the rejection of this hypothesis (Schröder *et al.*, 2018). Ribose which is released in the cytosol by *NSH1/2* is imported into the plastids where it is phosphorylated by *RBSK* for ribose recycling (Fig. 3). The block of ribose recycling in *rbsk* plants however did not cause any dark-induced phenotype as observed for *GSDA* and *NSH1* mutants (Jung *et al.*, 2011; Schröder *et al.*, 2018). It was concluded that the loss of ribose recycling is unlikely to be the cause of the *gsda* and *nsh1* darkness-induced phenotypes. This is consistent with the observation that *XDH* mutants are also affected by a similar darkness-induced phenotype, although *XDH* is located downstream of *NSH1/2* in the pathway and *XDH* mutants can thus recycle ribose (Brychkova *et al.*, 2008).

Brychkova *et al.* (2008) suggested a different role of purine catabolism to cope with extended darkness. They showed that the ureides allantoin and allantoate, which are downstream products of purine catabolism, accumulate in extended darkness and argued that they act as antioxidants (Fig. 3). The application of ureides to *xdh* leaf discs exposed to 48 h of darkness attenuated the formation of chlorosis (Brychkova *et al.*, 2008). Moreover, the authors observed that reactive oxygen species (ROS) increased over the course of extended darkness and demonstrated that the increase of ROS in *xdh* background could be quenched by the application of allantoin and allantoate. Because *GSDA*, *NSH1* and *XDH* mutants are substantially impaired in their ureide production, the supposed ROS quenching function of ureides may be a reasonable explanation why all three purine catabolism mutants show a darkness-induced phenotype. Moreover, it could explain why the recovery rates after the end of extended darkness were impaired for *xdh* and *gsda* plants, as reported by Brychkova *et al.* (2008) and Dahncke (2014). In both studies, increased protein degradation was observed in the *GSDA* and *XDH* mutants in extended darkness. Proteins involved in photosynthesis are particularly degraded during prolonged darkness (Masclaux *et al.*, 2000), so that the re-exposure to light can lead to excessive reduction of photosystems and the formation of ROS. The lack of ureides in *GSDA* and *XDH* mutants may result in reduced ROS scavenging capacity which could explain the observed increased cell damage and reduced recovery rates. Recovery rates of four-week-old rosettes after six days of darkness were 80% for wild-type plants and depending on *XDH* RNAi and mutant line only 20-45% (Brychkova *et al.*, 2008).

Data presented in this study from four-week-old vegetative rosettes confirmed the accumulation of allantoate after 48 h of extended darkness (Fig. 26). In line, the time course over 48 h of extended darkness in seedlings showed continuously rising allantoate and also uric acid concentrations (Fig. 23B). Allantoin concentrations were too low to be detected in seedlings. As metabolite concentrations in rosette leaves were generally lower than in seedlings the analysis of allantoin concentrations in rosettes was not attempted (Baccolini, 2019). For future allantoin measurements,

the method that was optimized for the quantification of allantoin in common bean nodules should be used (Chapter 7.8), as it is about sixty times more sensitive than the method used for the quantification of allantoin in *Arabidopsis* tissues. Surprisingly, assuming a factor of 10x to compare metabolite concentrations per dry weight and per fresh weight, the allantoate concentration in dark-stressed rosettes was 4.6-fold higher than in dark-stressed seedlings (Fig. 22, 26B). According to Brychkova *et al.* (2008), who measured an about sixfold higher allantoin than allantoate concentration in four-week-old rosettes after 48 hours of prolonged night, quantification of allantoin in the rosettes would have been possible here. Interestingly, gene expression data suggest that allantoin is specifically produced in extended darkness (Usadel *et al.*, 2008). The expression of genes encoding enzymes acting upstream of the ureide biosynthesis like *XMPP*, *GSDA*, *XDH* and *UOX* was upregulated by factors 16x, 4x, 3x and 2x, respectively, whereas the expression of genes encoding enzymes acting downstream like *ALN* and *AAH* was repressed by factors 6x and 4x, respectively. By contrast, under nitrogen starvation also *ALN* and *AAH* expression was shown to be upregulated indicating that ureides were likely catabolized for nitrogen remobilization (Soltabayeva *et al.*, 2018). Therefore, it is reasonable to assume that ureides play a special role in prolonged darkness, for example as ROS scavengers.

As mentioned in the beginning, the extension of the night causes the shortage of carbohydrates and energy for the plant. Although ribose recycling was not considered relevant to energy metabolism in the dark (Schröder *et al.*, 2018), an observation was made which led to further need of discussion. During the generation of *xmpp* complementation lines a chlorotic phenotype was observed when a segregating population of *xmpp:xs* was grown on agar plates supplemented with 1% sucrose (Fig. A - 10, *xs* = *35S-XMPP-HAStrep*). The phenotype did not develop when sucrose was not supplemented. This observation supported the assumption that purine catabolism may be indeed regulated depending on the energy status. Gene expression analysis showed that *XMPP* expression was fivefold repressed when *Arabidopsis* seedlings were supplemented with 34% sucrose (Greville, 2006). The cause of the chlorotic phenotype was not clarified, but germination of additional seeds on agar plates supplemented with up to 50 μ M guanosine excluded the possibility that it was caused by XMP dephosphorylation-induced guanylate deprivation, as the seedlings developed the same phenotype (not shown). It is possible that adenylate depletion due to a high XMP dephosphorylation rate could be the reason. Assuming that purine catabolism should not operate and *XMPP* should actually be suppressed under sugar supplementation, the strongly expressed *XMPP* in the overexpression line could cause the initiation of the constitutively ready purine catabolism and the depletion of adenylates.

The connection between purine catabolism and free adenylates in the dark will be discussed in the following. Estimates of cellular concentrations of free adenylates and purine nucleotides derived from potential mRNA degradation have been calculated (Calc. A - 1). The estimates show that the free adenylate pool size (287 μ M) of an *Arabidopsis* mesophyll cell is 4 - 20-fold greater than the sum of purine nucleotides which could be released by the degradation of all mRNA (15 - 75 μ M). This indicates that mRNA degradation is likely not the primary source fueling cytosolic purine catabolism. The increased guanosine concentration in dark-stressed rosettes with *gsda* background in contrast to the non-stressed rosettes showed that the deamination of guanosine to xanthosine by *GSDA* is induced in the dark (Fig. 26B). However, it is not possible to distinguish whether guanosine originates from cytosolic degradation of free guanylates, guanylates released from mRNA, or vacuolar RNA degradation. Prolonged darkness stimulates autophagy, which leads, among other things, to the degradation of rRNA (Floyd *et al.*, 2015). Since rRNA makes up 80% of total RNA, most of the RNA-derived nucleotides are released in the vacuole, where they are dephosphorylated to nucleosides that are exported to the cytosol. It would be interesting to know in what proportions from which sources

purine catabolism is fed under non-stressed and dark-stressed conditions, in particular whether from free adenylates or nucleotides from rRNA. This information could help to further elucidate the role of XMPP, which is involved in the degradation of cytosolic adenylates but not in the degradation of nucleotides in the vacuole. However, it is not easy to obtain such insights because metabolite analyses with mutants, as mentioned earlier, do not allow to draw quantitative conclusions, and feeding experiments with labeled metabolites can also misbalance pool sizes and thus affect and alter metabolic fluxes. All in all, the impression arises that the adenylate pool may be an important source fueling purine catabolism through the action of XMPP in extended darkness.

ATP, the main energy transferring molecule, is an energy-rich molecule comprising two high-energy phosphoanhydride bonds. But also AMP is energy-rich and its degradation via IMP, XMP, xanthosine, xanthine and uric acid leads to the formation of two NADH and one ribose (Fig. 28). Ribose is transported into the plastids where it is phosphorylated to ribose-5-phosphate (R5P) under consumption of one ATP (Schröder *et al.*, 2018). According to the suggestion of Xu *et al.* (2013), three R5P could be converted to two fructose-6-phosphate (F6P) and one glyceraldehyde-3-phosphate (GAP) through the non-oxidative PPP. F6P and GAP would be exported into the cytosol where they enter glycolysis. F6P would need to be activated by the phosphorylation to fructose-1,6-bisphosphate consuming ATP whereas GAP could directly enter the lower part of glycolysis. The produced pyruvate could be catabolized in the tricarboxylic acid cycle. About 31.6 ATP equivalents, as a measure for the stored energy, are estimated to result from AMP catabolism (Tab. 3). As the major part of ATP equivalents is generated by ribose degradation, similar numbers can be assumed for other nucleotides. However, the adenylates are especially interesting because they account for the major part of the nucleotides (Fig. 25, Straube *et al.*, 2021). For the catabolism of glucose and amino acids in comparison, the production of 32 and a range of 12.5 to 34 ATP equivalents were estimated, respectively (Tab. 3, Hildebrandt *et al.*, 2015). These estimates of the possible energy yields indicate that nucleotides might be suitable as alternative energy source.

Usadel *et al.* (2008) quantified starch, sugars, ATP and amino acids of five-week-old rosettes in the course of extended darkness. Conflicting with the idea that nucleotides could be used as energy source in the extended night, the ATP concentration increased in the first six hours. This increase of ATP in

Table 3 Potential energy yield from complete oxidation of AMP in comparison to glucose and selected amino acids. Numbers for glucose and amino acids were retrieved from Hildebrandt *et al.* (2015). Numbers for AMP were calculated as illustrated in figure 28. Assuming that four protons are required for the production of one ATP, NADH and FADH₂ correspond to 2.5 and 1.5 ATP equivalents, respectively.

Molecule	NADH	FADH ₂	Direct ATP	ATP equivalents
Glucose	10	2	4	32
AMP	10.3	1.7	3.3	31.6
Tyrosine	11	3	2	34
Leucine	10	4	1	32
Lysine	10	3	2	31.5
Isoleucine	9	3	2	29
Proline	8	3	1	25.5

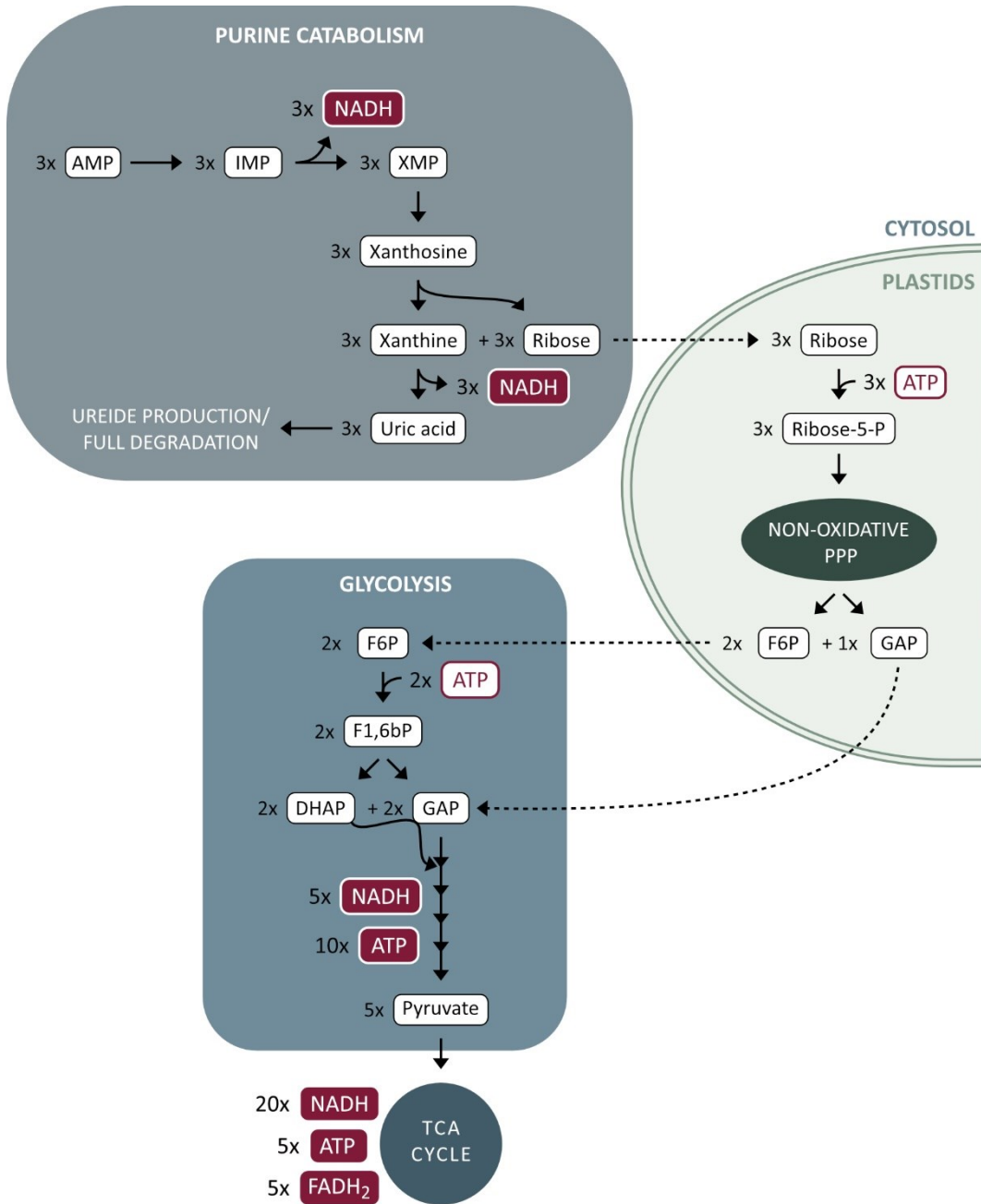


Figure 28 Possible pathway of complete AMP oxidation. Dashed lines represent transport processes. Solid lines represent enzymatic reactions. AMP, adenosine monophosphate; NADH, nicotinamide adenine dinucleotide; IMP, inosine monophosphate; ATP, adenosine triphosphate; XMP, xanthosine monophosphate; Ribose-5-P, ribose-5-phosphate; F6P, fructose-6-phosphate; GAP, glyceraldehyde-3-phosphate; F1,6bP, fructose-1,6-bisphosphate; DHAP, dihydroxyacetone phosphate; FADH₂, flavin adenine dinucleotide; PPP, Pentose Phosphate Pathway; TCA cycle, Tricarboxylic Acid Cycle.

the extended night was in tendency confirmed here in seedlings (Fig. 25). Moreover, this initial concentration increase affected also other adenylates and guanylates but is generally followed by a decrease after 48 h. The concentration of the sum of the purine nucleotides in wild-type seedlings at the end of the night was 108 nmol g⁻¹ FW and rose to 119 nmol g⁻¹ FW at 6 h of prolonged night but decreased to 63 nmol g⁻¹ FW at 48 h. It should be noted that adenylates accounted for 90% of the total concentration of purine nucleotides at all three time points. The origin of the nucleotides that led to the concentration increase in the first six hours is unknown. Assuming that 15 - 75 μM purine nucleotides could be released by the degradation of all mRNA of a mesophyll cell (Calc. A - 1) and assuming a mesophyll cell volume of 600 μL g⁻¹ FW (Koffler *et al.*, 2013), 9 - 45 nmol g⁻¹ FW purine nucleotides could be released in a dark-stressed rosette. The observed increase in concentration of total purine nucleotides was however comparatively high with 11 nmol g⁻¹ FW, of which adenylates accounted for 10.1 nmol g⁻¹ FW. These are just rough estimates, but they indicate that the increase in nucleotides and adenylates in particular may not be primarily caused by mRNA degradation. The origin of the temporary increase in purine nucleotides during the first six hours of darkness is unclear, but the findings suggest that adenylates are the main source fueling purine catabolism in the following period of darkness.

Usadel *et al.* (2008) showed that the starch and sucrose concentrations available at the end of the night decreased drastically within the first six hours of extended darkness. Coinciding, the concentrations of hexose-phosphates G6P and F6P were strongly reduced. After eight hours, the hexose phosphates had increased again and stabilized at concentrations equal to half of the previous concentration (Usadel *et al.*, 2008). The authors considered this as a sign for a rearrangement of plant metabolism to an alternative energy source. Interestingly, the authors reported that with the stabilization of hexose-phosphate concentrations, the ATP concentration was constantly decreasing. In this study, it was observed that adenylate and guanylate concentrations of seedlings had decreased accordingly after 48 h of extended darkness (Fig. 25). The rearrangement of amino acid metabolism becomes apparent after 24 h of extended darkness, when amino acid concentrations strongly increased (Usadel *et al.*, 2008). It can be assumed that the use of amino acids as alternative respiratory substrates was in full progress by then. The fast depletion of starch and sugars before the respiratory machinery was rearranged to the use amino acids released from protein degradation supports the hypothesis that nucleotides could serve as transitory energy source. The previous argumentation that the lack of the dark-induced phenotype in *rbsk* rosettes excludes a role of ribose recycling from nucleotides in adaption to extended darkness may be worth reevaluating. Purine catabolism mutants including *xmpp* could be analyzed for their sugar, sugar phosphate and nucleotide contents in context of extended darkness. In these mutants the recovery of hexose-phosphates after the initial reduction at about six hours of the dark period may be impaired due to the lack of the transitory energy supply from adenylate catabolism.

Another interesting finding directly related to the adenylates is that in yeast a close connection of purine catabolism to changes of the adenylate energy charge (AEC) in the respiro-fermentative transitions after the addition of glucose to respiratory growing yeast was demonstrated (Walther *et al.*, 2010). Supplied glucose was rapidly phosphorylated for the activation of glucose for glycolytic use which coincided with strong reductions in ATP and free phosphate concentrations. The authors demonstrated that this caused AMP deamination to IMP and the subsequent dephosphorylation to inosine, thereby maintaining the AEC. The authors proposed that the benefit of this conversion would be that IMP and inosine would not impair glycolytic reactions whereas an altered AEC would. The conversion to IMP and inosine would not only represent a rapid adjustment of the AMP concentration but could also be reversed in a rapid and energy-efficient manner by the hydrolysis of inosine to hypoxanthine and ribose, the salvage of hypoxanthine to IMP and the amination of IMP to AMP. After

the respiro-fermentative transition, the ATP concentration and subsequently AMP, IMP and inosine concentrations recovered. Such a mechanism is however unlikely to be operative in plants. In contrast to yeast, plants have a much higher ratio of adenylates to the sum of IMP and inosine pools. In the yeast respiro-fermentative transition, the adenylate : (IMP + inosine) ratio decreased from 6.9 to 0.7. In plants however the adenylate : (IMP + inosine) ratio is 35 and a substantial misbalance of AEC would thus be expected to cause a drastic increase of the inosine concentration. However, no indications were found that such a sharp increase in inosine concentration was ever observed. Another aspect is that from a physiological standpoint such perturbations of the AEC are unlikely in plants. Yeasts are exposed to strongly fluctuating nutrient availability in their environment, whereas the nutrient supply for the plant is normally not drastically changing. Especially with regard to sugars, plants build up a starch reservoir during the day that buffers the diurnal lack of energy supply in the night (Usadel *et al.*, 2008). A third argument is that the Arabidopsis SNF1-related protein kinase 1 (SnRK1) is likely not sensing changes of AEC (Emanuelle *et al.*, 2016), whereas its homologs AMP Kinase (AMPK) and Sucrose Non-Fermenting (SNF1) are responsible for AEC sensing and for the induction of metabolic changes in mammals and yeast, respectively. The *AMPK/SNF1/SnRK1* family is generally known to induce metabolic changes in response to low-energy conditions (Baena-González and Lunn, 2020).

Intriguingly, even though Arabidopsis SnRK1 is insensitive to AMP and ADP, it reacts to perturbations of sugar-phosphates (Emanuelle *et al.*, 2015; Emanuelle *et al.*, 2016). This fits with the hypothesis that nucleotides may serve as alternative transitory energy source in the early phase of an extended night, because the decrease of G6P and F6P concentrations coincided with the onset of the gradual nucleotide degradation (Fig. 25; Usadel *et al.*, 2008). The hypothesis is further supported by the analysis of *XMPP* expression in various *SnRK1*-related gene expression studies. In mesophyll protoplasts *XMPP* expression was sixfold induced after the induction of *KIN10* expression, which codes for a subunit of SnRK1 (Baena-González *et al.*, 2007). Consistently, *XMPP* expression was fivefold repressed in three-week-old *SnRK1α1/α2* mutants compared to wild-type plants after 6 h of extended night (Pedrotti *et al.*, 2018). In a co-expression network analysis Arias *et al.* (2014) listed *XMPP* as a central member of the sugar starvation network and showed that its expression pattern is similar to the genes involved in SnRK1 signaling.

A *SnRK1*-dependent induction of nucleotide catabolism would resemble the activation of the branched-chain amino acid (BCAA) catabolism to supply alternative respiratory substrates in the extended night, as proposed by Pedrotti *et al.* (2018). The authors demonstrated that SnRK1 controls basic leucine zipper (bZIP) transcription factors which directly induce promoter activity of genes involved in BCAA catabolism. Interestingly, *XMPP* transcription was induced upon the transfer of bZIP11 into the nucleus (Hanson *et al.*, 2008). In conclusion, SnRK1 signaling induces amino acid catabolism and likely also purine catabolism. Considering that the enzymes of purine catabolism are constitutively expressed and are able to cope with sudden changes in flux possibly channeled by the induced *XMPP*, it may be faster to mobilize energy from nucleotides than from amino acids (Fig. 26, 27). Experiments should be conducted to assess this hypothesis. As the onset of purine catabolism in extended darkness is characterized by the accumulation of ureides, a breakdown of ureide production in *SnRK1* mutants could affirm the control by the SnRK1 signaling. To check the relevance of ribose recycling, *NSH1* and *RBSK* mutants could be analyzed regarding their sugar concentrations. If the stabilization of the hexose-phosphates after their initial concentration decrease during the early phase of the extended night (Usadel *et al.*, 2008) is enabled by the switch to nucleotide catabolism as alternative energy source, the genetic block of ribose recycling is expected to impair this recovery and/or to potentially cause early protein degradation to make amino acids more rapidly available as alternative respiratory substrates. In this context it would be interesting to investigate

whether the *XMPP* mutant exhibits significant metabolic changes.

The metabolite analysis of seedlings and rosettes presented here showed no perturbation of purine catabolism pool sizes in the *XMPP* mutant in the dark. The energy aspect however may eventually provide a rationale for the existence of *XMPP*. In the absence of *XMPP*, XMP is aminated by GMPS to GMP hydrolyzing ATP to AMP. GMP is dephosphorylated to guanosine, which is deaminated by GSDA to xanthosine releasing ammonia (Fig. 3). The detour of the flux may not exceed GMPP and GSDA capacities, however it costs the hydrolysis of ATP to AMP and indirectly also the hydrolysis of ATP to ADP to re-assimilate the released ammonia into glutamine catalyzed by Glutamine Synthase. This makes the detour through GMP and guanosine less energy efficient, which may become critical under energy shortage. It thus appears possible that the *XMPP* mutant is partially impaired in the switch of energy sources upon carbon starvation and may display reduced sugar phosphate levels in the extended night. A high ammonia concentration resulting from the redirection of purine catabolism through GMP and guanosine may pose another problem. It would be interesting to determine ammonia concentrations in dark-stressed *XMPP* mutants and to elucidate whether ammonia may accumulate. Although the *XMPP* mutation can be compensated by the catabolic GMP route and does not affect downstream metabolite pool sizes in the dark, it may however decrease plant performance. Possible consequences of this impairment are not as apparent as in cases of the darkness-induced chlorotic phenotypes of *gsda*, *nsh1* and *xdh*, but there could be long-term consequences, such as growth inhibition after prolonged darkness or reduced seed yield, as already observed under long-day conditions (Fig. 20).

Another energy-relevant player is the *SnRK* antagonist *Target of Rapamycin (TOR)*. In general, TOR is known to promote anabolic reactions and to repress catabolic reactions. TOR takes over an antagonistic role to SnRK1/bZIP signaling in extended darkness. Under energy deprivation TOR is inhibited by SnRK1/bZIP which represses its inhibitory effect on autophagy (Heinemann and Hildebrandt, 2021). Gene expression data provided by Xiong *et al.* (2013) showed that the induction of genes involved in purine *de novo* biosynthesis and salvage as well as the repression of *XMPP* upon glucose addition are TOR-dependent. A connection of purine metabolism and TOR activity was demonstrated in human cell line. Independent of the energy status mammalian TOR complex 1 (mTORC1) of human cell lines was shown to sense purine nucleotide and amino acid concentrations and to inhibit downstream protein, RNA and ribosome synthesis when these are too low (Hoxhaj *et al.*, 2017). It was also shown, that a bidirectional control mechanisms exist between mTORC1 and purine nucleotide concentrations (Emmanuel *et al.*, 2017). The application of mTORC1 inhibitors reduce purine and pyrimidine *de novo* biosynthesis rates as well as low purine nucleotide concentrations inhibit mTORC1 activity. The same study reports that the mTORC1 signaling is especially sensitive to changes of adenylate concentrations. It is interesting to note, that reduced pyrimidine nucleotide concentrations did not impair mTORC1 activity (Emmanuel *et al.*, 2017; Hoxhaj *et al.*, 2017).

In *Arabidopsis* a similar observation was made. Kazibwe *et al.* (2020) investigated why a *Ribonuclease 2 (RNS2)* mutant exhibited constitutive autophagy activity. They demonstrated that autophagy in *rns2* could be repressed by the addition of purine nucleoside inosine and its nucleobase hypoxanthine in a TOR-dependent manner but not by the addition of pyrimidine nucleosides cytidine, uridine or thymidine. The authors claimed that the absence of *RNS2* causes a strong reduction of vacuolar RNA degradation and in the following cytosolic nucleosides and nucleotides concentrations. However, neither nucleosides nor nucleotide concentrations were determined. Nevertheless, it was convincingly demonstrated that inosine can act upstream on the TOR activation which led to the repression of autophagy. Similar to the observation in human cell line, autophagy was induced after the block of purine *de novo* biosynthesis and salvage reactions by the application of GAR

Discussion

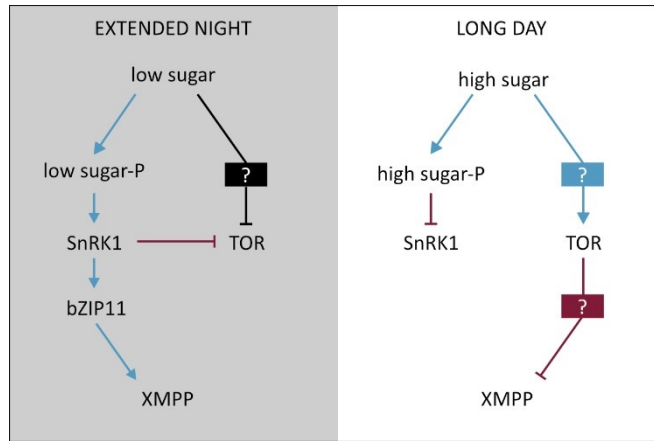


Figure 29 Model for XMPP expression depending on sugar availability. Grey box, potential control mechanisms operating in the extended night. The low concentrations of sugar phosphates (Sugar-P) leads to the activation of XMPP through SnRK1/bZIP11 signaling. At the same time SnRK1 inhibits TOR. White box, under sugar availability provided by photosynthesis or by exogenous sugar application high sugar-P concentrations inhibit the SnRK1 signaling. The sugar availability also leads to the activation of TOR which leads to the inhibition of XMPP expression. These regulatory mechanisms are likely not only affecting expression but possibly also translation and protein stability. SnRK1, SNF1-Related Protein Kinase 1. bZIP11, Basic Domain Leucine Zipper 11. TOR, Target of Rapamycin.

Formyltransferase (GART) and HGPRT and APRT inhibitors, respectively. Whether changes in nucleotide, nucleoside or nucleobase concentrations cause the activation of TOR in plants is not clear. Interestingly, IMP, inosine, and hypoxanthine concentrations in *Arabidopsis* seedlings appear to be affected by some type of light-dependent control, although the IMP-inosine-hypoxanthine pathway to xanthine is not involved in purine catabolism. The IMP concentration in wild-type seedlings is increased after six hours of light compared to the end of normal night (Fig. 25). A similar observation was made for inosine and hypoxanthine concentrations of wild-type seedlings after three hours of light compared to the end of the night (Fig. 23C). In the extended night, inosine concentration in seedlings are decreased (Fig. A - 7). It would be interesting to investigate whether inosine is involved in signaling processes induced by extended darkness. It was noticed that inosine concentrations in dark-stressed *gsda* and *nsh1* rosettes are strongly increased in comparison with wild-type plants (Fig. A - 8). A similar high hypoxanthine concentration would be expected in *xdh* rosettes. The inosine accumulation in *gsda* and *nsh1* rosettes was about $0.15 \mu\text{mol g}^{-1} \text{DW}$. This corresponds approximately to a concentration of $15 \text{ nmol g}^{-1} \text{FW}$. The concentrations of inosine and hypoxanthine used by Kazibwe *et al.* (2020) to induce the repression of constitutive autophagy in the *RNS2* mutant was $10 \text{ nmol g}^{-1} \text{medium}$. An important note is that *GSDA*, *NSH1* and *XDH* mutants are possibly affected by the repression of autophagy in extended darkness. Therefore, their dark-induced phenotypes may be caused by the impairment of autophagy rather than the impairment of nucleotide degradation. However, this does not mean that purine nucleotide degradation and XMPP in particular are not important in extended darkness.

The thoroughly compiled findings on purine catabolism in relation to its role in the prolonged night and carbon starvation, as well as new insights provided by this study, underscore the importance of purine catabolism under these conditions. Exciting new possible roles of purine catabolism were discussed. These include the use of nucleotides as a transient energy source in the early phase of the prolonged night and a possible role of purine metabolites in energy signaling. The accumulating ureides appear to be important ROS scavengers, but may also serve to temporarily store nitrogen that would otherwise be released upon complete degradation of the purine ring system. The consequences of impaired purine catabolism can be subtle and may manifest as decreased sugar-phosphate

concentrations, reduced recovery rates and plant growth upon the exposure to extended darkness or partially compromised seed production. More experiments aiming to elucidate the physiological role of purine catabolism in extended darkness and energy deprivation are required.

5.3.7 XMPP and purine catabolism in pathogen response

The application of defense-related stimuli like wounding, infection with *P. syringae* and treatment with methyl jasmonate (MeJA) increased *XMPP* transcript and protein amounts (Fig. 16). This indicates that *XMPP* and purine catabolism may also play a role in plant defense which has been previously suggested by Ma *et al.* (2016) who demonstrated that *XDH* plays two opposing roles upon the infection of *Arabidopsis* with the biotrophic fungus *Golovinomyces cichoracearum*. According to their model, *XDH* uses NADH, and not its normal substrate xanthine, in the epidermis cells at the infection site to generate superoxide radicals to defend against the invading pathogen. In the underlying mesophyll cells, *XDH* uses xanthine to produce uric acid as a ROS scavenger to protect the surrounding plant tissue from the superoxide radicals.

Interestingly, a promoter reporter study with marker genes of the salicylic acid (SA) and jasmonate (JA) metabolism showed that upon local infiltration of *Arabidopsis* leaves with *P. syringae* DC3000 carrying *AvrRpt2*, the induction of SA and JA occurs in a spatially separated manner (Betsuyaku *et al.*, 2018). SA signaling was restricted to the area close to the infection site and coincided with the loss of chlorophyll autofluorescence as consequence of cell death. Surrounding the infection site, JA signaling was active. Although the pathogens used by Ma *et al.* and Betsuyaku *et al.* are very different, they both will be discussed in context of a general plant defense response. The justification to compare the infection of *Arabidopsis* with two very different pathogens was drawn from a genome wide association study performed for the infection of *Arabidopsis* with different isolates of the necrotrophic fungus *Botrytis cinera* (Corwin *et al.*, 2016). This pathogen was chosen because no qualitative resistance alleles were known to confer resistance to *B. cinera* in *Arabidopsis*. With this plant-pathogen system the authors aimed to identify genes of the plant innate immune response which, commonly in contrast to the genes involved in the adaptive immune response, represent only a small part of the defense repertoire of a plant and are therefore difficult to identify. In this study, the *XMPP* was listed to be involved in the *Arabidopsis* innate immune response against *B. cinera* infection. Based on the fact that *XMPP* and purine catabolism seem to be involved in the *Arabidopsis* innate immune response independent of the pathogen, a single model summarizing the available data from different pathogen systems is proposed (Fig. 30).

Close to the infection site where SA signaling is active, *XDH* contributes to the oxidative burst to fight the pathogen or to induce the hypersensitive response-mediated cell death by using NADH to reduce oxygen to superoxide radicals. In cells surrounding the infection zone, JA signaling induces the expression of *XMPP* and *NSH2* which can deliver xanthine to *XDH*. Here, *XDH* uses xanthine as substrate producing uric acid. Uric acid contributes as a ROS scavenger to the protection of uninfected surrounding plant tissue from the oxidative burst at the infection site. According to the proposed model, it would be interesting to investigate whether *xmpp* or other mutants of genes involved in purine catabolism show a reduced containment of the oxidative burst, increased ROS concentrations or cell death on larger areas after infection with various pathogens. Except for the *XDH* mutants, altered infection rates are not expected, because other purine catabolic enzymes are not required for the *XDH*-dependent ROS formation.

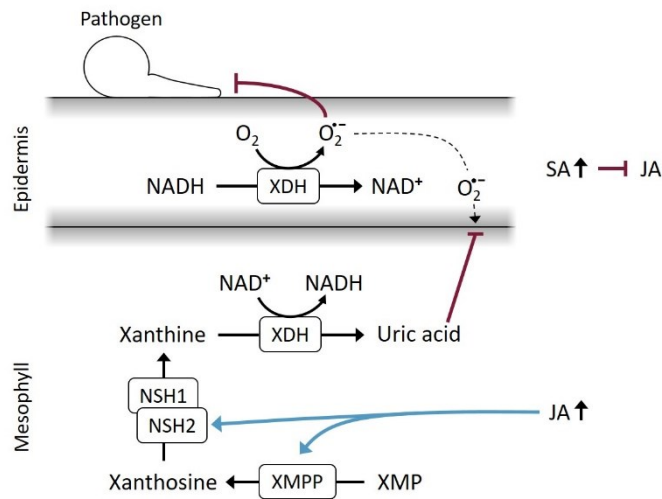


Figure 30 Model for the potential role of purine catabolism in plant defense. This model is based in its essence on the findings of Ma *et al.* (2016) that XDH plays opposing roles in epidermis and mesophyll cells upon infection with powdery mildew *Golovinomyces cichoracearum* UCSC1 and UMSG1. According to the assumptions discussed here, the illustrated processes may play a role in basal quantitative defense responses also against other pathogens like *Botrytis cinera* or *Pseudomonas syringae* (Corwin *et al.*, 2016; Betsuyaku *et al.*, 2018). After the perception of an invading pathogen by the plant two modes of reactions are initiated which act spatially separated. At the infections site salicylic acid (SA) signaling is induced and the XDH produces superoxide radicals by the oxidation of NADH. These radicals can serve to fight the pathogen or to induce ROS-dependent hypersensitive response and cell death. In the cells surrounding the infection site, jasmonate (JA) signaling induces the expression of XMPP and NSH2 which provide xanthine to XDH. This causes XDH to produce the ROS scavenger uric acid instead of superoxide radicals.

6 Summary

Purine metabolism is a fundamental pathway of plant primary metabolism and is also known to be used in tropical legumes to produce ureides for long-distance nitrogen transport. Some enzymes and transporters involved in ureide biosynthesis are still unknown. This work describes the identification of the novel XMP Phosphatase (XMPP) that has been shown here to be involved in ureide biosynthesis in nodules of tropical legumes. To characterize XMPP and as a positive control also Xanthine Dehydrogenase (XDH) in nodules, a system was established in our laboratory to produce soybean nodules carrying gene knockouts mediated by CRISPR-Cas9 mutation. The analysis of *XDH* CRISPR nodules showed that it is in principle possible to produce knockout nodules in soybean. However, the conditions in tetraploid soybean were too challenging so that no conclusive results could be obtained for the characterization of XMPP in soybean. The main obstacles were the low mutation rates and the complexity of the metabolic pathway, as the loss of XMPP can be compensated by the catabolic GMP route. In a joint experiment of several laboratory members the analysis of XMPP in common bean nodules was aimed instead, because the generation and identification of knockout nodules in diploid common bean was simpler due to its low ploidy. Common bean *xmpp* nodules were successfully generated and their metabolite analysis showed that XMPP catalyzes the dephosphorylation of XMP *in vivo* and that XMP dephosphorylation is probably the main route to ureide biosynthesis.

Because XMPP is conserved in vascular plants, another objective of this work was its characterization in *Arabidopsis*. This showed that dephosphorylation of XMP is an entry point into purine catabolism and is occurring in seed and seedling development, vegetative and reproductive rosettes, and that it is of particular importance in prolonged darkness and likely also under biotic stress. Analysis of non-stressed and dark-stressed vegetative showed that in extended darkness I) the flux through purine catabolism increases, II) ureides accumulate, III) a large amount of XMPP protein is produced, IV) while protein amounts of other purine catabolic enzymes (*GSDA*, *NSH1*, *XDH*) remain barely unchanged without limiting the metabolic flux in the wild type. The latter indicates that purine catabolism is probably kept in a stand-by state ready to cope with increased metabolic flux through the pathway. The expression of the XMPP protein was found to be under tight control and to be strongly induced in prolonged night and plant defense. The high affinity for XMP as well as the high catalytic activity suggest that the abundant XMPP can direct metabolic flux to GMP biosynthesis into irreversible nucleotide degradation under these conditions. XMPP appears to be an important switch that initiates purine catabolism through XMP dephosphorylation. Therefore, it is surprising that *xmpp* plants did not develop a phenotype in the prolonged night. This can be explained by the fact that the catabolic GMP route can compensate for the loss of XMPP. Evaluation of the results of this work and findings from earlier studies suggest that purine catabolism is probably less energy efficient in the *xmpp* mutant, which could be the cause of its reduced seed yield. Regarding the role of XMPP in the extended night, a new model was proposed suggesting that adenylates may serve as a temporary alternative energy source at the beginning of the extended night when the starch reservoir is depleted and amino acids are not yet available as alternative respiratory substrates. In this process, the formation of ureides could serve to keep the nitrogen organically bound, which would otherwise be released by the full degradation of ureides. Interestingly, the review of data reported in previous studies and online-accessible gene expression data revealed that metabolites of purine catabolism may play a role in energy signaling. It is possible that *GSDA*, *NSH1* and *XDH* mutants could likely be inhibited in autophagy due to their accumulation of purine nucleosides or nucleobases. Experiments under energy shortage are required to elucidate the role of purine catabolism in energy metabolism. Regarding the role in plant defense, it has been suggested that XMPP and purine catabolism may be part of the innate immune response to produce uric acid and possibly also allantoin and allantoate as ROS scavengers to contain the oxidative burst at the infection site and to protect the surrounding plant tissue.

7 Material and Methods

7.1 Plant material and cultivation

Soybean

Here, the optimized procedure for the production of soybean root nodules is described. The protocol was adapted from Kereszt *et al.* (2007). Soybean cultivar Williams 82 was used. Growth conditions were (14 h light of $260 \mu\text{mol m}^{-2} \text{s}^{-1}$, 28°C / 10 h dark, 25°C) at 70% relative humidity. Seeds were surface-sterilized in a solution of 70 % (v/v) ethanol and 3 % (w/v) hydrogen peroxide. The volume of this solution was five times bigger than the approximate volume of the soybean seeds. After gently shaking for two minutes, sterilization solution was replaced with sterile water. After shaking another two minutes, the water was replaced again. This washing step was repeated four more times. Finally, seeds were scattered on autoclaved Seramis (Westland Deutschland GmbH), which was soaked with nutrient solution (Tab. 4). Seeds were covered with a thin layer of Seramis. The plant tray was covered with a lid, which was sealed air-tight to reach high humidity. About four days after seed germination when the hypocotyls of the seedlings were straightened, but the cotyledons were not yet unfolded, the seedlings were infected with *Agrobacterium rhizogenes* strain K599. The agrobacteria induce the formation of hairy roots and transfer DNA of interest. Here, agrobacteria were used to transfer the CRISPR constructs H276, H277, H313 or V112, aiming to generate *gsda1 gsda2 gsda3*, *xdh1-1 xdh1-2*, *xmpp1 xmpp2* knockout or control nodules, respectively. CRISPR constructs contained a *GFP* expression cassette. Prior to the infection, agrobacteria were plated from the glycerol stock to YEB medium (0.5% (w/v) meat extract; 0.1% (w/v) yeast extract; 0.5% (w/v) tryptone; 0.5% (w/v) sucrose; 2 mM MgSO_4 pH 7.2; for solid medium 1.5% (w/v) agar) containing $100 \mu\text{g mL}^{-1}$ rifampicin and $100 \mu\text{g mL}^{-1}$ spectomycin. After two days, a single colony was streaked on a new plate. After another day, bacteria were resuspended in 1 mL of liquid YEB medium, containing the mentioned antibiotics, and were spread on a new plate. The next day, bacterial lawn was scraped together and the bacteria were used to infect soybean seedlings. A needle was dipped into the bacteria mass and the seedling hypocotyl was pierced 3 mm below the cotyledon node. Excess bacteria mass was streaked from the needle on both sites of the piercing hole. This promotes the induction of hairy roots on two sides of the hypocotyl. After the infection, the seedlings were potted to 12 cm pots holding nutrient solution-soaked Seramis. Thereby, the seedling was covered deep in Seramis so that the infection site was below the surface and only the cotyledons were reaching the surface. Care had to be taken that the infection site was always covered with moist Seramis to support the development of hairy roots. If necessary more Seramis was added. Developing hairy roots were inspected three weeks after *A. rhizogenes* infection using fluorescence microscopy. The coexpression of GFP allowed to identify and remove roots which were not carrying the CRISPR construct. After the first root inspection seedling roots were inoculated with *Bradyrhizobium japonicum* strain 110spc4 to produce nodules. Rhizobia were previously grown on AG medium (0.1% (w/v) yeast extract, 0.1% (w/v) L-arabinose, 0.1% (w/v) sodium gluconate, 5.5 mM 2-(N-morpholino)ethanesulfonic acid (MES) pH6.9; 6.9 mM 4-(2-hydroxyethyl)-1-piperazineethanesulfonic acid (HEPES) pH6.9; 26 μM FeCl_3 ; 264 μM MgSO_4 ; 88 μM CaCl_2 ; 1.8 mM Na_2SO_4 ; 6.0 mM NH_4Cl ; 349 μM Na_2HPO_4 , 1.5% (w/v) agar) containing $100 \mu\text{g mL}^{-1}$ spectomycin. For the inoculation 50 mL of rhizobia suspension with optical density at 600 nm of 0.4 - 0.5 was diluted in 1.5 L to inoculate 100 seedlings with each 15 mL. Each plant was fertilized three times a week with 15 mL of threefold diluted modified B&D nutrient solution (Tab. 4). KNO_3 was included for the first three weeks which was stopped with the rhizobia inoculation to avoid a nitrogen-dependent impairment of nodulation. It is critical to not stop nitrogen supply too early because the

fast growing soybean quickly suffer from nitrogen deficiency. After 2.5 more weeks, a second root inspection was performed to keep individual hairy roots separated. Each hairy root is induced by an individual transformation event so that the hairy roots are genetically distinct and thus have to be separated. After a total of about nine weeks the hairy roots and nodules were harvested separately. Nodule sections were produced using a Leica VT1000S vibratome. Nodules were glued to the vibratome plate using superglue. The nodules were submerged in a mix of 50 mM NaH₂PO₄ and 50 mM Na₂HPO₄ for a final pH of 7.5 and were cut into 60 µm sections. Nodule morphology was inspected using Nikon binocular microscope SMZ25 with and without GFP-Long-path filter (Nikon P2-EFL GFP-L).

Table 4 Composition of adjusted B&D nutrient solution used for the cultivation of soybean Williams 82. The final nutrient solution was threefold diluted and was applied on three days of the week.

Compound	Stock concentration (mM)	Final concentration (µM)
CaCl ₂ · 2 H ₂ O	200	100
CaSO ₄ · 2 H ₂ O	10	500
KH ₂ PO ₄	375	3750
K ₂ HPO ₄ · 3 H ₂ O	125	1250
Fe-Citrate · H ₂ O	20	40
MgSO ₄ · 7 H ₂ O	1000	2000
Na ₂ SO ₄	200	200
K ₂ SO ₄	500	1000
MnSO ₄ · H ₂ O	4	8
H ₃ BO ₄	4	8
ZnSO ₄ · 7 H ₂ O	4	8
CuSO ₄ · 5 H ₂ O	1	2
CoSO ₄ · 7 H ₂ O	0.2	0.4
Na ₂ MoO ₄ · 2 H ₂ O	0.2	0.4
NiCl ₂ · 6 H ₂ O	0.2	0.4
KNO ₃ *	2000*	2000*

*KNO₃ was only included in the first three weeks before rhizobia were applied.

Common bean cultivar G19833 was cultivated under the same growth conditions as soybean but was grown in 2:1 vermiculite perlite mix and were inoculated with *Rhizobium tropici* strain CIAT899 for the formation of nodules. Generation of common bean nodules was performed by Luisa Voß according to Voß (2020).

Arabidopsis

Arabidopsis thaliana ecotype Columbia-0 was used. The T-DNA mutants *xmpp-1* (SALK067037) generally referred to as *xmpp* and *xmpp-2* (SALK131244, At2g32150; Zhu, 2016), *nsh1* (SALK083120, At2g36310; Jung *et al.*, 2011), *gsda* (GK432D08, At5g28050; Dahncke and Witte, 2013) and *uox* (SALK131438, At2g26230; Hauck *et al.*, 2014) were obtained from the SALK and GABI-Kat collections (Alonso *et al.*, 2003; Kleinboelting *et al.*, 2012). The mutants *xmpp-1*, *nsh1*, *gsda* and *uox* were used to generate double and triple mutants by crossing. Complementation lines of *xmpp*, *xmpp gsda* and *xmpp nsh1 gsda* were generated by transformation with constructs H453 for TwinStrep-XMPP, H469 for untagged XMPP, X130 for XMPP-HAStrep expression. Complementation lines were generated by floral dipping as described by Baccolini (2019). *Arabidopsis* was cultivated under long-day conditions (16 h light of 85 µmol m⁻² s⁻¹, 22°C / 8 h dark, 20°C) at 60% relative humidity. For metabolite analysis of *Arabidopsis* seeds, six individual plants of each genotype were grown next to each other in a randomized setup. Xanthosine, guanosine and guanine were quantified directly after seed harvest.

Material and Methods

Nucleotide analysis was performed with six months old seeds. Seedlings were grown on half-strength Murashige and Skoog (MS) medium prepared as described by Schröder (2019). For metabolite analysis, each plate contained all genotypes representing one biological replicate. To equalize germination, plates were stored in the dark at 4°C for two days before transfer to the growth chamber. Five days after germination half of the seedlings were transferred into the dark while the other half was kept under long-day conditions. After 48 h, whole seedlings were harvested. For the metabolite analysis of rosettes, eighteen individual plants of each genotype were grown next to each other in a randomized set up. Four-week-old plants were divided in three groups. One group was exposed to an extended night by additional 48 h hours in the dark. Another group was kept under long-day conditions for 48 h. The third group was grown for three more weeks until they were producing seeds. Rosettes were harvested dividing each rosette in two halves of young and old leaves. Samples of the same material were taken to produce immunoblots corresponding to the metabolite data. For the characterization of the complementation lines, seedlings were grown on separate plates for 10 days after germination and were either placed into the dark for 48 h or were kept under long-day conditions for 48 h. Allopurinol treatment of seedlings was performed by applying 500 µL of 200 µM allopurinol per plate at the end of the night when the extended night was starting. For this a 20 mM allopurinol stock solution was prepared in dimethyl sulfoxide which was diluted in water to a working solution of 200 µM. For the MeJA treatment 500 µL of 500 µM MeJA were applied per rosette. A MeJA stock solution of 50 mM was prepared in 100% ethanol which was diluted in water to generate the working solution. For the wounding stimulus a rosette leaf was three times gently pressed in between plastic tweezers. Infiltration of four-week-old Arabidopsis plants with *P. syringae* strain ES4326 suspension with an optical density at 600 nm of 0.1 was performed by Björn Heinmann. Infiltrated and non-infiltrated systemic leaves were harvested five hours after infiltration. For the *uox* suppressor test seeds were germinated on half-strength MS medium. To equalize germination, plates were stored in the dark for two days at 4°C before they were transferred to the growth chamber. Each plate contained all genotypes representing one biological replicate. Three biological replicates were generated. Seed for individual plates were obtained from independent mother plants grown in parallel with all other plants of the experiment. The germination rate was quantified 22 days after the transfer to long-day conditions.

7.2 Cloning

CRISPR Constructs

CRISPR approach was based on the system used by Xie *et al.* (2015) to produce multiple gRNAs from a single polycistronic gene. For this gRNAs were cloned in between tRNAs which *in vivo* will be cleaved by the tRNA-processing system releasing the gRNAs. Vector pGTR (refers to V113) from Xie *et al.* was obtained from Addgene and was used to generate the so-called guide array containing gRNAs, a gRNA scaffold and tRNAs which was eventually cloned into vector pB-CRISPR-35S:GFP (V112, unpublished Marco Herde) for expression of CRISPR machinery and GFP in hairy roots. First, online tools CRISPR-P and CRISPR-PLANT were used to find possible gRNA binding sites (Lei *et al.*, 2014; Xie *et al.*, 2014). Multiple criteria were applied for the selection of gRNAs: 1) Binding sites were located in the first half of the corresponding transcript. 2) Secondary structures of gRNA scaffold were assessed using online tools mfold web server and RNAfold WebServer (Zuker, 2003; Gruber *et al.*, 2008) and showed characteristic two 3' hairpin structures but no secondary 5' structures longer than 7 nt within the first 20 nucleotides. 3) gRNA did not contain more than five consecutive thymidines as it could function as

a stop signal of transcription. 4) gRNA should have a GC content of 40 - 70% (Wang *et al.*, 2014). More criteria recommended by Doench *et al.* (2014) were applied as far as possible: 5) No cytosine at position 3, 6) Cytosine was preferred and guanine avoided at position 16. 7) Guanine was preferred and cytosine avoided at position 20. 8) CGG and not TGG was the preferred PAM sequence. 9) Guanine was avoided for the position after the PAM sequence. 10) Guide RNAs with higher adenine content in the middle were preferred. Sequences encoding gRNAs and primers used for the amplification of these are listed in table (Tab. 5). The gRNA scaffold assembly and amplification was performed as described by Xie *et al.* (2015) which introduced Bpil restriction sites. The gRNA scaffold was cloned into the expression vector V112 using Bpil. The coding sequence of Arabidopsis *XMPP* was amplified from cDNA obtained from flower RNA introducing NcoI and XmaI sites with the primers N188 and N189 or ClaI and XmaI sites with the primers N359 and N360. Via ClaI and XmaI, the coding sequence was introduced into pXCS-HASTrep (Witte *et al.*, 2004; vector V13; construct X130) to generate a C-terminally hemagglutinin (HA)- and Strep-tagged protein by transient expression in *N. benthamiana*. For the production of an N-terminally Strep-tagged protein, the coding sequence was cloned into pXNS2cpmv-strep (from Baccolini and Witte, 2019; V90 construct X144) via NcoI and XmaI. With the NEBuilder HiFi DNA Assembly Kit and protocol (New England Biolabs) XMPP point mutants were generated to produce C-terminally HASTrep-tagged XMPP-S250A (construct H465) and XMPP-S250D (H466) by transient expression in *N. benthamiana*. Primers N359 and P1111 with 2904 and P1112 were

Table 5: Information about CRISPR constructs used to produce knockout nodules. Clone numbers are set in parentheses. For soybean each gene was targeted with two gRNAs. Primers used to amplify sequences coding for gRNA are listed. Note, the combination of primers is different than the pairs mentioned here, depending on which gRNAs are cloned in which order into the gRNA array. See Xie *et al.* (2015) for details.

Gene	Accession	Sequence encoding gRNA (5' to 3')	Primers
Soybean			
<i>XMPP</i> CRISPR construct (H313)			
<i>XMPP1</i>	Glyma.10G248900	gRNA1: AGGCCTCGATATCACTGCAG	P709 and P710
	both	gRNA3: ACCTACGGAAGCACCCCTTGC	P711 and P712
<i>XMPP2</i>	Glyma.20G144800	gRNA2: AGGCCATGATATCACCCGCAG	P713 and P714
<i>XDH</i> CRISPR construct (H277)			
<i>XDH1-1</i>	Glyma.13G340300	gRNA1: TGCAAACCGTTGGGAGGCAT	P721 and P722
	both	gRNA2: TGGGACTAACTAGGCTGTG	P723 and P724
<i>XDH1-2</i>	Glyma.15G034000	gRNA3: GGTCTGACCGGGACAAAACCT	P725 and P726
		gRNA4: AGGGATGCACGTGATTACAG	P727 and P728
<i>GSDA</i> CRISPR construct (H276)			
<i>GSDA1</i>	Glyma.09G080100	gRNA1: TCAGTAGCTTCTGCGTTTGC	P281 and P282
	both	gRNA3: GGGGTAGACTGTGAAGATGG	P277 and P278
<i>GSDA2</i>	Glyma.15G186100	gRNA2: GCGTTTGCTGGACATAAGGA	P715 and P716
<i>GSDA3</i>	Glyma.20G37210	gRNA4: AGTAACCTCAGCATGGGCAG	P717 and P718
		gRNA5: GCTTCTGCTGCTACTGCTAA	P719 and P720
Common bean			
<i>XMPP</i> CRISPR construct (H1040)	Phvul.007G056000	ACTGACTCGCAAACCGGCGA	P2325 and P2331
<i>XDH1</i> CRISPR construct (H1041)	Phvul.005G148000	GTTTCGTAGAGTGTAGCTGA	P2329 and P2332

Material and Methods

used to introduce the changes encoding the S250A mutation. Primers N359 and P1113 with 2904 and P1114 were used to introduce the changes encoding the S250D mutation. To obtain the complementation lines *xmpp gsda::sX* and *xmpp nsh1 gsda::sX*, and *xmpp::X* clones H453 and H469 were generated, respectively. For H453, a genomic fragment of 999 bp upstream of the *XMPP* translation start codon was cloned with an introduced coding sequence for a TwinStrep tag for N-terminal tagging. For this, pXNS2pat-Strep-sl (V28) was generated by cloning the annealed primers 1709 and 1710 into the binary vector pAMPAT-MCS (accession number AY436765) opened with XhoI and EcoRI. V28 was used to generate pXNS2patTwinStrep-sl (V163) by opening V28 with KasI and NcoI and introducing a second Strep tag with a preceding linker sequence formed by the annealed primers P1097 and P1098. *XMPP* genomic DNA was amplified using the primers N188 and N189 and cloned into V163 via NcoI and XmaI. Into this construct the *XMPP* promoter, amplified with the primers P1094 and P1103, was cloned via AscI and XhoI replacing a 35S promoter cassette (construct H453). For H469, *XMPP* coding sequence was amplified from Arabidopsis cDNA with primers P359 and P1155 introducing ClaI and XmaI sites. Via ClaI and XmaI the coding sequence was introduced into V13 for expression of untagged XMPP in *xmpp::X* complementation line. To produce untagged Arabidopsis XMPP in *Escherichia coli* strain BL21 (DE3) for antibody production, *XMPP* amplified with the primers N188 and N189 from Arabidopsis cDNA was cloned into pET30nco-CTH (from Myrach *et al.*, 2017; V48) using ClaI and SmaI for the *XMPP* cDNA and ClaI and EcoRV for the vector (construct H325). The coding sequence of soybean *XMPP2* was amplified from root cDNA introducing ClaI and XmaI sites with primers P634 and P635. The coding sequence was cloned into pXCScpmv-HA-Strep (from Myrach *et al.*, 2017; V69; construct H330) to produce C-terminally HAStrep-tagged soybean XMPP by transient expression in *N. benthamiana*.

7.3 Transformation of bacteria

Transformation of *Escherichia coli* strains Dh10B (Invitrogen) in the cloning process and BL21 (Novagen) to produce XMPP as antigen for the antibody production, as well as *A. rhizogenes* (strain K599; Kereszt *et al.*, 2007) for the induction of soybean hairy roots and *A. tumefaciens* (strain GV3101::pMP90RK; Koncz and Schell, 1986) for transient and stable expression of XMPP variants in *N. benthamiana* and Arabidopsis were performed by electroporation as described by Baccolini (2019).

7.4 Fragment length analysis

For the identification of nodules which were successfully mutated by CRISPR-Cas9 and subsequent NHEJ, fragment length analysis (FLA) was performed. Genomic DNA isolated from fresh or freeze-dried roots or nodules can be used to amplify fragments spanning the gRNA binding sites. Primers were prepared so that each primer set was specific for one gRNA binding site and in case of soybean for only one of the homologs. For soybean *XMPP1* gRNA 1 binding site primers P1918 and P1919, and for *XMPP1* gRNA 3 binding site primers P1920 and P1921 were used. For soybean *XMPP2* gRNA 2 binding site primers P1923 and P1924, and for *XMPP2* gRNA 3 binding site primers P1920 and P1922 were used. For common bean *XMPP* gRNA and *XDH* gRNA binding sites primers P2497 with P2498 and P2499 with P2500 were used, respectively. Forward primers contained an M13 tail so that in the second part of the amplification program the dye-labelled M13 primer could bind. The composition of the reaction mix and the used temperature program are listed in Table 6. Either JOE- or FAM-dye-labelled M13

primer was used (Ju *et al.*, 1995). Wild-type DNA and DNA from potential knockout nodules were labelled differently. After amplification, 1 μ L of wild-type and 1 μ L of sample reaction mixtures were mixed with 0.2 μ L of Orange 500 DNA Size Standard (Nimagen) and 10 μ L Hi-Di Formamid (Thermo Fisher Scientific) and denatured for 5 min at 95 °C followed by a quick cooling on ice. FLA was performed with ABIPRISM 310 Genetic Analyzer using POP-7 polymer (Thermo Fisher Scientific) and GeneMapper ID version 3.2 software was used for the analysis of size chromatograms.

Table 6 Composition of reaction mixture and temperature program used to amplify fragments for FLA. F- and R-primer refer to forward and reverse primers. Either M13 primer coupled to JOE or FAM dye was used.

A Fragment amplification		B Temperature program			
Component	Conc.	Purpose	Temp. (°C)	Time (m:ss)	Cycles
Fusion HF Buffer ^a	1x	Initial denaturation	95	6:00	
dNTPS (each)	0.25 mM	Denaturation	95	0:30	30x
F-primer (M13-tailed)	50 nM	Annealing	60	0:20	
R-primer	250 nM	Elongation	72	0:20	
M13 primer with dye	125 nM	Denaturation	95	0:30	7x
gDNA	0.1-10 ng μ L ⁻¹	Annealing	52	0:45	
Phusion ^a	2.5% (v/v)	Elongation	72	0:20	
^a F630L, ThermoFisher Scientific		Final Elongation	72	5:00	

7.5 Protein affinity purification and phosphatase activity assay

N. benthamiana were grown under long-day conditions (16 h light of 85 μ mol m⁻² s⁻¹, 22°C / 8 h dark, 20°C) and were used for transient expression of Strep-tagged proteins from constructs X130, X144, H465, H466 and H330 according to Baccolini and Witte (2019) and Werner *et al.* (2008). The affinity purification was performed as described by Baccolini and Witte but with an adjusted extraction buffer (Buffer E) containing 100 mM HEPES (pH 8.0), 100 mM NaCl, 5 mM EDTA (pH 8.0), 0.005% Triton-X100, 10 mM dithiothreitol, 1:625 diluted Bioblock (IBA Life Sciences), 1:10 diluted protease inhibitor (complete protease inhibitor cocktail, Roche). Phosphatase activity was measured at 22°C with the Enzc hek Phosphate Assay Kit (Thermo Fisher Scientific) according to the manufacturer's instructions but in a total volume of 200 μ L. In brief, 2-amino-6-mercapto-7-methyl-purine (MESG) and inorganic phosphate produced from the XMPP-dependent reaction serve as two substrates for purine nucleoside phosphorylase, resulting in a product exhibiting an absorbance at 360 nm. Absorption changes were recorded using Shimadzu UV-2700 spectrophotometer. For kinetic measurements, XMPP amounts were adjusted to obtain linear initial rates at all XMP concentrations. Protein concentrations were determined with bovine serum albumin standards in a Coomassie-stained sodium dodecyl sulfate (SDS) gel using an Odyssey Fc Imager (LI-COR Biosciences; Coomassie Brilliant Blue R 250, Roth). To determine the kinetic constants, the data were plotted and fitted with the GraphPad Prism 4 software. For the substrate screen and for testing whether XMPP is inhibited by guanosine or xanthosine, XMPP with a C-terminal HA-Strep tag (expressed from X130) was used.

7.6 Immunoblots

Mini-PROTEAN Tetra Cell System was used for SDS polyacrylamide gel electrophoresis. When working with XMPP, GSDA and NSH1, 0.75 mm thick gels containing 10% acrylamide were used loading 15 μL of sample. The additional stacking gel always contained 4% acrylamide. For the preparation of immunoblots to detect XDH, 1.5 mm thick gels including 8% acrylamide and a loading volume of 30 μL were used. Proteins were extracted with buffer E from the affinity purification using a 1:2 tissue to buffer ratio. For the anti-XDH immunoblot the protein transfer to a nitrocellulose membrane (0.45 μm pore size, Thermo Fisher Scientific) was performed by tank blotting using the Mini Trans-Blot Cell (BioRad) according to manufacturer's instructions. The blot was performed 16 h overnight in blotting buffer (38.4 mM Tris HCl, pH 9.2; 32 mM glycine; 0.4 mM SDS) at room temperature (RT). For all other immunoblots semi-dry blotting to the nitrocellulose membrane was performed using the turbo program for mini gels of Trans-Blot Turbo Transfer System (Biorad) according to the manufacturer's instructions using the same blotting buffer. The membrane was blocked with 5% milk powder in TBS-T (20 mM TRIS HCl, pH 7.6; 150 mM NaCl; 0.1% (v/v) Tween 20) and was incubated with primary antibodies. For the detection of XMPP the custom-made rabbit polyclonal anti-XMPP antibody (1 $\mu\text{g mL}^{-1}$) in TBS-T with 0.5% (w/v) milk powder was incubated overnight at 4 °C. For the detection of GSDA, custom-made rabbit anti-serum was used in a 1:500 dilution for 1 h at RT (Dahncke and Witte, 2013). For the detection of NSH1, custom-made rabbit polyclonal anti-NSH1 antibody (0.2 $\mu\text{g mL}^{-1}$; Baccolini and Witte, 2019) was used for 1 h at RT. For the detection of XDH, monoclonal anti-XDH antibody (RD2, iTUBS antibody facility) was used in a 1:5000 dilution at RT. The membrane was washed three times for 10 min with TBS-T and incubated with secondary antibodies in TBS-T for 1 h at room temperature and washed as before. For the detection of XMPP, goat anti-rabbit IgG horseradish peroxidase conjugate antibody (RABHRP1, 1:10,000, Sigma-Aldrich) was used. For the detection of GSDA and NSH1 anti-rabbit IgG alkaline phosphatase conjugate antibody (A3562, 1:10,000, Sigma-Aldrich) was used. For the detection of XDH anti-mouse IgG alkaline phosphatase conjugate antibody (A9316, 1:10,000, Sigma-Aldrich) was used. For detection of XMPP, SuperSignal West Femto Maximum Sensitivity Substrate (Thermo Fisher Scientific) was used according to the manufacturer's instructions. The chemiluminescence was detected by a Lumi-Imager F1 (Roche). For the detection of GSDA, NSH1 and XDH, 5-bromo-4-chloro-3-indolyl-phosphate (BCIP) and nitro blue tetrazolium (NBT) were used according to Baccolini (2019). Total protein concentrations of rosette leaves were determined using Bradford (Serva) according to manufacturer's instructions for microtiter plate assay. Bovine serum albumin was used to produce a concentration standard row. In a 96-well plate 50 μL of sample or standard were added per well. For each sample and standard three technical replicates were prepared. Bradford 5x stock solution was mixed with water in ratio 2:7.5. A multi-channel pipette was used to add 200 μL Bradford working solution to each well. After 5 min of incubation the absorption of each well was measured at 595 nm using Thermo Fisher Scientific Multiskan GO Microplate Spectrophotometer.

7.7 Production of custom-made polyclonal anti-XMPP antibody

Untagged Arabidopsis XMPP protein was produced in *E. coli* strain BL21 using construct H325 and precipitated in inclusion bodies. Inclusion bodies were isolated as described by Baccolini and Witte (2019) and were used for commercial antibody production (by immunoGlobe). Production of antisera and affinity purification of the antibody was performed by immunoGlobe.

7.8 Metabolite analysis

The extraction method was adapted from Hauck *et al.* (2014). For metabolite analysis, frozen or freeze-dried plant material was homogenized with steel beads using a mixer mill MM 400 (Retsch). When working with frozen material, tube racks were pre-cooled in liquid nitrogen. Ten milligrams of seeds were frozen in liquid nitrogen and were ground with one 4 mm steel bead and five 2 mm steel beads for 4.5 min at 28 s⁻¹. For frozen seedlings, 50 mg were ground with five 2 mm steel beads for 4.5 min at 28 s⁻¹. For freeze-dried rosette leaves, 10 mg were ground as performed for the seedlings. Freeze-dried nodules were homogenized using a 7 mm steel bead and 1 mg was used for the metabolite analysis. For the extraction, 10 mM ammonium acetate buffer (pH 7.5) pre-warmed to 60°C was used and samples were immediately transferred to a heat block at 95°C for shaking at 1000 rpm for 10 min. For seeds, rosette leaves and nodules 1 mL and for seedlings 500 µL of extraction buffer were added. Following the heat treatment, samples were chilled on ice for 5 min. After centrifugation at 20 000g for 10 min at 4°C, 80% of the supernatant was transferred to a new tube to remove beads and cell debris. By centrifugation at 45,000g for 15 min at 4°C particles which might block the HPLC system were removed.

Xanthosine, xanthine, guanosine, guanine, inosine, uric acid, allantoin and allantoate in *Arabidopsis* tissues and soybean nodules were quantified using an Agilent HPLC 1200 system with a Polaris 5 C18-A 50 x 4.6 mm column (Agilent Technologies) coupled to an Agilent 6460C series triple quadrupole mass spectrometer. Except for uric acid and allantoin, measurements were performed in the positive ion mode. Ammonium acetate (10 mM, pH 7.5) and 100% methanol served as solvents A and B as described by Baccolini and Witte (2019). The flow rate was 0.8 mL min⁻¹ and the injection volume of samples was 20 µL. Seed extracts were diluted 50-fold except for the quantification of allantoin and inosine which were quantified in undiluted extracts. Seedling extracts were not diluted for the quantification of xanthosine, xanthine, inosine, hypoxanthine, uric acid and allantoate and 100-fold diluted for the quantification of guanosine. Rosette extracts were 100-fold diluted. Soybean nodule extracts were used undiluted except for the quantification of xanthine in xanthine accumulating nodules which required a 10-fold dilution of extracts. External standard dilutions spiked 1:10 into the wild-type matrix were used for quantification of xanthosine, xanthine, guanosine, guanine and inosine. For the quantification of uric acid, allantoin and allantoate, the *xmpp gsdA* matrix was used. The MS parameters are listed in table 7. Measurements failing the quality criteria for retention time, qualifier to quantifier ratio or signal to noise ratio below seven were called “not detected” (Chapter 7.8). The quantification of nucleotides was performed by Henryk Straube as described by Straube *et al.* (2021). As the chromatography with the Polaris 5 C18-A 50 x 4.6 mm limited the detection sensitivity for allantoin and uric acid, a new chromatography using SeQuant ZIC-cHILIC 3µm, 100Å 150 x 2.1 mm (Merck Millipore) was established with Dr. Marco Herde, which was used for the analysis of common bean nodules. Solvent A was acetonitrile and 50 mM ammonium acetate pH5.8 in a 95:5 ratio and solvent B was water, 50 mM ammonium acetate pH5.8 and acetonitrile in a 50:45:5 ratio. For HILIC chromatography solvent of metabolite extracts were removed by freeze-drying overnight and replaced by 1.5-fold bigger volume of HILIC solvent A. Injection volume was 10 µL and flow rate 0.3 mL min⁻¹. The solvent B gradient was as follows: 0.0 min, 0% B; 5.0 min, 5% B; 10.0 min, 25% B; 15.0 min, 30% B; 17.0 min, 65% B; 20.0 min, 95% B; 31.0 min, 95% B; 31.1 min, 5%; 40.1 min, 5%.

Material and Methods

Table 7 LC-MS parameters.

MS source parameter	Positive ion mode	Negative ion mode
Ion source	AJS ESI	AJS ESI
Gas temperature	300 °C	350 °C
Gas flow	12 L min ⁻¹	12 L min ⁻¹
Nebulizer	30 psi	40 psi
Sheath gas heater	300 °C	350 °C
Sheath gas flow	11 L min ⁻¹	12 L min ⁻¹
Capillary	4,000 V	2,500 V

Analyte	Ion mode	Retention time (min) ^a	Precursor ion (m/z)	Product ion ^b (m/z)	Fragmen- tor (V)	Collision energy (V)	Qualifier ratio
Allantoate	pos.	0.9	177.1	117.0	60	25	21.9 – 36.1
				74.0	60	25	
Allantoin	neg.	0.9	157.0	113.9	96	15	96-6 – 144-0
				96.9	96	15	
XMP ^c	pos.	1.0	365.0	212.9	84	3	58.6 – 85.9
				153.0	84	15	
Uric acid	neg.	1.3	167.0	124.0	91	14	11.1 – 22.3
				69.2	91	20	
Xanthosine	pos.	1.8	285.1	153.0	60	5	13.6 – 23.3
				135.9	60	35	
Xanthine	Pos.	2.4	153.1	109.0	100	15	47.9 – 75.1
				55.2	100	33	
Guanine	pos.	2.2	152.1	135.0	118	18	43.9 – 66.5
				110.0	118	22	
Hypoxanthine	pos.	2.5	137.1	118.9	117	22	67.6 – 95.3
				110.0	117	22	
Inosine	pos.	5.8	269.1	136.9	55	14	7.9 – 12.1
				118.9	55	40	
Guanosine	pos.	6.1	284.1	152.0	90	10	26.0 – 39.5
				135.0	90	45	

^a Retention times are affected by matrix and can vary depending on the analyzed tissue.

^b The first listed product ion was used for quantification.

^c XMP was only quantified in nodules like this. In Arabidopsis seeds it was performed according to Straube *et al.* (2021).

7.9 Statistical Analyses

Data for the determination of kinetic constants were plotted and analyzed using the GraphPad Prism 4 software. For metabolite data, the R software version 4.0.5, RStudio version 1.2.5042 and CRAN packages multcomp and sandwich were used to perform two-sided Tukey's pairwise comparisons and to consider heteroscedasticity of the data set with the sandwich variance estimator (Herberich *et al.*, 2010; Pallmann and Hothorn, 2016). Using the same packages, two-sided Dunnett's comparisons to the reference group (XMPP + 10 μ M XMP) were performed for the inhibitor test. Two-sided t tests assuming variance homogeneity were performed with Microsoft Excel 2016.

7.10 Software

Data acquisition: UV probe version 2.51 was used to record absorption changes during enzyme assays using Shimadzu UV-2700 Spectrophotometer. GeneMapper ID version 3.2 was used to analyze size chromatograms generated by ABI PRISM 310 Genetic Analyzer. Skanit Software 3.2 was used with Thermo Fisher Scientific Multiskan GO Microplate Spectrophotometer to measure the absorption of extracts in different wells. LumiAnalyst version 3.1 was used to take pictures of the chemiluminescence detection using Roch Lumi-Imager F1. LC-MS data were collected by MassHunter Workstation Software Data LC/MS Data Acquisition B.07.01. Leica Application Suite X version 3.7.2.22383 was used for the generation of pictures using Leica TCS SP8 confocal microscope. NIS-Elements version 4.30.02 was used to operate Nikon binocular microscope SMZ25. MassHunter Workstation Software Quantitative Analysis B.09.01 was used to analyze LC-MS data. Microsoft Excel 2016 was used for data analysis. Microsoft Word 2016 was used for writing this manuscript. R software version 4.0.5 and RStudio version 1.2.5042 were used for statistical analysis. GraphPad Prism 4 and Affinity Designer and Photo version 1.9.2.1035 were used for the preparation of figures. GraphPad Prism 4 was also used to plot Michaelis Menten curves. Genevestigator (Hruz *et al.*, 2008) and eFP browser (Winter *et al.*, 2007) were used to access online accessible transcript data. PhosPhAt 4.0 was used to search for phosphorylation sites (Heazlewood *et al.*, 2008). CLUSTAL 2.1 Multiple Sequence Alignment tool (Larkin *et al.*, 2007) at Usegalaxy.org (Afgan *et al.*, 2018) applying default settings and BoxShade at ExPASy version 3.2. were used to generate multiple sequence alignments.

8 References

- Afgan, E. Baker, D. Batut, B. van den Beek, M. Bouvier, D. Cech, M., *et al.* (2018). The Galaxy platform for accessible, reproducible and collaborative biomedical analyses: 2018 update. *Nucleic Acids Research*. Vol. 46. No. W1, p. W537-W544. doi: 10.1093/nar/gky379
- Alonso, J. M. Stepanova, A. N. Lisse, T. J. Kim, C. J. Chen, H. Shinn, P., *et al.* (2003). Genome-wide insertional mutagenesis of *Arabidopsis thaliana*. *Science*. Vol. 301. No. 5633, p. 653–657. doi: 10.1126/science.1086391
- Apodaca, L. U.S. Geological Survey (2020). *Mineral Commodity Summary 2020*, <https://pubs.er.usgs.gov/publication/mcs2020>. Accessed January 23, 2021.
- Arias, M. C. Pelletier, S. Hilliou, F. Wattebled, F. Renou, J.-P. and D'Hulst, C. (2014). From Dusk till Dawn: The *Arabidopsis thaliana* Sugar Starving Responsive Network. *Frontiers in Plant Science*. Vol. 5, p. 482ff. doi: 10.3389/fpls.2014.00482
- AtGenExpress: Methyl Jasmonate time course in wildtype seedlings, ME00337 in AT-00110* (2015).
- Atkins, C. A. (1981). Metabolism of purine nucleotides to form ureides in nitrogen-fixing nodules of cowpea (*Vigna unguiculata* L. Walp.). *FEBS letters*. Vol. 125. No. 1, p. 89–93. doi: 10.1016/0014-5793(81)81003-4
- Baccolini, C. (2019). *Analysis of in vivo Purine Nucleotide Catabolism in Arabidopsis thaliana with Focus on Nucleoside Hydrolase 2*. Dissertation. Hannover, Germany: Leibniz Universität Hannover, Institut für Pflanzenernährung.
- Baccolini, C. and Witte, C.-P. (2019). AMP and GMP Catabolism in *Arabidopsis* Converge on Xanthosine, Which Is Degraded by a Nucleoside Hydrolase Heterocomplex. *The Plant Cell*. Vol. 31. No. 3, p. 734–751. doi: 10.1105/tpc.18.00899
- Baena-González, E. and Lunn, J. E. (2020). SnRK1 and trehalose 6-phosphate - two ancient pathways converge to regulate plant metabolism and growth. *Current Opinion in Plant Biology*. Vol. 55, p. 52–59. doi: 10.1016/j.pbi.2020.01.010
- Baena-González, E. Rolland, F. Thevelein, J. M. and Sheen, J. (2007). A central integrator of transcription networks in plant stress and energy signalling. *Nature*. Vol. 448. No. 7156, p. 938–942. doi: 10.1038/nature06069
- Barbottin, A. Lecomte, C. Bouchard, C. and Jeuffroy, M.-H. (2005). Nitrogen Remobilization during Grain Filling in Wheat: Genotypic and Environmental Effects. *Crop Science*. Vol. 45. No. 3, p. 1141–1150. doi: 10.2135/cropsci2003.0361
- BASF, Badische Anilin- & Sodafabrik in Ludwigshafen am Rhein (1908). *Verfahren zur Synthetischen Darstellung von Ammoniak aus den Elementen*. No. DE235421. Deutschland.
- Bergersen, F. J. (1958). The Bacterial Component of Soybean Root Nodules; Changes in Respiratory Activity, Cell Dry Weight and Nucleic Acid Content with Increasing Nodule Age. *Microbiology*. Vol. 19. No. 2, p. 312–323. doi: 10.1099/00221287-19-2-312
- Bergmann, H. Preddie, E. and Verma, D. P. (1983). Nodulin-35: A Subunit of Specific Uricase (Uricase II) Induced and Localized in the Uninfected Cells of Soybean Nodules. *The EMBO journal*. Vol. 2. No. 12, p. 2333–2339.
- Betsuyaku, S. Katou, S. Takebayashi, Y. Sakakibara, H. Nomura, N. and Fukuda, H. (2018). Salicylic Acid and Jasmonic Acid Pathways are Activated in Spatially Different Domains Around the Infection Site During Effector-Triggered Immunity in *Arabidopsis thaliana*. *Plant and Cell Physiology*. Vol. 59. No. 1, p. 8–16. doi: 10.1093/pcp/pcx181

- Bouwman, A. F. Boumans, L. J. M. and Batjes, N. H. (2002). Estimation of global NH₃ volatilization loss from synthetic fertilizers and animal manure applied to arable lands and grasslands. *Global Biogeochemical Cycles*. Vol. 16. No. 2, p. 8.1-8.14. doi: 10.1029/2000GB001389
- Broughton, W. J. and Dilworth, M. J. (1971). Control of leghaemoglobin synthesis in snake beans. *Biochemical Journal*. Vol. 125. No. 4, p. 1075–1080.
- Brychkova, G. Alikulov, Z. Fluhr, R. and Sagi, M. (2008). A Critical Role for Ureides in Dark and Senescence-induced Purine Remobilization is Unmasked in the *Atxdh1* Arabidopsis Mutant. *The Plant Journal*. Vol. 54. No. 3, p. 496–509. doi: 10.1111/j.1365-313X.2008.03440.x
- Buey, R. M. Ledesma-Amaro, R. Velázquez-Campoy, A. Balsera, M. Chagoyen, M. Pereda, J. M. d., et al. (2015). Guanine Nucleotide Binding to the Bateman Domain Mediates the Allosteric Inhibition of Eukaryotic IMP Dehydrogenases. *Nature Communications*. Vol. 6, p. 8923. doi: 10.1038/ncomms9923
- Cao, D. Takeshima, R. Zhao, C. Liu, B. Jun, A. and Kong, F. (2017). Molecular Mechanisms of Flowering under Long Days and Stem Growth Habit in Soybean. *Journal of Experimental Botany*. Vol. 68. No. 8, p. 1873–1884. doi: 10.1093/jxb/erw394
- Carter, A. M. and Tegeder, M. (2016). Increasing Nitrogen Fixation and Seed Development in Soybean Requires Complex Adjustments of Nodule Nitrogen Metabolism and Partitioning Processes. *Current Biology*. Vol. 26. No. 15, p. 2044–2051. doi: 10.1016/j.cub.2016.06.003
- Carter, E. L. Flugga, N. Boer, J. L. Mulrooney, S. B. and Hausinger, R. P. (2009). Interplay of metal ions and urease. *Metallomics*. Vol. 1. No. 3, p. 207–221. doi: 10.1039/b903311d
- Coletto, I. Pineda, M. and Alamillo, J. M. (2019). Molecular and Biochemical Analysis of XDH from *Phaseolus vulgaris* Suggest that Uric Acid Protects the Enzyme against the Inhibitory Effects of Nitric Oxide in Nodules. *Plant Physiology and Biochemistry*. Vol. 143, p. 364–374. doi: 10.1016/j.plaphy.2019.09.008
- Corwin, J. A. Copeland, D. Feusier, J. Subedy, A. Eshbaugh, R. Palmer, C., et al. (2016). The Quantitative Basis of the Arabidopsis Innate Immune System to Endemic Pathogens Depends on Pathogen Genetics. *PLOS Genetics*. Vol. 12. No. 2, p. e1005789. doi: 10.1371/journal.pgen.1005789
- Dahncke, K. (2014). *Charakterisierung der Guanosindeaminase von Arabidopsis thaliana und Evaluation ihrer Bedeutung für den Purinnukleotidabbau*. Dissertation. Berlin: Freie Universität Berlin, Abteilung Biochemie der Pflanze.
- Dahncke, K. and Witte, C.-P. (2013). Plant Purine Nucleoside Catabolism Employs a Guanosine Deaminase Required for the Generation of Xanthosine in Arabidopsis. *The Plant Cell*. Vol. 25. No. 10, p. 4101–4109. doi: 10.1105/tpc.113.117184
- Doench, J. G. Hartenian, E. Graham, D. B. Tothova, Z. Hegde, M. Smith, I., et al. (2014). Rational Design of Highly Active sgRNAs for CRISPR-Cas9-mediated Gene Inactivation. *Nature Biotechnology*. Vol. 32. No. 12, p. 1262–1267. doi: 10.1038/nbt.3026
- Emanuelle, S. Doblin, M. S. Stapleton, D. I. Bacic, A. and Gooley, P. R. (2016). Molecular Insights into the Enigmatic Metabolic Regulator, SnRK1. *Trends in Plant Science*. Vol. 21. No. 4, p. 341–353. doi: 10.1016/j.tplants.2015.11.001
- Emanuelle, S. Hossain, M. I. Moller, I. E. Pedersen, H. L. van de Meene, A. M. L. Doblin, M. S., et al. (2015). SnRK1 from Arabidopsis thaliana is an atypical AMPK. *The Plant Journal*. Vol. 82. No. 2, p. 183–192. doi: 10.1111/tpj.12813
- Emmanuel, N. Rangunathan, S. Shan, Q. Wang, F. Giannakou, A. Huser, N., et al. (2017). Purine Nucleotide Availability Regulates mTORC1 Activity through the Rheb GTPase. *Cell Reports*. Vol. 19. No. 13, p. 2665–2680. doi: 10.1016/j.celrep.2017.05.043

References

- Erisman, J. W. Sutton, M. A. Galloway, J. Klimont, Z. and Winiwarter, W. (2008). How a Century of Ammonia Synthesis Changed the World. *Nature Geoscience*. Vol. 1. No. 10, p. 636–639. doi: 10.1038/ngeo325
- Evans, H. J. and Kliewer, M. (1964). Vitamin B12 compounds in relation to the requirement if cobalt for higher plants and nitrogen-fixing organisms. *Annals of the New York Academy of Sciences*. Vol. 112, p. 735–755. doi: 10.1111/j.1749-6632.1964.tb45052.x
- Floyd, B. E. Morriss, S. C. MacIntosh, G. C. and Bassham, D. C. (2015). Evidence for autophagy-dependent pathways of rRNA turnover in Arabidopsis. *Autophagy*. Vol. 11. No. 12, p. 2199–2212. doi: 10.1080/15548627.2015.1106664
- Foresti, W. A. M. (2020). *The role of Guanosine Deaminase for Ureide Biosynthesis in the Nodule of Phaseolus vulgaris*. M. Sc. Thesis. Hannover: Leibniz Universität Hannover, Institut für Pflanzenernährung.
- Freitas, D. S. Rodak, B. W. Carneiro, M. A. C. and Guilherme, L. R. G. (2019). How does Ni fertilization affect a responsive soybean genotype? A dose study. *Plant and Soil*. Vol. 441. No. 1-2, p. 567–586. doi: 10.1007/s11104-019-04146-2
- Fujihara, S. and Yamaguchi, M. (1978). Effects of Allopurinol 4-Hydroxypyrazolo(3,4-d)Pyrimidine on the Metabolism of Allantoin in Soybean Plants. *Plant Physiology*. Vol. 62. No. 1, p. 134–138. doi: 10.1104/pp.62.1.134
- Greville, K. (2006). *Investigating the links between organic acid and carbohydrate regulation of gene expression*. GSE6158, AT-00063, <https://www.ncbi.nlm.nih.gov/geo/query/acc.cgi?acc=GSE6158>. Accessed July 04, 2021.
- Gruber, A. R. Lorenz, R. Bernhart, S. H. Neuböck, R. and Hofacker, I. L. (2008). The Vienna RNA websuite. *Nucleic Acids Research*. Vol. 36. No. Web Server issue, p. W70-74. doi: 10.1093/nar/gkn188
- Gutierrez, R. A. Ewing, R. M. Cherry, J. M. and Green, P. J. (2002). Identification of Unstable Transcripts in Arabidopsis by cDNA Microarray Analysis: Rapid Decay is Associated with a Group of Touch- and Specific Clock-controlled Genes. *Proceedings of the National Academy of Sciences of the United States of America*. Vol. 99. No. 17, p. 11513–11518. doi: 10.1073/pnas.152204099
- Hanks, J. F. Schubert, K. and Tolbert, N. E. (1983). Isolation and Characterization of Infected and Uninfected Cells from Soybean Nodules: Role of Uninfected Cells in Ureide Synthesis. *Plant Physiology*. Vol. 71. No. 4, p. 869–873.
- Hanson, J. Hanssen, M. Wiese, A. Hendriks, M. M. W. B. and Smeekens, S. (2008). The sucrose regulated transcription factor bZIP11 affects amino acid metabolism by regulating the expression of ASPARAGINE SYNTHETASE1 and PROLINE DEHYDROGENASE2. *The Plant Journal*. Vol. 53. No. 6, p. 935–949. doi: 10.1111/j.1365-313X.2007.03385.x
- Hauck, O. K. Scharnberg, J. Escobar, N. M. Wanner, G. Giavalisco, P. and Witte, C.-P. (2014). Uric acid Accumulation in an Arabidopsis Urate Oxidase Mutant Impairs Seedling Establishment by Blocking Peroxisome maintenance. *The Plant Cell*. Vol. 26. No. 7, p. 3090–3100. doi: 10.1105/tpc.114.124008
- Heazlewood, J. L. Durek, P. Hummel, J. Selbig, J. Weckwerth, W. Walther, D., et al. (2008). PhosPhAt: A database of phosphorylation sites in Arabidopsis thaliana and a plant-specific phosphorylation site predictor. *Nucleic Acids Res*. Vol. 36. No. Database issue, p. D1015-21. doi: 10.1093/nar/gkm812
- Heinemann, B. and Hildebrandt, T. M. (2021). The role of amino acid metabolism in signaling and metabolic adaptation to stress induced energy deficiency in plants. *Journal of Experimental Botany*. Vol. 72. No. 13, p. 4634–4645. doi: 10.1093/jxb/erab182

- Heinemann, K. J. Yang, S.-Y. Straube, H. Medina-Escobar, N. Varbanova-Herde, M. Herde, M., *et al.* (2021). Initiation of cytosolic plant purine nucleotide catabolism involves a monospecific xanthosine monophosphate phosphatase. *Nature Communications*. Vol. 12. No. 1, p. 793. doi: 10.1038/s41467-021-27152-4
- Hellriegel, H. and Wilfarth, H. (1889). Erfolgt die Assimilation des Freien Stickstoffs durch die Leguminosen unter Mitwirkung Niederer Organismen? *Berichte der Deutschen Botanischen Gesellschaft*. Vol. 7. doi: 10.1111/j.1438-8677.1889.tb05680.x
- Herberich, E. Sikorski, J. and Hothorn, T. (2010). A robust procedure for comparing multiple means under heteroscedasticity in unbalanced designs. *PLoS One*. Vol. 5. No. 3, p. e9788. doi: 10.1371/journal.pone.0009788
- Hildebrandt, T. M. Nunes Nesi, A. Araújo, W. L. and Braun, H.-P. (2015). Amino Acid Catabolism in Plants. *Molecular plant*. Vol. 8. No. 11, p. 1563–1579. doi: 10.1016/j.molp.2015.09.005
- Hoagland, D. R. and Arnon, D. I. (1950). The water-culture method for growing plants without soil. *California Agricultural Experiment Station*. Vol. 347, p. 22.
- Hoxhaj, G. Hughes-Hallett, J. Timson, R. C. Ilagan, E. Yuan, M. Asara, J. M., *et al.* (2017). The mTORC1 Signaling Network Senses Changes in Cellular Purine Nucleotide Levels. *Cell Reports*. Vol. 21. No. 5, p. 1331–1346. doi: 10.1016/j.celrep.2017.10.029
- Hruz, T. Laule, O. Szabo, G. Wessendorp, F. Bleuler, S. Oertle, L., *et al.* (2008). Genevestigator v3: A reference expression database for the meta-analysis of transcriptomes. *Advances in bioinformatics*. Vol. 2008, p. 420747. doi: 10.1155/2008/420747
- IPCC, Intergovernmental Panel on Climate Change (2013). *Climate Change 2013: The Physical Science Basis: Working Group I Contribution to the Fifth Assessment Report of the Intergovernmental Panel on Climate Change*. Cambridge University Press.
- Irani, S. and Todd, C. D. (2016). Ureide Metabolism under Abiotic Stress in *Arabidopsis thaliana*. *Journal of Plant Physiology*. Vol. 199, p. 87–95. doi: 10.1016/j.jplph.2016.05.011
- Johnson, M. C. and Kollman, J. M. (2020). Cryo-EM Structures Demonstrate Human IMPDH2 Filament Assembly Tunes Allosteric Regulation. *eLife*. Vol. 9, p. 213. doi: 10.7554/eLife.53243
- Ju, J. Ruan, C. Fuller, C. W. Glazer, A. N. and Mathies, R. A. (1995). Fluorescence energy transfer dye-labeled primers for DNA sequencing and analysis. *Proceedings of the National Academy of Sciences of the United States of America*. Vol. 92. No. 10, p. 4347–4351. doi: 10.1073/pnas.92.10.4347
- Jung, B. Flörchinger, M. Kunz, H.-H. Traub, M. Wartenberg, R. Jeblick, W., *et al.* (2009). Uridine-ribohydrolase is a key regulator in the uridine degradation pathway of *Arabidopsis*. *The Plant Cell*. Vol. 21. No. 3, p. 876–891. doi: 10.1105/tpc.108.062612
- Jung, B. Hoffmann, C. and Möhlmann, T. (2011). *Arabidopsis* nucleoside hydrolases involved in intracellular and extracellular degradation of purines. *The Plant Journal*. Vol. 65. No. 5, p. 703–711. doi: 10.1111/j.1365-313X.2010.04455.x
- Kazibwe, Z. Soto-Burgos, J. MacIntosh, G. C. and Bassham, D. C. (2020). TOR mediates the autophagy response to altered nucleotide homeostasis in a ribonuclease mutant. *Journal of Experimental Botany*. Vol. 71. No. 22, p. 6907–6920. doi: 10.1093/jxb/eraa410
- Kereszt, A. Li, D. Indrasumunar, A. Nguyen, C. D. T. Nontachaiyapoom, S. Kinkema, M., *et al.* (2007). *Agrobacterium Rhizogenes*-mediated Transformation of Soybean to Study Root Biology. *Nature Protocols*. Vol. 2. No. 4, p. 948–952. doi: 10.1038/nprot.2007.141
- Kirchberger, S. Tjaden, J. and Neuhaus, H. E. (2008). Characterization of the *Arabidopsis* Brittle1 transport protein and impact of reduced activity on plant metabolism. *The Plant journal : for cell and molecular biology*. Vol. 56. No. 1, p. 51–63. doi: 10.1111/j.1365-313X.2008.03583.x

References

- Kleinboelting, N. Huep, G. Kloetgen, A. Viehoveer, P. and Weisshaar, B. (2012). GABI-Kat SimpleSearch: New features of the Arabidopsis thaliana T-DNA mutant database. *Nucleic Acids Research*. Vol. 40. No. Database issue, p. D1211-5. doi: 10.1093/nar/gkr1047
- Klepikova, A. V. Kasianov, A. S. Gerasimov, E. S. Logacheva, M. D. and Penin, A. A. (2016). A high resolution map of the Arabidopsis thaliana developmental transcriptome based on RNA-seq profiling. *The Plant Journal*. Vol. 88. No. 6, p. 1058–1070. doi: 10.1111/tpj.13312
- Koffler, B. E. Bloem, E. Zellnig, G. and Zechmann, B. (2013). High resolution imaging of subcellular glutathione concentrations by quantitative immunoelectron microscopy in different leaf areas of Arabidopsis. *Micron*. Vol. 45, p. 119–128. doi: 10.1016/j.micron.2012.11.006
- Koncz, C. and Schell, J. (1986). The promoter of TL-DNA gene 5 controls the tissue-specific expression of chimaeric genes carried by a novel type of Agrobacterium binary vector. *Molecular and General Genetics MGG*. Vol. 204. No. 3, p. 383–396. doi: 10.1007/BF00331014
- Kwasnik, A. Wang, V. Y.-F. Krzyszton, M. Gozdek, A. Zakrzewska-Placzek, M. Stepniak, K., *et al.* (2019). Arabidopsis DXO1 Links RNA Turnover and Chloroplast Function Independently of its Enzymatic Activity. *Nucleic Acids Research*. Vol. 47. No. 9, p. 4751–4764. doi: 10.1093/nar/gkz100
- Larkin, M. A. Blackshields, G. Brown, N. P. Chenna, R. McGettigan, P. A. McWilliam, H., *et al.* (2007). Clustal W and Clustal X version 2.0. *Bioinformatics*. Vol. 23. No. 21, p. 2947–2948. doi: 10.1093/bioinformatics/btm404
- Laursen, T. Møller, B. L. and Bassard, J.-E. (2015). Plasticity of specialized metabolism as mediated by dynamic metabolons. *Trends in Plant Science*. Vol. 20. No. 1, p. 20–32. doi: 10.1016/j.tplants.2014.11.002
- Ledermann, R. Bartsch, I. Remus-Emsermann, M. N. Vorholt, J. A. and Fischer, H.-M. (2015). Stable Fluorescent and Enzymatic Tagging of Bradyrhizobium diazoefficiens to Analyze Host-Plant Infection and Colonization. *Molecular Plant-Microbe Interactions*. Vol. 28. No. 9, p. 959–967. doi: 10.1094/MPMI-03-15-0054-TA
- Lei, Y. Lu, L. Liu, H.-Y. Li, S. Xing, F. and Chen, L.-L. (2014). CRISPR-P: A web tool for synthetic single-guide RNA design of CRISPR-system in plants. *Molecular plant*. Vol. 7. No. 9, p. 1494–1496. doi: 10.1093/mp/ssu044
- Lescano, C. I. Martini, C. Gonzalez, C. A. and Desimone, M. (2016). Allantoin accumulation mediated by allantoinase downregulation and transport by Ureide Permease 5 Confers Salt Stress Tolerance to Arabidopsis Plants. *Plant Molecular Biology*. Vol. 91. No. 4-5, p. 581–595. doi: 10.1007/s11103-016-0490-7
- Lodwig, E. and Poole, P. (2003). Metabolism of Rhizobium Bacteroids. *Critical Reviews in Plant Sciences*. Vol. 22. No. 1, p. 37–78. doi: 10.1080/713610850
- Lu, Y. Zhu, J. and Liu, P. (2005). A two-step strategy for detecting differential gene expression in cDNA microarray data. *Current Genetics*. Vol. 47. No. 2, p. 121–131. doi: 10.1007/s00294-004-0551-3
- Ma, X. Wang, W. Bittner, F. Schmidt, N. Berkey, R. Zhang, L., *et al.* (2016). Dual and Opposing Roles of Xanthine Dehydrogenase in Defense-Associated Reactive Oxygen Species Metabolism in Arabidopsis. *The Plant Cell Online*. Vol. 28. No. 5, p. 1108–1126. doi: 10.1105/tpc.15.00880
- MacIntosh, G. C. and Bassham, D. C. (2011). The connection between ribophagy, autophagy and ribosomal RNA decay. *Autophagy*. Vol. 7. No. 6, p. 662–663. doi: 10.4161/auto.7.6.15447
- Masclaux, C. Valadier, M. H. Brugière, N. Morot-Gaudry, J. F. and Hirel, B. (2000). Characterization of the sink/source transition in tobacco (Nicotiana tabacum L.) shoots in relation to nitrogen management and leaf senescence. *Planta*. Vol. 211. No. 4, p. 510–518. doi: 10.1007/s004250000310

- Merchante, C. Stepanova, A. N. and Alonso, J. M. (2017). Translation regulation in plants: An interesting past, an exciting present and a promising future. *The Plant Journal*. Vol. 90. No. 4, p. 628–653. doi: 10.1111/tpj.13520
- Mergner, J. Frejno, M. List, M. Papacek, M. Chen, X. Chaudhary, A., *et al.* (2020). Mass-spectrometry-based draft of the Arabidopsis proteome. *Nature*, p. 1–6. doi: 10.1038/s41586-020-2094-2
- Mitra, R. (2018). *Arabidopsis thaliana* mutant leaves treated with *Pseudomonas syringae* ES4326: GSE18978 in AT-00406, <https://www.ncbi.nlm.nih.gov/geo/query/acc.cgi?acc=GSE18978>. Accessed April 05, 2021.
- Mohammadi-Dehcheshmeh, M. Ebrahimie, E. Tyerman, S. D. and Kaiser, B. N. (2014). A novel method based on combination of semi-in vitro and in vivo conditions in *Agrobacterium rhizogenes*-mediated hairy root transformation of Glycine species. *In Vitro Cellular & Developmental Biology - Plant*. Vol. 50. No. 2, p. 282–291. doi: 10.1007/s11627-013-9575-z
- Moll, R. H. Kamprath, E. J. and Jackson, W. A. (1982). Analysis and Interpretation of Factors Which Contribute to Efficiency of Nitrogen Utilization. *Agronomy Journal*. Vol. 74. No. 3, p. 562–564. doi: 10.2134/agronj1982.00021962007400030037x
- Montalbini, P. and Della Torre, G. (1995). Allopurinol Metabolites and Xanthine Accumulation in Allopurinol-Treated Tobacco. *Journal of Plant Physiology*. Vol. 147. No. 3-4, p. 321–327. doi: 10.1016/S0176-1617(11)82160-7
- Myrach, T. Zhu, A. and Witte, C.-P. (2017). The assembly of the plant urease activation complex and the essential role of the urease accessory protein G (UreG) in delivery of nickel to urease. *The Journal of biological chemistry*. Vol. 292. No. 35, p. 14556–14565. doi: 10.1074/jbc.M117.780403
- Nakanishi, T. and Sekimizu, K. (2002). SDT1/SSM1, a multicopy suppressor of S-II null mutant, encodes a novel pyrimidine 5'-nucleotidase. *Journal of Biological Chemistry*. Vol. 277. No. 24, p. 22103–22106. doi: 10.1074/jbc.M200573200
- Nelson, D. R. Bellville, R. J. and Porter, C. A. (1984). Role of Nitrogen in Seed Development of Soybean. *Plant Physiology*. Vol. 74. No. 1, p. 128–133.
- Nguyen, J. Machal, L. Vidal, J. Perrot-Rechenmann, C. and Gadai, P. (1986). Immunochemical Studies on Xanthine Dehydrogenase of Soybean Root Nodules: Ontogenic Changes in the Level of Enzyme and Immunocytochemical Localization. *Planta*. Vol. 167. No. 2, p. 190–195. doi: 10.1007/BF00391414
- Pallmann, P. and Hothorn, L. A. (2016). Analysis of means: A generalized approach using R. *Journal of Applied Statistics*. Vol. 43. No. 8, p. 1541–1560. doi: 10.1080/02664763.2015.1117584
- Pareek, V. Tian, H. Winograd, N. and Benkovic, S. J. (2020). Metabolomics and Mass Spectrometry Imaging Reveal Channeled de novo Purine Synthesis in Cells. *Science*. Vol. 368. No. 6488, p. 283–290. doi: 10.1126/science.aaz6465
- Pate, J. S. and Atkins, C. A. (1983). *Nitrogen Uptake, Transport and Utilization in Nitrogen fixation: Volume 3: Legumes*, editor W. J. Borughton, p. 245–298 (Oxford: Clarendon Press).
- Pedrotti, L. Weiste, C. Nägele, T. Wolf, E. Lorenzin, F. Dietrich, K., *et al.* (2018). Snf1-RELATED KINASE1-Controlled C/S1-bZIP Signaling Activates Alternative Mitochondrial Metabolic Pathways to Ensure Plant Survival in Extended Darkness. *The Plant Cell*. Vol. 30. No. 2, p. 495–509. doi: 10.1105/tpc.17.00414
- Perchlik, M. and Tegeder, M. (2017). Improving Plant Nitrogen Use Efficiency through Alteration of Amino Acid Transport Processes. *Plant Physiology*. Vol. 175. No. 1, p. 235–247. doi: 10.1104/pp.17.00608
- Prather, M. J. Hsu, J. DeLuca, N. M. Jackman, C. H. Oman, L. D. Douglass, A. R., *et al.* (2015). Measuring and modeling the lifetime of nitrous oxide including its variability. *Journal of geophysical research. Atmospheres*. Vol. 120. No. 11, p. 5693–5705. doi: 10.1002/2015JD023267

References

- Raychaudhuri, A. and Tipton, P. A. (2002). Cloning and Expression of the Gene for Soybean Hydroxyisourate Hydrolase. Localization and Implications for Function and Mechanism. *Plant Physiology*. Vol. 130. No. 4, p. 2061–2068. doi: 10.1104/pp.011049
- Reisenhauer, H. M. (1960). Cobalt in Nitrogen Fixation by a Legume. *Nature*. Vol. 186. No. 4722, p. 375–376. doi: 10.1038/186375a0
- Riegler, H. Geserick, C. and Zrenner, R. (2011). Arabidopsis thaliana nucleosidase mutants provide new insights into nucleoside degradation. *The New phytologist*. Vol. 191. No. 2, p. 349–359. doi: 10.1111/j.1469-8137.2011.03711.x
- Schmidt, A. Su, Y.-H. Kunze, R. Warner, S. Hewitt, M. Slocum, R. D., et al. (2004). UPS1 and UPS2 from Arabidopsis mediate high affinity transport of uracil and 5-fluorouracil. *Journal of Biological Chemistry*. Vol. 279. No. 43, p. 44817–44824. doi: 10.1074/jbc.m405433200
- Schmiechen, C. M. (2019). *Investigation of the protein interactome of xanthosine monophosphate phosphatase (XMPP)*. M. Sc. Thesis. Hannover: Leibniz Universität Hannover, Institut für Pflanzenernährung.
- Schmutz, J. Cannon, S. B. Schlueter, J. Ma, J. Mitros, T. Nelson, W., et al. (2010). Genome sequence of the palaeopolyploid soybean. *Nature*. Vol. 463. No. 7278, p. 178–183. doi: 10.1038/nature08670
- Schröder, R. (2019). *The Identification and Characterisation of a Ribokinase and a Putative D-Ribose Permease in Arabidopsis thaliana*. Dissertation. Hannover: Leibniz Universität Hannover, Institut für Pflanzenernährung.
- Schröder, R. Y. Zhu, A. Eubel, H. Dahncke, K. and Witte, C.-P. (2018). The Ribokinases of Arabidopsis thaliana and Saccharomyces cerevisiae are Required for Ribose Recycling from Nucleotide Catabolism, which in Plants is Not Essential to Survive Prolonged Dark Stress. *The New phytologist*. Vol. 217. No. 1, p. 233–244. doi: 10.1111/nph.14782
- Schubert, K. R. (1986). Products of Biological Nitrogen Fixation in Higher Plants: Synthesis, Transport, and Metabolism. *Annual Review of Plant Biology*. Vol. 37, p. 539–574.
- Schubert, K. R. and Boland, M. J. (1990). *The Ureides in Intermediary nitrogen metabolism*, editor B. J. Mifflin, p. 197–282 (San Diego CA u.a. Acad. Pr).
- Shelp, B. J. and Atkins, C. A. (1983). Role of Inosine Monophosphate Oxidoreductase in the Formation of Ureides in Nitrogen-Fixing Nodules of Cowpea (Vigna unguiculata L. Walp.). *Plant Physiology*. Vol. 72. No. 4, p. 1029–1034. doi: 10.1104/pp.72.4.1029
- Shelp, B. J. Atkins, C. A. Storer, P. J. and Canvin, D. T. (1983). Cellular and Subcellular Organization of Pathways of Ammonia Assimilation and Ureide Synthesis in Nodules of Cowpea (Vigna unguiculata L. Walp). *Archives of Biochemistry and Biophysics*. Vol. 224. No. 2, p. 429–441. doi: 10.1016/0003-9861(83)90229-1
- Smith, P. M.C. and Atkins, C. A. (2002). Purine Biosynthesis. Big in Cell Division, Even Bigger in Nitrogen Assimilation. *Plant Physiology*. Vol. 128. No. 3, p. 793–802. doi: 10.1104/pp.010912
- Soltabayeva, A. Srivastava, S. Kurmanbayeva, A. Bekturova, A. Fluhr, R. and Sagi, M. (2018). Early Senescence in Older Leaves of Low Nitrate-Grown Atxdh1 Uncovers a Role for Purine Catabolism in N Supply1OPEN. *Plant Physiology*. Vol. 178. No. 3, p. 1027–1044. doi: 10.1104/pp.18.00795
- Straube, H. Niehaus, M. Zwittian, S. Witte, C.-P. and Herde, M. (2021). Enhanced nucleotide analysis enables the quantification of deoxynucleotides in plants and algae revealing connections between nucleoside and deoxynucleoside metabolism. *The Plant Cell*. Vol. 33. No. 2, p. 270–289. doi: 10.1093/plcell/koaa028
- Strogies, M. and Gniffke, P. Umweltbundesamt (2020). *Berichterstattung unter der Klimarahmenkonvention der Vereinten Nationen und dem Kyoto-Protokoll 2020: Nationaler Inventarbericht zum Deutschen Treibhausgasinventar 1990 – 2018*.

- Suzuki, N. Miller, G. Salazar, C. Mondal, H. A. Shulaev, E. Cortes, D. F., *et al.* (2013). Temporal-spatial interaction between reactive oxygen species and abscisic acid regulates rapid systemic acclimation in plants. *The Plant Cell*. Vol. 25. No. 9, p. 3553–3569. doi: 10.1105/tpc.113.114595
- Sweetlove, L. J. and Fernie, A. R. (2018). The role of dynamic enzyme assemblies and substrate channelling in metabolic regulation. *Nature Communications*. Vol. 9. No. 1, p. 2136. doi: 10.1038/s41467-018-04543-8
- Szabo, E. X. Reichert, P. Lehniger, M.-K. Ohmer, M. Francisco Amorim, M. de Gowik, U., *et al.* (2020). Metabolic Labeling of RNAs Uncovers Hidden Features and Dynamics of the Arabidopsis Transcriptome. *The Plant Cell*. Vol. 32. No. 4, p. 871–887. doi: 10.1105/tpc.19.00214
- Takagi, H. Watanabe, S. Tanaka, S. Matsuura, T. Mori, I. C. Hirayama, T., *et al.* (2018). Disruption of ureide degradation affects plant growth and development during and after transition from vegetative to reproductive stages. *BMC plant biology*. Vol. 18. No. 1, p. 287. doi: 10.1186/s12870-018-1491-2
- Tegeder, M. (2014). Transporters Involved in Source to Sink Partitioning of Amino Acids and Ureides: Opportunities for Crop Improvement. *Journal of Experimental Botany*. Vol. 65. No. 7, p. 1865–1878. doi: 10.1093/jxb/eru012
- Thal, B. (2017). *Towards the analysis of mitochondrial physiology in nitrogen fixing root nodules*. doctoral thesis. Hannover, Germany: Leibniz Universität Hannover, Institute of Plant Genetics.
- Tian, H. Xu, R. Canadell, J. G. Thompson, R. L. Winiwarter, W. Suntharalingam, P., *et al.* (2020). A comprehensive quantification of global nitrous oxide sources and sinks. *Nature*. Vol. 586. No. 7828, p. 248–256. doi: 10.1038/s41586-020-2780-0
- Triplett, E. W. (1985). Intercellular Nodule Localization and Nodule Specificity of Xanthine Dehydrogenase in Soybean. *Plant Physiology*. Vol. 77. No. 4, p. 1004–1009. doi: 10.1104/pp.77.4.1004
- Triplett, E. W. Blevins, D. G. and Randall, D. D. (1980). Allantoic Acid Synthesis in Soybean Root Nodule Cytosol via Xanthine Dehydrogenase. *Plant Physiology*. Vol. 65. No. 6, p. 1203–1206. doi: 10.1104/pp.65.6.1203
- Udvardi, M. and Poole, P. S. (2013). Transport and Metabolism in Legume-Rhizobia Symbioses. *Annual Review of Plant Biology*. Vol. 64, p. 781–805. doi: 10.1146/annurev-arplant-050312-120235
- Umweltbundesamt (2011). *Stickstoff - Zu viel des Guten?* <http://www.umweltbundesamt.de/sites/default/files/medien/publikation/long/4058.pdf>. Accessed May 26, 2016.
- Umweltbundesamt (2020). *Prozessdetails: Chem-AnorgAmmoniak-DE-2020: Prozessorientierte Basisdaten für Umweltmanagementsysteme*, <https://www.probas.umweltbundesamt.de/php/prozessdetails.php?id=%7B79A3BA36-8F46-48C1-B379-0D3ABA48F561%7D#nachoben>. Accessed April 08, 2021.
- Usadel, B. Bläsing, O. E. Gibon, Y. Retzlaff, K. Höhne, M. Günther, M., *et al.* (2008). Global Transcript Levels Respond to Small Changes of the Carbon Status During Progressive Exhaustion of Carbohydrates in Arabidopsis Rosettes. *Plant Physiology*. Vol. 146. No. 4, p. 1834–1861. doi: 10.1104/pp.107.115592
- van den Bosch, K. A. and Newcomb, E. H. (1986). Immunogold Localization of Nodule-specific Uricase in Developing Soybean Root Nodules. *Planta*. Vol. 167. No. 4, p. 425–436. doi: 10.1007/BF00391217
- Vaughn, K. C. Duke, S. O. Duke, S. H. and Henson, C. A. (1982). Ultrastructural Localization of Urate Oxidase in Nodules of *Sesbania exaltata*, *Glycine max* and *Medicago sativa*. *Histochemistry*. Vol. 74. No. 3, p. 309–318. doi: 10.1007/BF00493430
- Völker, J., Mohaupt, V., Arle, J., Baumgarten, C., Blondzik, K., Borchardt, D., *et al.* Umweltbundesamt (2016). *Die Wasserrahmenrichtlinie – Deutschlands Gewässer 2015*.

References

- Voß, L. (2020). *Determination of Expression Domains of the Ureide Biosynthesis Pathway in Phaseolus vulgaris Nodules and the Role of the Glucose Transporter in Ureide Generation*. M. Sc. Thesis. Hannover: Leibniz Universität Hannover, Institut für Pflanzenernährung.
- Walther, T. Novo, M. Rössger, K. Létisse, F. Loret, M.-O. Portais, J.-C., *et al.* (2010). Control of ATP Homeostasis During the Respiro-fermentative Transition in Yeast. *Molecular Systems Biology*. Vol. 6, p. 344. doi: 10.1038/msb.2009.100
- Wang, T. Wei, J. J. Sabatini, D. M. and Lander, E. S. (2014). Genetic Screens in Human Cells Using the CRISPR-Cas9 System. *Science*. Vol. 343. No. 6166, p. 80–84. doi: 10.1126/science.1246981
- Watanabe, S. Matsumoto, M. Hakomori, Y. Takagi, H. Shimada, H. and Sakamoto, A. (2014). The Purine Metabolite Allantoin Enhances Abiotic Stress Tolerance Through Synergistic Activation of Abscisic Acid Metabolism. *Plant, Cell & Environment*. Vol. 37. No. 4, p. 1022–1036. doi: 10.1111/pce.12218
- Webb, M. A. and Newcomb, E. H. (1987). Cellular Compartmentation of Ureide Biogenesis in Root Nodules of Cowpea (*Vigna unguiculata* (L.) Walp.). *Planta*. Vol. 172. No. 2, p. 162–175. doi: 10.1007/BF00394584
- Weir, B. S. (2016). *The Current Taxonomy of Rhizobia*, <http://www.rhizobia.co.nz/taxonomy/rhizobia>. Accessed May 26, 2016.
- Werner, A. K. Sparkes, I. A. Romeis, T. and Witte, C.-P. (2008). Identification, Biochemical Characterization, and Subcellular Localization of Allantoate Amidohydrolases from Arabidopsis and Soybean. *Plant Physiology*. Vol. 146. No. 2, p. 418–430. doi: 10.1104/pp.107.110809
- Werner, A. K. and Witte, C.-P. (2011). The Biochemistry of Nitrogen Mobilization: Purine Ring Catabolism. *Trends in Plant Science*. Vol. 16. No. 7, p. 381–387. doi: 10.1016/j.tplants.2011.03.012
- Winter, D. Vinegar, B. Nahal, H. Ammar, R. Wilson, G. V. and Provart, N. J. (2007). An "Electronic Fluorescent Pictograph" browser for exploring and analyzing large-scale biological data sets. *PLOS ONE*. Vol. 2. No. 8, p. e718. doi: 10.1371/journal.pone.0000718
- Witte, C.-P. (2011). Urea metabolism in plants. *Plant science : an international journal of experimental plant biology*. Vol. 180. No. 3, p. 431–438. doi: 10.1016/j.plantsci.2010.11.010
- Witte, C.-P. and Herde, M. (2020). Nucleotide Metabolism in Plants. *Plant Physiology*. Vol. 182. No. 1, p. 63–78. doi: 10.1104/pp.19.00955
- Witte, C.-P. Noël, L. D. Gielbert, J. Parker, J. E. and Romeis, T. (2004). Rapid one-step protein purification from plant material using the eight-amino acid StrepII epitope. *Plant Molecular Biology*. Vol. 55. No. 1, p. 135–147. doi: 10.1007/s11103-004-0501-y
- Xie, K. Minkenberg, B. and Yang, Y. (2015). Boosting CRISPR/Cas9 Multiplex Editing Capability with the Endogenous tRNA-processing System. *Proceedings of the National Academy of Sciences of the United States of America*. Vol. 112. No. 11, p. 3570–3575. doi: 10.1073/pnas.1420294112
- Xie, K. Zhang, J. and Yang, Y. (2014). Genome-wide prediction of highly specific guide RNA spacers for CRISPR-Cas9-mediated genome editing in model plants and major crops. *Molecular plant*. Vol. 7. No. 5, p. 923–926. doi: 10.1093/mp/ssu009
- Xiong, Y. McCormack, M. Li, L. Hall, Q. Xiang, C. and Sheen, J. (2013). Glucose-TOR Signalling Reprograms the Transcriptome and Activates Meristems. *Nature*. Vol. 496. No. 7444, p. 181–186. doi: 10.1038/nature12030
- Xu, Y.-F. Létisse, F. Absalan, F. Lu, W. Kuznetsova, E. Brown, G., *et al.* (2013). Nucleotide Degradation and Ribose Salvage in Yeast. *Molecular Systems Biology*. Vol. 9, p. 665. doi: 10.1038/msb.2013.21
- Yin, Y. Katahira, R. and Ashihara, H. (2014). Metabolism of purine nucleosides and bases in suspension-cultured Arabidopsis thaliana. *European Chemical Bulletin*. Vol. 3. No. 9, p. 925–934.

- Zhang, Y. and Fernie, A. R. (2021). Metabolons, enzyme-enzyme assemblies that mediate substrate channeling, and their roles in plant metabolism. *Plant communications*. Vol. 2. No. 1, p. 100081. doi: 10.1016/j.xplc.2020.100081
- Zhu, A. (2016). *Identification and Characterization of Pyrimidine 5'-Nucleotidases in Arabidopsis thaliana*. PhD. Hannover, Germany: Leibniz Universität Hannover, Institut für Pflanzenernährung.
- Zrenner, R. Stitt, M. Sonnewald, U. and Boldt, R. (2006). Pyrimidine and Purine Biosynthesis and Degradation in Plants. *Annual Review of Plant Biology*. Vol. 57, p. 805–836. doi: 10.1146/annurev.arplant.57.032905.105421
- Zuker, M. (2003). Mfold web server for nucleic acid folding and hybridization prediction. *Nucleic Acids Research*. Vol. 31. No. 13, p. 3406–3415. doi: 10.1093/nar/gkg595

9 List of Figures

Figure 1 Development of global nitrogen fertilizer use, global meat production and world population after the invention of the Haber-Bosch process at the beginning of the 20 th century. _____	1
Figure 2 Structure of purine and pyrimidine nucleotides. _____	3
Figure 3 Purine Metabolism. _____	5
Figure 4 Ureide Biosynthesis. _____	11
Figure 5 Determination of kinetic constants of the XMPP candidate from soybean. _____	13
Figure 6 Different nutrient solutions were tested for the cultivation of soybean cultivar Williams 82. _____	15
Figure 7 Lecaton, Seramis and <i>Nullerde</i> were tested for their suitability to grow soybean for the production of transgenic nodules. _____	17
Figure 8 Illustration of the optimization success in soybean cultivation. _____	19
Figure 9 Assessment of the morphology of <i>XMPP</i> CRISPR, <i>GSDA</i> CRISPR and <i>XDH</i> CRISPR nodules. _	22
Figure 10 Quantification of xanthine, allantoin and allantoate concentrations in <i>XDH</i> CRISPR and control nodules. _____	23
Figure 11 Assessment of knockout rates in <i>XMPP</i> CRISPR nodules. _____	24
Figure 12 Analysis of <i>xmpp</i> and <i>xdh</i> nodules of common bean. _____	26
Figure 13 Phylogenetic analysis of the SDT-like family. _____	28
Figure 14 Determination of kinetic constants and substrate specificity of XMPP. _____	29
Figure 15 <i>XMPP</i> is highly transcribed but its protein could not be detected despite a sensitive anti-XMPP antibody. _____	30
Figure 16 Detection of XMPP protein under conditions which induce <i>XMPP</i> gene expression. _____	31
Figure 17 Quantification of XMP, adenylates and guanylates in seed extracts of <i>XMPP</i> genetic variants in the context of other mutants of purine catabolism. _____	34
Figure 18 Quantification of intermediates downstream of XMP in seed extracts of <i>XMPP</i> genetic variants in the context of other mutants of purine catabolism genes. _____	36
Figure 19 Inhibitory effect of guanosine or xanthosine on XMPP activity. _____	36
Figure 20 Quantification of seed yield and seed diameter of <i>XMPP</i> genetic variants in the context of other mutants of purine catabolism genes. _____	37
Figure 21 Partial genetic suppression of the <i>uox</i> seed germination phenotype by the <i>XMPP</i> mutation. _____	39
Figure 22 Quantification of intermediates downstream of XMP in <i>XMPP</i> genetic variants in the context of other mutants of purine catabolism genes in seedlings under long-day or extended-night conditions. _____	41
Figure 23 Effect of allopurinol on seedlings. _____	43
Figure 24 Purine nucleotide concentrations in <i>XMPP</i> genetic variants in the context of other mutants of purine catabolism genes in seedlings under long-day or extended-night conditions. _____	45
Figure 25 Purine nucleotide concentrations in wild-type seedlings under long-day or extended-night conditions. _____	46
Figure 26 Quantification of intermediates downstream of XMP in <i>XMPP</i> genetic variants in the context of other mutants of purine catabolism genes in vegetative rosettes, dark-stressed vegetative rosettes and reproductive rosettes. _____	48
Figure 27 Immunoblots for XMPP, GSDA, NSH1 and XDH detection in extracts of vegetative rosettes, dark-stressed vegetative rosettes and reproductive rosettes. _____	49
Figure 28 Possible pathway of complete AMP oxidation. _____	66

Figure 29 Model for <i>XMPP</i> expression depending on sugar availability.	70
Figure 30 Model for the potential role of purine catabolism in plant defense.	72

Figure A - 1 Sequence alignment of soybean <i>XMPP1</i> and <i>XMPP2</i> genomic DNA.	96
Figure A - 2 Illustration of the fragment length analysis.	98
Figure A - 3 Corrected coding sequence of common bean <i>XMPP</i> .	99
Figure A - 4 Immunoblot of complementation lines.	99
Figure A - 5 Determination of kinetic constants of <i>XMPP</i> phosphorylation site mutants.	100
Figure A - 6 Quantification of inosine in seed extracts of <i>XMPP</i> genetic variants in the context of other mutants of purine catabolism genes.	100
Figure A - 7 Relative inosine quantification in <i>XMPP</i> genetic variants in the context of other mutants of purine catabolism genes in seedlings under long-day or extended-night conditions.	101
Figure A - 8 Quantification of inosine in <i>XMPP</i> genetic variants in the context of other mutants of purine catabolism genes in vegetative rosettes, dark-stressed vegetative rosettes and reproductive rosettes.	101
Figure A - 9 Comparison of metabolite concentrations in young and old leaves of vegetative rosettes, dark-stressed vegetative rosettes and reproductive rosettes.	102
Figure A - 10 Chlorotic phenotype in the segregating population of complementation line <i>xmpp::Xs</i> germinated on agar plates including 1% sucrose.	102
Calculation A - 1 Estimation of cellular adenylate concentrations and concentrations of purine nucleotides that could be released from mRNA degradation in the cytosol.	103

10 List of Tables

Table 1 Extract of the candidate list from the comparative transcriptome analysis.	12
Table 2 Molar composition of nutrient solutions tested for cultivation of soybean cultivar Williams 82.	14
Table 3 Potential energy yield from complete oxidation of AMP in comparison to glucose and selected amino acids.	65
Table 4 Composition of adjusted B&D nutrient solution used for the cultivation of soybean Williams 82.	75
Table 5: Information about CRISPR constructs used to produce knockout nodules.	77
Table 6 Composition of reaction mixture and temperature program used to amplify fragments for FLA.	79
Table 7 LC-MS parameters.	82

11 Appendix

Additional Figures

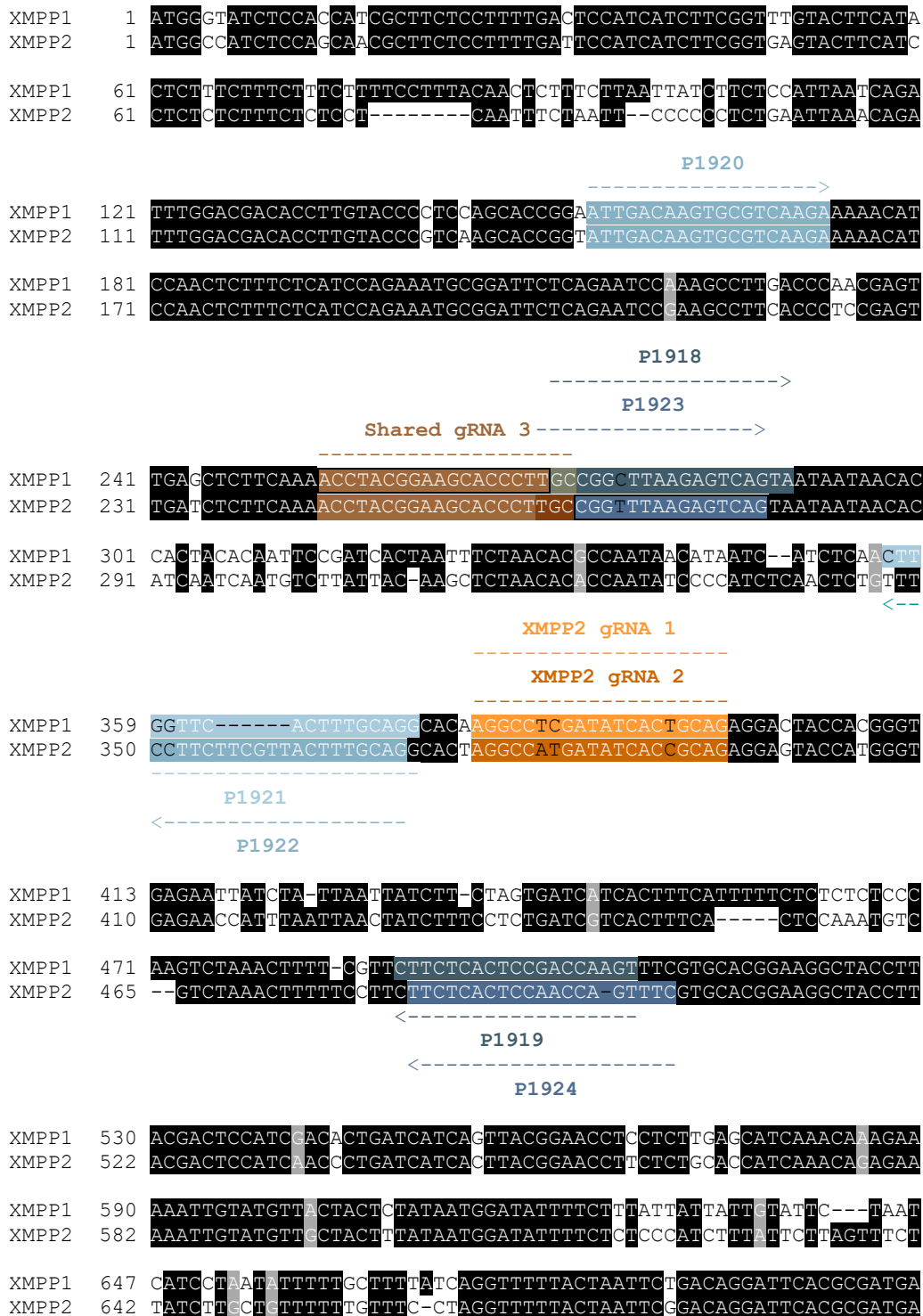


Figure A - 1 Sequence alignment of soybean *XMPP1* and *XMPP2* genomic DNA. Guide RNA binding sites are marked in orange and brown, primer binding sites for fragment length analysis are marked in blue. *XMPP1* = Glyma.10g248900, *XMPP2* = Glyma.20g144800. Continued on the following page.

```

XMPP1 707 GGGCGCTGGATAGCTTGGGCTCAAGGACTGTTTCGAGCAAATCATATGCTTCGAGACTA
XMPP2 701 GGTCTGTTGGATAGCTTGGGATCAAGGACTGTTTCGAGCAAATCATATGTTTCGAGACTA

XMPP1 767 TAAACCCGAACCTTCCCTATTCAACCCGACCCGACGAATTCCCATCCTCCTTAAACCTT
XMPP2 761 TAAACCCGAACCTTCGATATTCCACCCGACCCGATGAATTCCCATCCTCCTTAAACCGT

XMPP1 827 CGCTCGACGCCTTCAAGATCGCGCTTGACGCTGCCAACGTGGATCCTCGTGTACGGTAA
XMPP2 821 CTCTCGACGCCTTCAAGATCGCCCTTGACGCTGCCAACGTGGATCCTCGTGTACGGTAA

XMPP1 887 GAC-----GACGAAGTCAGCAACCTCAACCAAAATCGTGATTGATTTCAAT--AACTCAA
XMPP2 881 GACAAGACGACCAGTCAAACACCTCAACCTATACGCCATTGATTTCAATGAAACTAAA

XMPP1 940 CTTGATCCAAGTTAAATTAGACCCAAAT-----GTCTCCGATAAAATTTTGATTCTAA
XMPP2 941 CTTTATCCAAGAAAATACTACTCAAATCTAAGTGTGTAGATAAAACTTTGAATTCAAA

XMPP1 994 TTTTATAA--TAAAAAATGTTGATTAAGGAAAACTCTATATAAATTAGTCAACCAATT
XMPP2 1001 TTATATAAATAGAAAAACGTGATTAAGAAAAGAAATCTAATAAATTAGTCAACCAATT

XMPP1 1053 TTCCFACAAAAATATCATATAAATTAATCGTGCACAAAATCAATCCTATGAGTATGGTTA
XMPP2 1061 TTTGTACAGAAATGATCATGAAATTAATAATGGACAAAATCATTCCTATGA-CACGGTTA

XMPP1 1113 TAAAAATAGTCAACAACGAAACGGTTCGTCACTTCCTTGTTCGGCGATGTTGTTT
XMPP2 1120 TAAAAA-----ACATACGAAACCGTTCGTCACTTCCTTGTTCGGCGATGTCGTGTT

XMPP1 1173 TGACAGTGAACCCAAATTAGATTATATTTAAGGAAATGTTAGAAAGGATCGTTTTTAA
XMPP2 1174 TTACAGTGAACCCAAATTACATTATATTTAAGGAAAAGTCAGAAAGGATCATTTTTAA

XMPP1 1233 TTTTTTATAAGAAATCATTGTGATGATAATGATTTTCTAGATTTTATGCTATATAT
XMPP2 1234 TTTTTTATCACAAGTTATTGAGATGATAATGATTTTGTATATTTTTATGTTATATAT

XMPP1 1291 GCAGTTCTTTCTGGATGACAGCGTTCGCAATATTGCCGCGGGAAAAGAAATGGGTCTCCA
XMPP2 1294 GCAGTTCTTTCTGGATGACAGCGTTCGCAATATTGCCGCGGGAAAAGAAATGGGTCTCCA

XMPP1 1351 CACTGTTCTGGTAATTTCTTAACGACGTCGTA-TAATCATAAAACTGTATTATTAAAG
XMPP2 1354 CACTGTTCTGGTAATTTCTTAGACGACTAATAATTAATTAATTTAAGTTGTTTAGTTAC

XMPP1 1410 GTGAT-TTAAATGTAA-----AATATT-----GAATGTTATAGGTTGGGAAGACAA
XMPP2 1414 ATAAATATCAATAATTATCATGACTGTTTCTTTGGGATGTTATAGGTTGGGAAGACACA

XMPP1 1456 GAAAAGCAAAGGAGCTGACTATGCTGTGGAGAGTGTGCATCACTTGGCACAAGTGATCCC
XMPP2 1474 GAAAAGCAAAGGAGCAGACTATGCAGTGGAGTGTGTGAATCACTTGGCACAAGTGATCCC

XMPP1 1516 AGAGATATGGGCAAACGAAATGGACGGTGGTGTATCCAACGATGACACGTTCCGAAGAGTGA
XMPP2 1534 AGAGATATGGGCAAACGAAATGGACGGTGGAGGATCAAACGATGACACGTTCCGAAGAGTGA

XMPP1 1576 ATTGGAGGCCGTA CTCTGCTCTGGTTGGAGCTTGA
XMPP2 1594 ATTGGAGGCCGTA CTCTGCTCTGGTTGGAGCTTGA

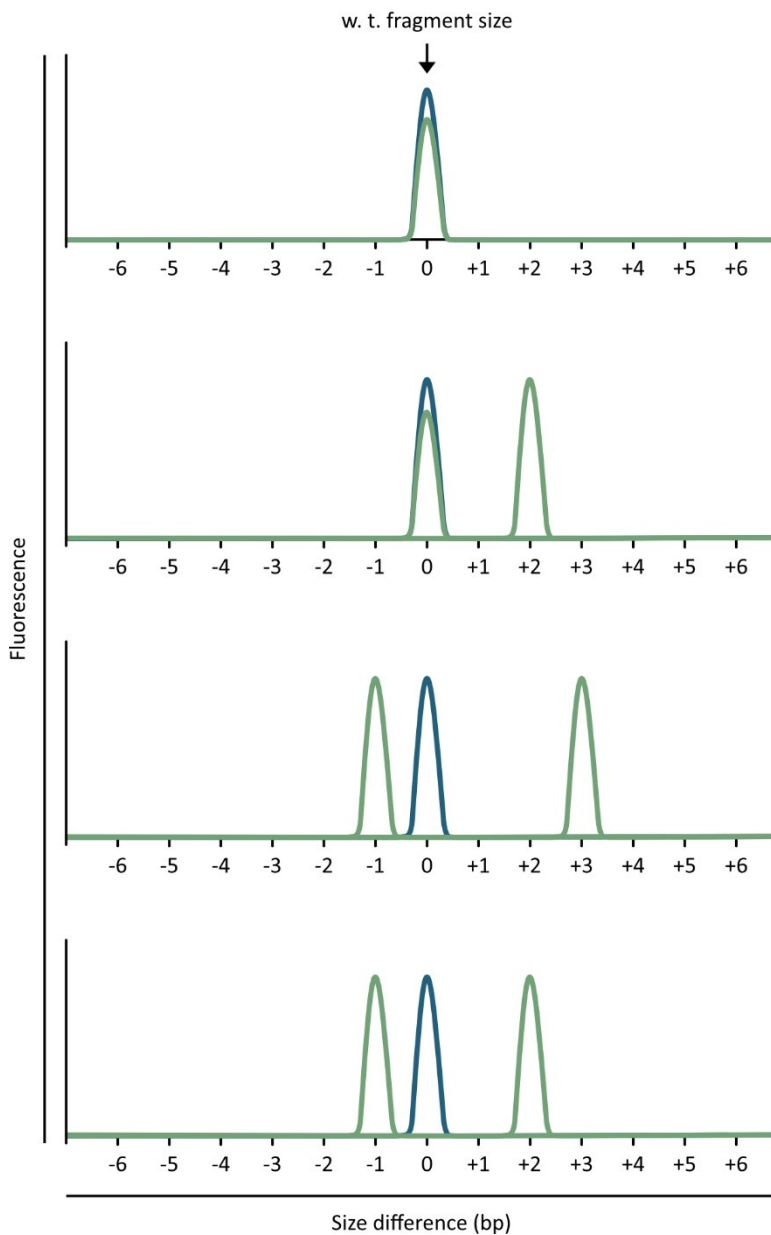
```

Figure A - 1 Sequence alignment of soybean XMPP1 and XMPP2 genomic DNA. Continued from previous page.

Appendix

A

■ FAM-labelled w. t. fragment ■ JOE-labelled fragments possibly containing mutations



B

Conclusions:

All fragments are w. t. size
→ No knockout

At least one fragment of w. t. size
At least one fragment with 2 bp insertion
→ No knockout

No fragment of w. t. size
At least one fragment with 1 bp deletion
At least one fragment with 3 bp insertion
→ No knockout (in-frame insertion)

No fragment of w. t. size
At least one fragment with 1 bp deletion
At least one fragment with 2 bp insertion
→ Knockout

Figure A - 2 Illustration of the fragment length analysis. FLA was performed to identify *XMPP* CRISPR hairy roots that were null mutants for both *XMPP* paralogs. Four FLAs were required for one hairy root because each paralog was targeted by two gRNAs giving in total four potential mutation sites. For each FLA, a primer pair was designed that bound to only one of the paralogs and that was specific for only one gRNA binding site. PCR was used to generate dye-labeled fragments of wild-type and *XMPP* CRISPR hairy root DNA, the size difference of which was determined by capillary gel electrophoresis-coupled fluorescence detection. When wild-type DNA was used, a fragment of wild-type size was generated. This was labeled with the green-fluorescent dye JOE. When DNA from an *XMPP* CRISPR hairy root was used, up to four fragments of different sizes could be generated. Since soybean is tetraploid, four alleles can be mutated differently. However, a smaller number of fragments with different sizes was usually observed. Fragments amplified from *XMPP* CRISPR hairy roots were labeled with the blue-fluorescent dye FAM. A, Exemplary chromatograms of a FLA. Wild-type fragment size was set to 0 so that the number of inserted or deleted base pairs could be read from the x-axis. B, Evaluation of the chromatograms illustrates the principle of FLA. Note, not all successful knockouts can be detected by FLA. All insertions or deletions that are 3 bp or multiples of 3 bp were excluded because in-frame mutations do not necessarily prevent the formation of functional protein.

```
>Coding sequence Phaseolus XMPP Phvul.007g05600
ATGGGTATTAACCTCCCTCGTTTTCCCCTTTTCGACGCCATCATCTTTGATTTGGACGACACCTTGTACCCCTCCA
CCACCGGAATCGACCGCTGCGTCAAGAGGAACATCGAACTCTTTCTCATCGAGAAATGCGGATTCTCAGAATC
CAAAGCGGCTCATCTCCGAGTTGAATTATTCAAACCTACGGAAGCACCCCTCGCCGGTTTGGCAGCAGCTTGGC
TATGATATCACCGCAGAGGAATACCACAGTTTCGTGCACGGAAGGCTACCTTACGACTCGATCAAGCCTGACG
TTCAGTTACGCAACCTGCTCTGCACTATCAAACAAAGAAAAATTGTTTTTACCAATTCGGATAGGATCCACGC
GATGAGAGCGTTGGATAGGCTTGGGATCAGTGACTGTTTCGAGCAGGTTATTTGCTTCGAGACTATTAACCCG
AATCTCCCAACTCGACCCGACCCGACGAATTTCCCGTCTCTCAAACCCCTCGCTGGACGCTTTTCAGGATCG
CGCTAGACGCTGCCAACGTGGAGCCTCGTCGTACGCTGTTTCTGGATGATAGCGTTCCGAACATTGCCGCGGG
AAGAGAAATGGGTCTGCAGACAGTTTTGGTTGGAAAGACAGTGAAGCAAGGAAGCAACTATGCGGTGGAG
TTTGTAACAACGTAGCGCAAGCGATTCCGGAGATATGGGCAAATAAAATGGAGGATAAGGATGAAACGATTA
```

Figure A - 3 Corrected coding sequence of common bean XMPP. First exon of was wrongly annotated at the Phytozome data base. The correct sequence was identified by a multiple sequence alignment with soybean an Arabidopsis homologs which was confirmed by the amplification from cDNA performed by Luisa Voss.

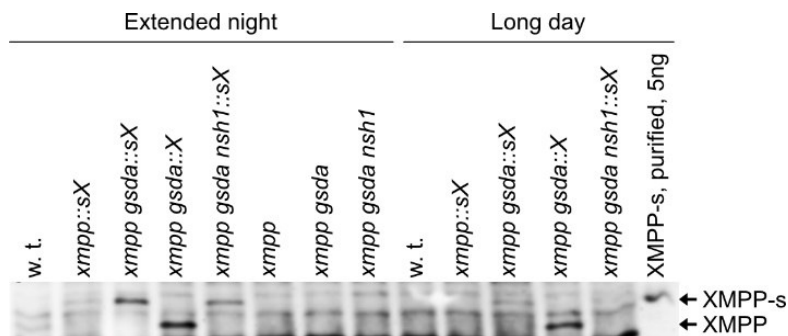


Figure A - 4 Immunoblot of complementation lines. Arabidopsis seedlings were grown on half-strength MS plates under long-day conditions (16 h day/ 8 h night, 22°C/ 20°C). Ten days after germination, one half of the Arabidopsis seedlings was subjected to 48 h of extended night whereas the other half was kept under long-day conditions. Complementation lines “::sX” contained a transgene encoding an N-terminally TwinStrep-tagged XMPP under the control of the native promoter. Complementation line “::X” contained a transgene encoding an untagged XMPP under the control of the 35S promoter. Loading volume of extracts was 15 µL. For comparison 5 ng of purified XMPP-HAStrep (XMPP-s) was loaded. XMPP protein was detected using custom-made anti-XMPP antibody. Protein bands of XMPP with and without tag are marked with arrows.

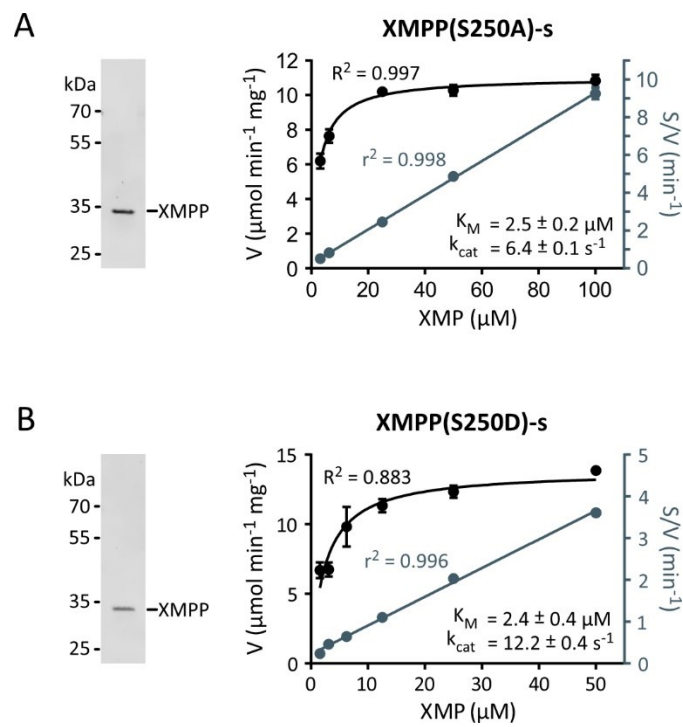


Figure A - 5 Determination of kinetic constants of XMPP phosphorylation site mutants. Potential phosphorylation site S250 was identified using PhosPhAt 4.0 (Heazlewood *et al.*, 2008). Mutants S250A and S250D were generated encoding for C-terminally HAStrep-tagged (XMPP-s) variants. Substitution of serine by alanine (A) and asparagine (D) served to prevent or mimic the phosphorylation of this site, respectively. **A**, XMPP(S250A)-s affinity purified from leaf extracts of *N. benthamiana* after transient expression. Left panel, Coomassie-stained SDS-gel with the purified enzyme. Right panel, determination of the kinetic constants with the data fitted according to Michaelis Menten (left axis) or Hanes (right axis). Error bars are SD, $n_t = 3$. **B**, XMPP(S250S)-s affinity purified from leaf extracts of *N. benthamiana* after transient expression. Left panel, Coomassie-stained SDS-gel with the purified enzyme. Right panel, determination of the kinetic constants with the data fitted according to Michaelis Menten (left axis) or Hanes (right axis). Error bars are SD, $n_t = 3$.

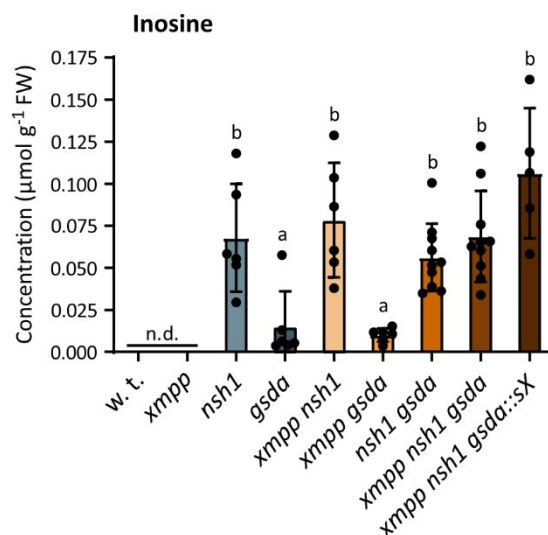


Figure A - 6 Quantification of inosine in seed extracts of XMPP genetic variants in the context of other mutants of purine catabolism genes. Additional data of experiment shown in Figure 18. The complementation line *xmpp nsh1 gsda::sx* contained a transgene encoding an N-terminally TwinStrep-tagged XMPP under the control of the native promoter (Figure A - 4). Error bars are SD, $n_b = 5 - 6$ for all but *nsh1 gsda* and *xmpp nsh1 gsda* with $n_b = 10$. A biological replicate (n_b) is a seed sample from an independent mother plant grown in parallel with all other plants of the experiment. Measurements not matching quality criteria (Chapter 7.8) were called not detected ("n.d.") and are not shown. Statistical analysis with two-sided Tukey's pairwise comparisons using the sandwich variance estimator. Different letters indicate p values < 0.05.

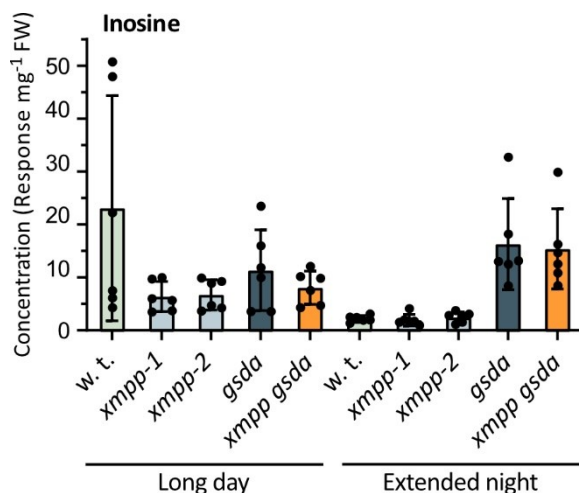


Figure A - 7 Relative inosine quantification in XMPP genetic variants in the context of other mutants of purine catabolism genes in seedlings under long-day or extended-night conditions. Additional data of experiment shown in figure 22. Seedlings were grown under long-day conditions (16 h day/ 8 h night, 22°C/ 20°C). At the end of the fifth night after germination, one half of the seedlings was kept under long-day conditions, whereas the other half was kept in the dark for 48 h. Error bars are SD, $n_b = 6$. Two-sided Tukey’s pairwise comparisons using the sandwich variance estimator were employed for statistical analyses. Different letters indicate p values < 0.05. Samples from long-day and extended-darkness conditions were independently analyzed indicated by small and capital letters.

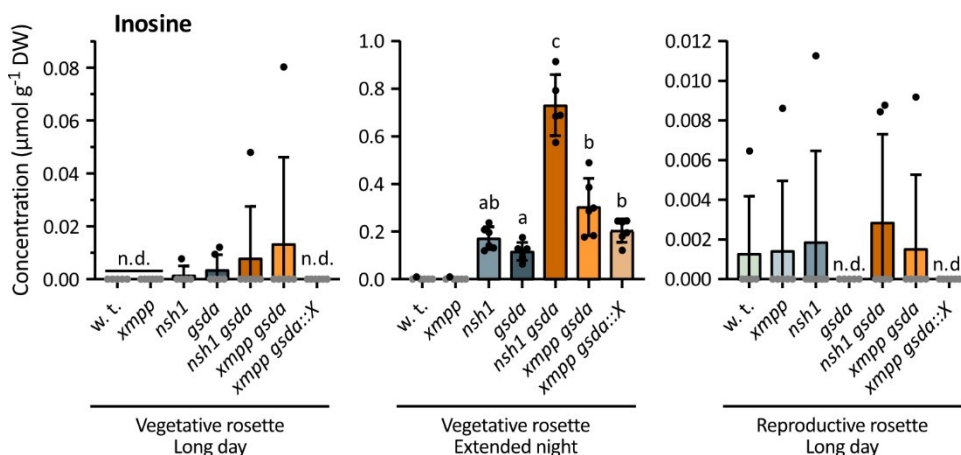


Figure A - 8 Quantification of inosine in XMPP genetic variants in the context of other mutants of purine catabolism genes in vegetative rosettes, dark-stressed vegetative rosettes and reproductive rosettes. Additional data of experiment shown in figure 26. Arabidopsis were grown under long-day conditions (16 h day/ 8 h night, 22°C/ 20°C). After four weeks, at the time before bolting, one third of the plants were subjected to 48 h of darkness beginning at the end of the night. Another third stayed for the same time under long-day conditions. Another third was grown three more weeks under long-day conditions until seeds were being produced. Rosettes were separated into young leaves and old leaves. Detailed results are only presented for young leaves. Fig. A – 9 gives an impression of the metabolite concentrations in old leaves. Samples of plant material used for metabolite analysis was used to prepare immunoblots for the detection of XMPP, GSDA, NSH1 and XDH proteins (Fig. 27). The complementation line *xmpp gsda::X* contained a transgene encoding an untagged XMPP under the control of the 35S promoter. Error bars are SD, $n_b = 5 - 6$. Measurements that failed quality criteria (Chapter 7.8) were called not detected (“n.d.”) are shown as grey data points set to 0. Statistical analysis was performed with groups that comprised at least three valid measurements. Two-sided Tukey’s pairwise comparisons using the sandwich variance estimator were employed for statistical analyses. Different letters indicate p values < 0.05.

Appendix

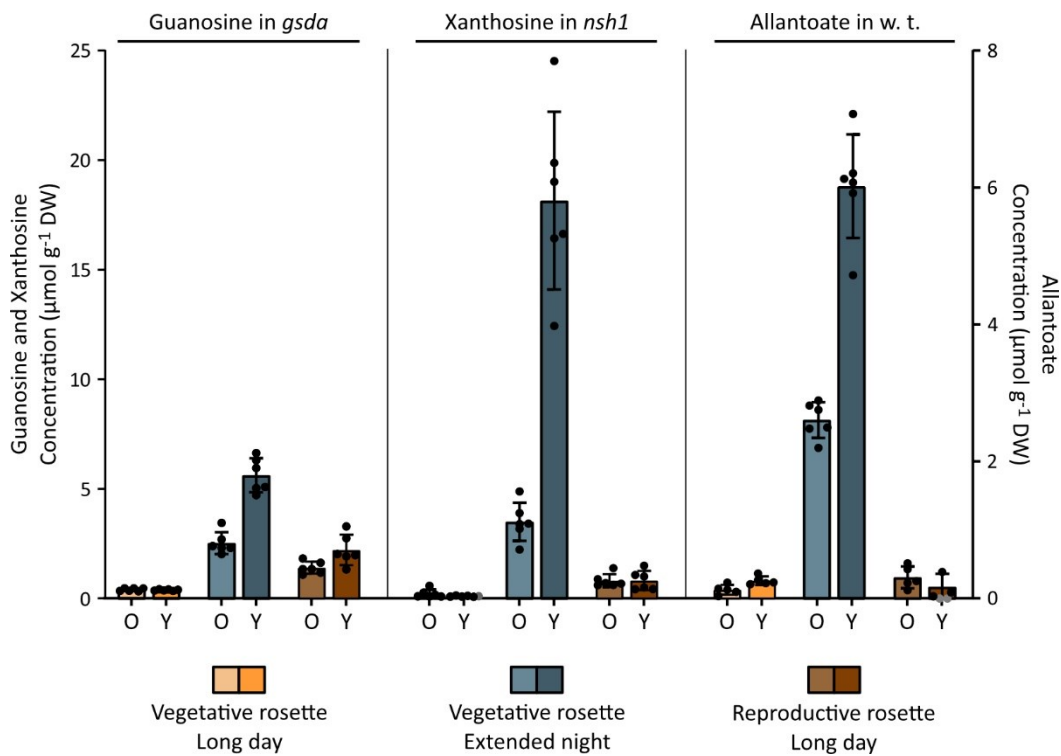


Figure A - 9 Comparison of metabolite concentrations in young and old leaves of vegetative rosettes, dark-stressed vegetative rosettes and reproductive rosettes. Additional data of experiment shown in figure 26. Arabidopsis were grown under long-day conditions (16 h day/ 8 h night, 22°C/ 20°C). After four weeks, at the time before bolting, one third of the plants were subjected to 48 h of darkness beginning at the end of the night. Another third stayed for the same time under long-day conditions. Another third was grown three more weeks under long-day conditions until seeds were being produced. Rosettes were separated into young leaves and old leaves. Detailed results are only presented for young leaves (Fig. 26). Samples of plant material used for metabolite analysis was used to prepare immunoblots for the detection of XMPP, GSDA, NSH1 and XDH proteins (Fig. 27). The complementation line *xmpp gsdA::X* contained a transgene encoding an untagged XMPP under the control of the 35S promoter. Error bars are SD, $n_b = 5$. Measurements that failed quality criteria (Chapter 7.8) are shown as grey data points set to 0.



Figure A - 10 Chlorotic phenotype in the segregating population of complementation line *xmpp::Xs* germinated on agar plates including 1% sucrose. The complementation line contained a transgene encoding an C-terminally HASTrep-tagged XMPP under the control of the 35S promoter.

Calculation A - 1 Estimation of cellular adenylate concentrations and concentrations of purine nucleotides that could be released from mRNA degradation in the cytosol.

1. Adenylates:
 - a. According to Straube et al. (2021) the sum of adenylates in a Arabidopsis seedling mesophyll cell accounts for 287 μM .
 - i. This refers to the total cell volume and not only the nucleotide-containing compartments.
 - ii. The concentration of the sum of adenylates the cellular ADP and AMP concentrations were derived from 1. The ATP concentration (Straube et al.; fig. 2a) and from the ATP to ADP and ATP to AMP ratios (Straube et al.; fig. 7b)
2. RNA:
 - a. According to Kerk et al. (2003) a Arabidopsis mesophyll cell (from cotyledons, plant age unknown) contains 100 - 500 pg RNA.
 - b. 100 - 500 pg RNA contains 0.2 - 1 pmol nucleotides, assuming that RNA consist of equal parts ATP, GTP, CTP and UTP (average molecular weight: 499 g mol⁻¹).
 - c. According to Yoo et al. (2007) a Arabidopsis mesophyll protoplast has an average diameter of 40 μm , which would correspond to a volume of 33.51 pL.
 - d. 0.2 - 1 pmol nucleotides per 33.51 pL corresponds to 6 - 30 mM nucleotides of the total mesophyll cell RNA.
 - e. Assuming that mRNA accounts for 5% of the total RNA and that only half of the nucleotides are purine nucleotides, the degradation of the total mesophyll cell mRNA would release 15 - 75 μM purine nucleotides.

According to these estimations a mesophyll cell would contain 4 - 20-fold more free adenylates (287 μM) than purine nucleotides which could be released from the complete degradation of the mRNA (15 - 75 μM).

Additional Tables

Table A - 1 Overview about purine nucleotides and their corresponding nucleosides and nucleobases.

Nucleotide	AMP	IMP	XMP	GMP
Nucleoside	Adenosine	Inosine	Xanthosine	Guanosine
Nucleobase	Adenine	Hypoxanthine	Xanthine	Guanine

Table A - 2 List of Primers.

Primer	Sequence 5' to 3'
N188	TCCATGGATTTCTCTCCGATCAACTGC
N189	ACCCGGGTCACGCACCGACGGCTGC
N359	TATCGATAAAATGGATTTCTCTCCGATCAACTGC
N360	TCCCGGGCGCACCGACGGCTGCTATT
1033	GTGAACGATTCTGGACCTGCCTC
1034	GAGAGGTTACATGTTCAACCAAC
1709	TCGAGCTCAAATGGGTTCTGCATGGTCTCATCCTCAATTTGAAAAAGGCCACCATGG
1710	AATTCATGGTGGCGCCTTTTCAAATTGAGGATGAGACCATGCAGAACCCATTTTGAGC
2904	GCTGGCCAGCTCCACGTCG
P243	TCCCGGGATGGTGAGCAAGGGCGAGGAGACCAC
P244	TGAGCTCTCACTTGTACAGCTCGTCCATGCCGTCGG
P277	TAGGTCTCCCTGTGAAGATGGGTTTTAGAGCTAGAA
P278	ATGGTCTCAACAGTCTACCCCTGCACCAGCCGGGAA
P281	TAGGTCTCCTTCTGCGTTTGGGTTTTAGAGCTAGAA
P282	ATGGTCTCAAGAAGCTACTGATGCACCAGCCGGGAA
P709	TAGGTCTCCCGATATCACTGCAGGTTTTAGAGCTAGAA
P634	GGCCATATGGCCATCTCCAGCAACGCTTC
P635	GTGCCCGGGTCAAGCTCCAACCACAGCACACGCG
P710	ATGGTCTCAATCGAGGCCCTGCACCAGCCGGGAA
P711	TAGGTCTCCAAGCACCTTGGGTTTTAGAGCTAGAA
P712	ATGGTCTCAGCTTCCGTAGGTTGCACCAGCCGGGAA
P713	TAGGTCTCCATCACCGCAGGTTTTAGAGCTAGAA
P714	ATGGTCTCATGATATCATGGCCTTGCACCAGCCGGGAA
P715	TAGGTCTCCTGGACATAAGGAGTTTTAGAGCTAGAA
P716	ATGGTCTCATCCAGCAAACGCTGCACCAGCCGGGAA
P717	TAGGTCTCCCAGCATGGGAGGTTTTAGAGCTAGAA
P718	ATGGTCTCAGCTGAGGTTACTTGCACCAGCCGGGAA
P719	TAGGTCTCCCTGCTACTGCTAAGTTTTAGAGCTAGAA
P720	ATGGTCTCAGCAGCAGAAGCTGCACCAGCCGGGAA
P721	TAGGTCTCCGTTGGGAGGCATGTTTTAGAGCTAGAA
P722	ATGGTCTCACAACGGTTTGCATGCACCAGCCGGGAA
P723	TAGGTCTCCAAGTCTAGGCTGTGGTTTTAGAGCTAGAA
P724	ATGGTCTCAAGTTTAGTCCCATGCACCAGCCGGGAA
P725	TAGGTCTCCGGGACAAAAGTGTTTTTAGAGCTAGAA
P726	ATGGTCTCATCCCGGTCAGACCTGCACCAGCCGGGAA
P727	TAGGTCTCCACGTGATTACAGGTTTTAGAGCTAGAA
P728	ATGGTCTCAACGTGCATCCCTTGCACCAGCCGGGAA
P1094	TGGCGCGCCTGCTGGTTAGATAGATTTCATGGC
P1097	GCGCCGGTTCCGGTGGGGGCTCCGGGGGAAGTGCATGGTCCCATCCGCAGTTCGAGAAAGGTGGTTC
P1098	CATGGAACCACCTTTCTCGAACTGCGGATGGGACCATGCACCTCCCCCGGAGCCCCACCGGAACCG
P1103	ACTCGAGTACAAGAGAACAAGTAAGTAAGAAAATATA
P1111	CATACCCTCCAGCTCAGCCTTGCTCCGTTCTGATC
P1112	GATCAGACGGAGCAAGGCTGAGCTGGAGGGTATG

To be continued on the following page.

Table A - 3 List of Primers. *Continued from previous page.*

Primer	Sequence 5' to 3'
P1113	CATACCCTCCAGCTCATCCTTGCTCCGTCTGATC
P1114	GATCAGACGGAGCAAGGATGAGCTGGAGGGTATG
P1918	GTAAAACGACGGCCAGTGCCGGCTTAAGAGTCAGTA
P1919	ACTTGGTCGGAGTGAGAAG
P1920	GTAAAACGACGGCCAGTATTGACAAGTGCCTCAAGA
P1921	CCTGCAAAGTGAACCAAG
P1922	CTGCAAAGTAACGAAGAAGG
P1923	GTAAAACGACGGCCAGTTGCCGGTTAAGAGTCAG
P1924	GAAACTGGTTGGAGTGAGAA
P1155	TCCCGGGTCACGCACCGACGGCTGCTATT
P2497	GATTCTCAGAATCCAAAGCG
P2498	CTGTGGTATTCTCTGCGGT
P2499	AGGGAGAACACGATGTTAACG
P2500	TCCAATTGCACGGTCTACAA

Curriculum Vitae

Name	Katharina Johanna Heinemann, née Winkel
Date of Birth	13 th February 1992
Place of Birth	Hildesheim
Education	2016 – 2021: Institute of Plant Nutrition, Leibniz Universität Hannover 2014 – 2016: Master of Science Pflanzenbiotechnologie, Leibniz Universität Hannover 2011 – 2014: Bachelor of Science Pflanzenbiotechnologie, Leibniz Universität Hannover 2011: General university entrance qualification, Gymnasium Sarstedt

Publications

1. Heinemann, K. J., Yang, S. Y., Straube, H., Medina-Escobar, N., Varbanova-Herde, M., Herde, M., Rhee, S., Witte, C.-P. Initiation of cytosolic plant purine nucleotide catabolism involves a monospecific xanthosine monophosphate phosphatase. *Nature Communications*. Vol. 12, No. 6846 (2021). Doi: <https://doi.org/10.1038/s41467-021-27152-4>.

Conference Contributions

1. Heinemann, K. J., Yang, S. Y., Medina-Escobar, N., Varbanova-Herde, M., Herde, M., Rhee, S., Witte, C.-P. Identification of a highly substrate-specific phosphatase representing an entry point into purine nucleotide catabolism, Talk at Doctoral Researchers Conference 2019 of GRK1798 – Signaling at the Plant-Soil Interface, 25 - 27th September 2019, Hannover.
2. Heinemann, K. J., Yang, S. Y., Medina-Escobar, N., Varbanova-Herde, M., Herde, M., Rhee, S., Witte, C.-P. Identification of a highly substrate-specific phosphatase representing an entry point into purine nucleotide catabolism, Talk at 32nd Molecular Biology of Plants Conference, 18th - 21st February 2019, Dabringhausen.
3. Winkel, K. J., Medina-Escobar, N., Varbanova-Herde, M., Herde, M., Witte, C.-P. Identification and Characterization of Enzymes and Transporters Involved in the Ureide Biosynthesis in the Soybean Nodule, Poster at Doctoral Researchers Conference 2017 of GRK1798 – Signaling at the Plant-Soil Interface, 27 - 29th September 2017, Bad Salzdetfurth.
4. Winkel, K. J., Herde, M., Witte, C. P. Identification and Characterization of Enzymes and Transporters Involved in the Ureide Biosynthesis in the Soybean Nodule, Talk at Black Forest Summer School 2017, 24 - 27th July 2017, Bernau im Schwarzwald.